Magnets, Superconductors and Cryostats
TE-MSC

May 2016
Internal Note 2015-11
EDMS Nr: 1563784

Analysis of the measurements performed on TF prototype current leads tested in Hefei in July 2015

Authors: T. Spina and A. Ballarino

Keywords: **Current leads, TF prototype, electro-thermal performance, 3D FE model**

Abstract

To check the design and manufacture process of the HTS current leads (68 kA) for the toroidal field ITER magnets (TF) before the series production, several tests on TF prototypes were performed in Hefei (at ASIPP center) in nominal operating condition [1].

In the present study, the data obtained from such measurements are analysed and compared to the ITER specified performance targets. The experimental values are compared to the 3D FE model predictions.

Contents

Abstract 1

1. TEST SUMMARY 3

2. LOFA (CASE 4.1) 5

2.1 Voltage drop over HEX 5

2.2 Current 7

2.3 HTS warm and cold end Temperatures 7

2.4 Minimum LOFA time 9

2.5 Minimum HTS overheating time constant 11

3. STEADY STATE (CASE 4.1) 13

3.1 Mass flow rate in HEX section 13

3.2 Pressure drop in 50 K GHe circuit in HEX 14
3.3 Voltage drop over HEX 17
4. UNDER/OVER CURRENT (CASES 6.1, 6.2, 6.3, 6.4, 6.5) 19
4.1 Voltage drop over HEX 19
4.2 Mass flow rate in HEX 22
4.3 Pressure drop in 50K GHe circuit in HEX 26
4.4 HTS warm end temperature 29
4.5 LOFA time for under/over current 31
4.6 Current 39
4.7 Summary under/over current analysis 40
4 STAND BY (CASES 2.2 and 3.2) 41
4.1 Current 41
4.2 Mass flow rate 43
4.3 Pressure drops over HEX 44
4.4 HTS warm end temperature 46
5 OVER COOLING (CASES 5.10, 5.11) 46
5.1 Pressure drop in 50K GHe circuit in HEX 47
5.2 HTS warm end temperature and mass flow rate in HEX 48
5.3 Voltage drop over HEX only case 5.11 50
6 TEMPERATURE PROFILE 53
6.1 Experimental data 53
6.2 3D FE thermo-hydraulic and electrical model 57
6.3 Comparison between experimental and simulated data 58
7 JOINT RESISTANCES (CASE 10.1) 59
SUMMARY 77
ACKNOWLEDGMENT: 78
References 78

1. TEST SUMMARY

Figure 1 Overview of the measurements performed in July 2015 in Hefei. (Courtesy of P. Bauer **[2]**). Data set: Cernox in middle of U-bend= MAG-HTS-CLU:MT011-T; Full current= MAG-HTS-CL-MI-001:IT; Ubend joint temp= MAG-FDR-STT:Ebloxx2-1

In Figure 1 an overview of the full set of measurements performed in Hefei in 2015 is shown.

Two TF prototypes were tested during the month of July and in this note we will refer to them as CL1 and CL2.

In this analysis, for each test, the time has been normalized and all the parameters (temperature, voltage and pressure drop, mass flow rate) are plotted as a function of time expressed in minutes or seconds.

In Figure 2 the relevant cryogenic scheme and instrumental diagrams are reported. Further details can be found in the Report "ASIPP_Test Procedure for the ITER Current Leads Prototypes" [1].

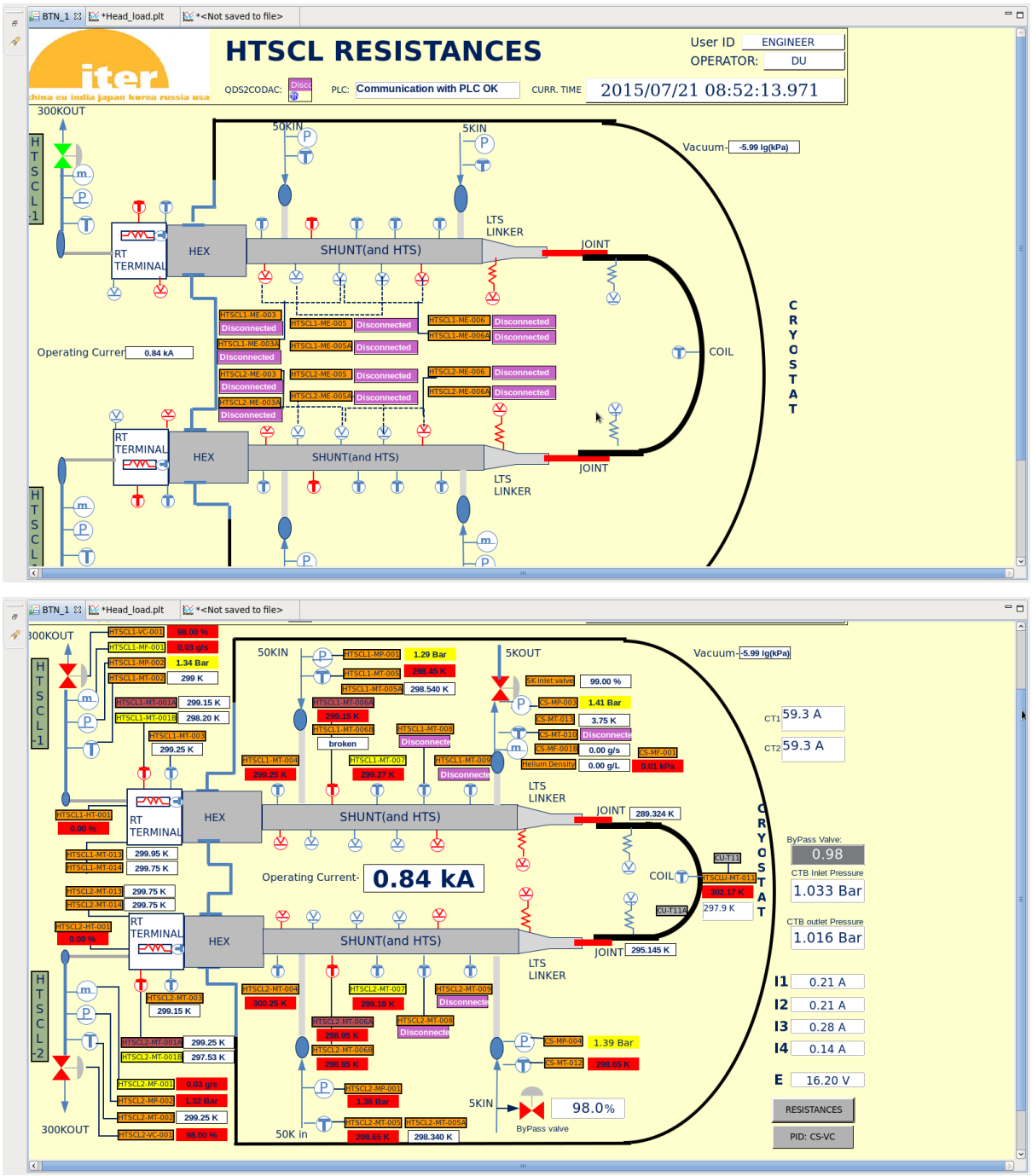

Figure 2 Relevant cryogenic scheme and instrumental diagrams **[1]**.

2. LOFA (CASE 4.1)

In this section the main results on the LOFA tests are presented and discussed. As reported in Figure 1, these tests were performed on the 5th and on the 6th of July 2015 for CL2 and CL1 respectively. The technical details of the data acquisition are reported in [1].

2.1 Voltage drop over HEX

In Figure 3 the Voltage drops over HEX for both the current leads are shown.

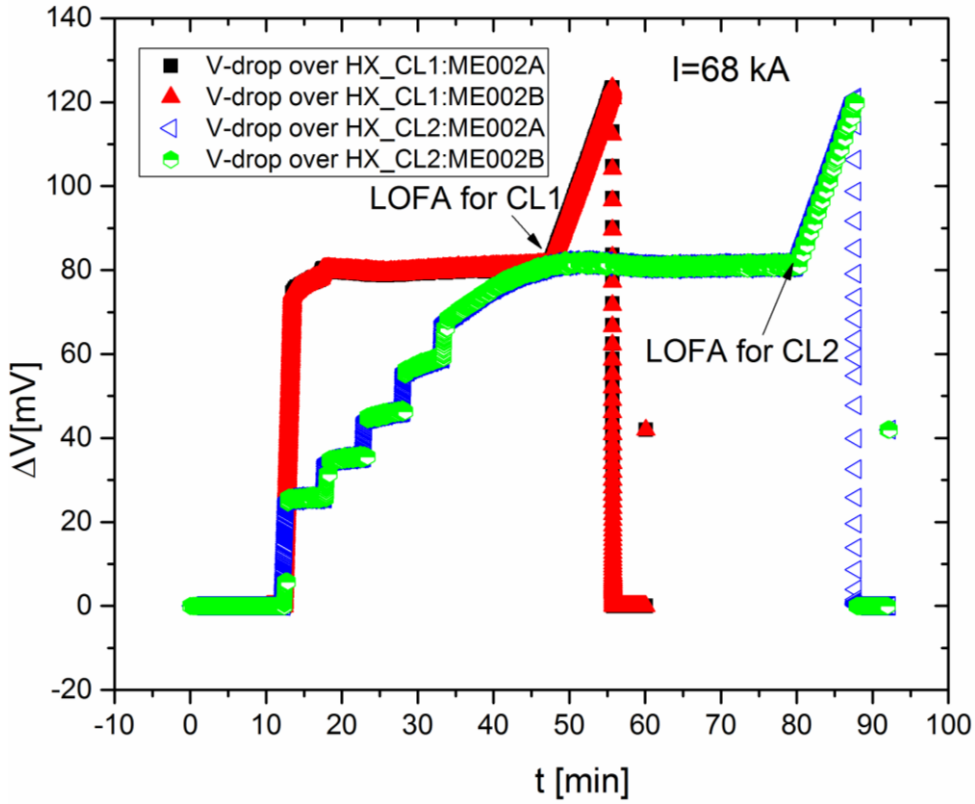

Figure 3 Voltage drop over HEX for CL1 (red and black curved) and CL2 (green and blue curves).

In Figure 4 and Figure 5 the voltage drops over HEX are plotted together with the current and the mass flow rate for both the current leads under study. The maximum value of the voltage drop over HEX reached during the transition regime is 123.09 mV for CL1 and 120.35 mV for CL2.

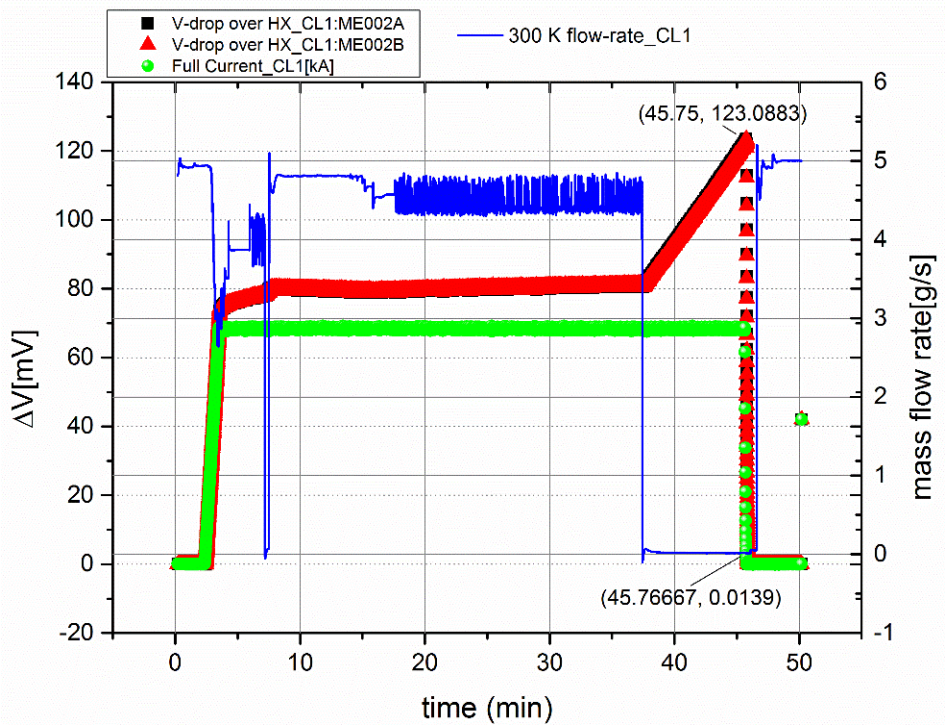

Figure 4 Transitory regime for CL1 starting after 33 minutes in nominal steady state conditions.

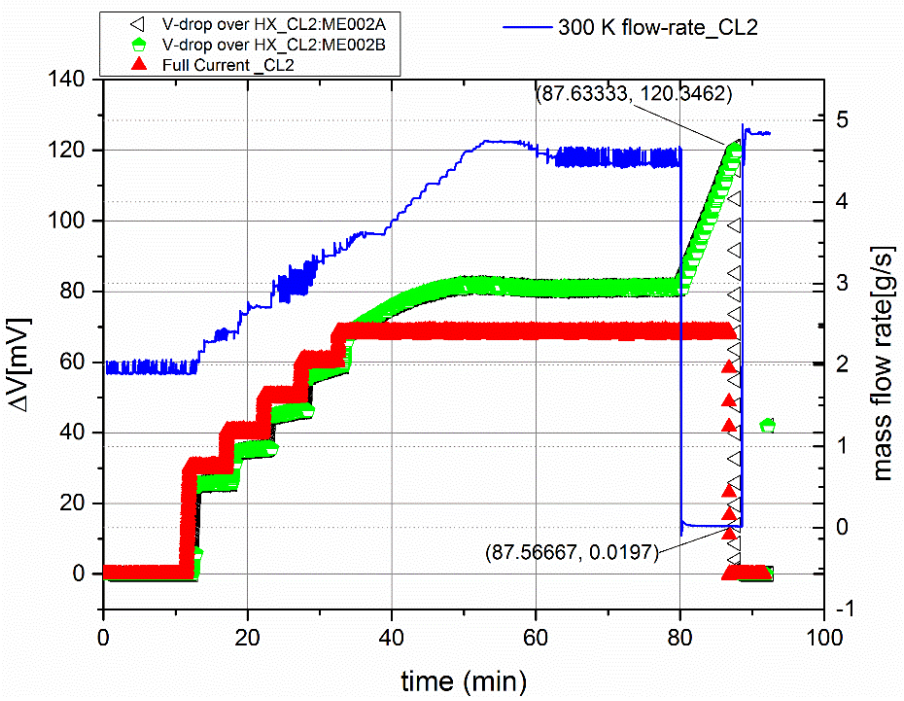

Figure 5 Transitory regime for CL2 starting after 40 minutes in nominal steady state conditions.

2.2 Current

In Figure 6 the current in steady state for both leads is shown. Results from two tests are reported.

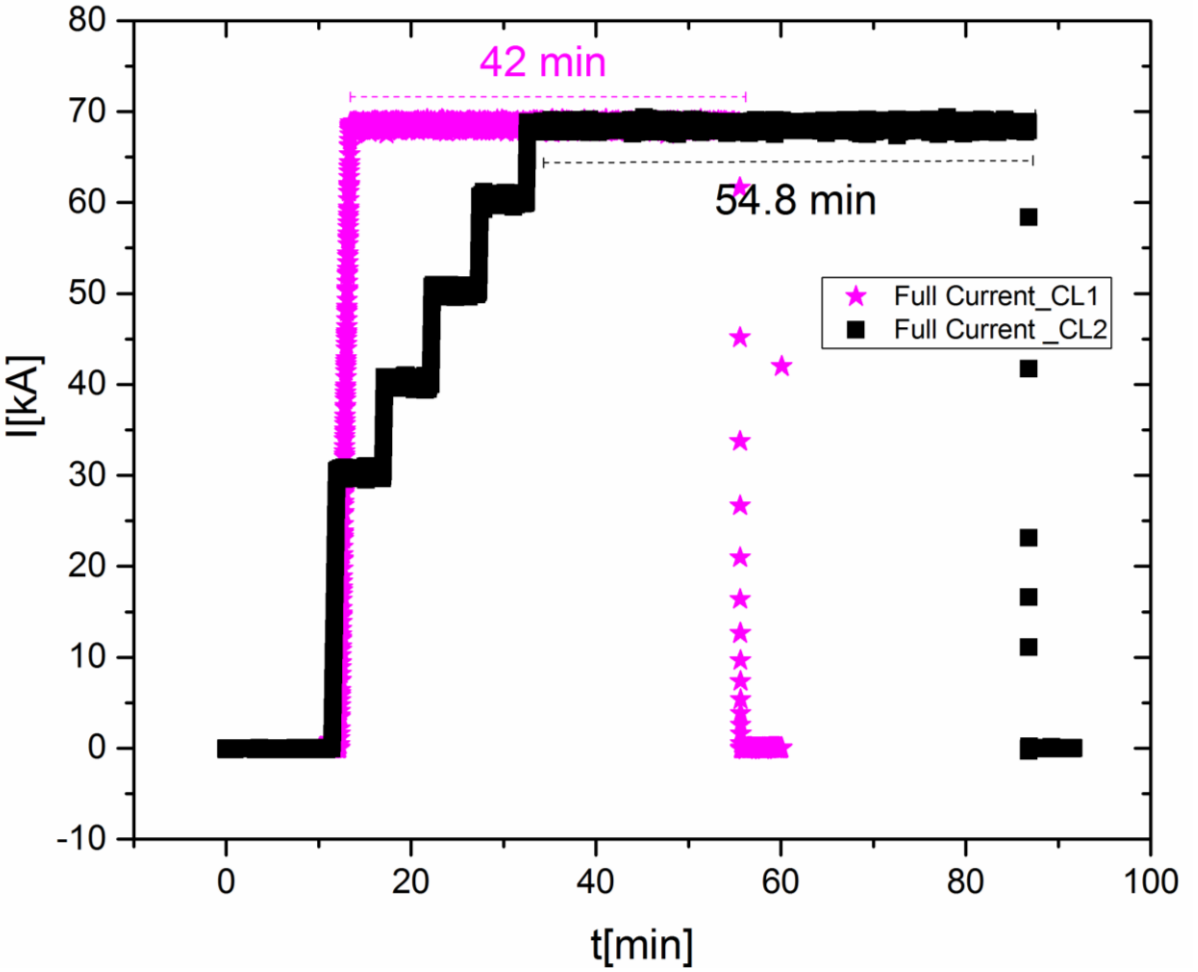

Figure 6 Current for CL1 in pink and for CL2 in black. Data set: MAG-HTS-CL-MI-001:IT

2.3 HTS warm and cold end Temperatures

In Figure 7 and in Figure 8 the HTS cold and warm end temperatures for the two CLs are plotted as a function of time.

As shown in Figure 7 the HTS cold end temperature is in the range between 4.7 K and 5 K while in Figure 8 it was found that the HTS warm end temperature has the lowest value ~65 K and the highest value ~99 K. **These values are in agreement with the TF requirement**.

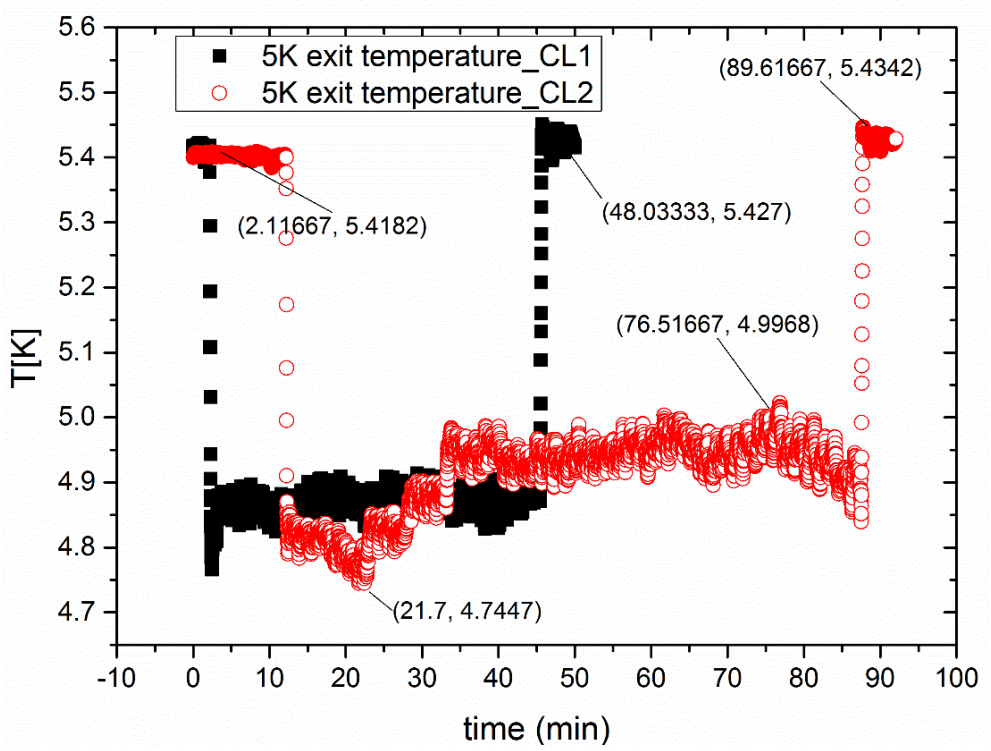

Figure 7 HTS cold end temperature for CL1 in black and for CL2 in red. Data set: MAG-HTS-CS:MT010-TT for CL1 and MAG-HTS-CS:MT010-TT for CL2

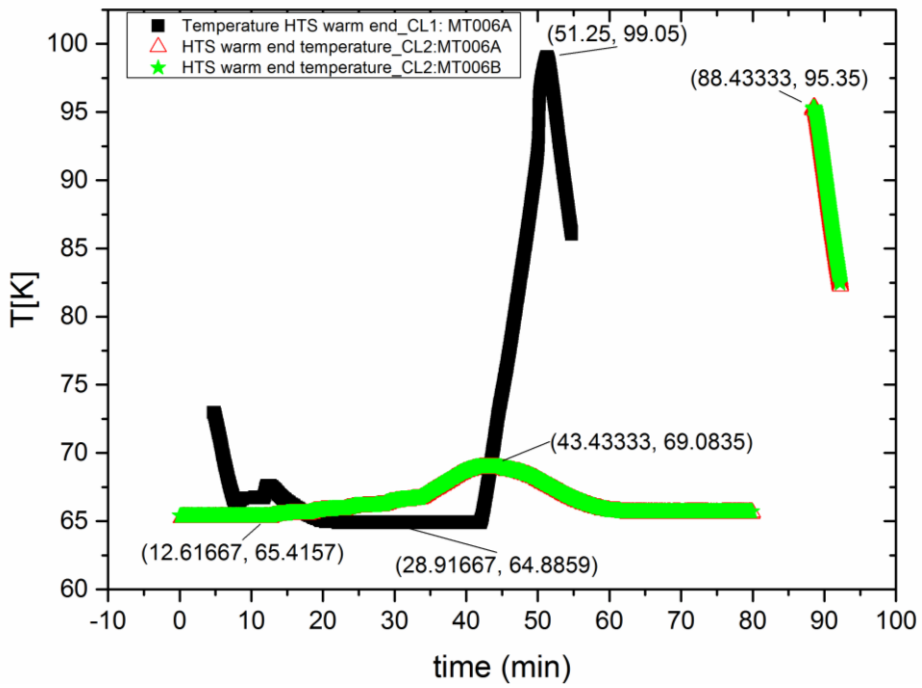

Figure 8 HTS warm end temperature for CL1 in black and for CL2 in red and green. Data set: MAG-HTS-CS:MT006A for CL1 and MAG-HTS-CS:MT006A\B for CL2.

2.4 Minimum LOFA time

As shown in Figure 9, the minimum LOFA time for CL1 is 484 s from the time when the mass flow goes to zero (light blue curve in Figure 9) to the end when the voltage across the HTS reaches 0.3 mV. **The ITER specifics form requests 400 s** (see Table 1).

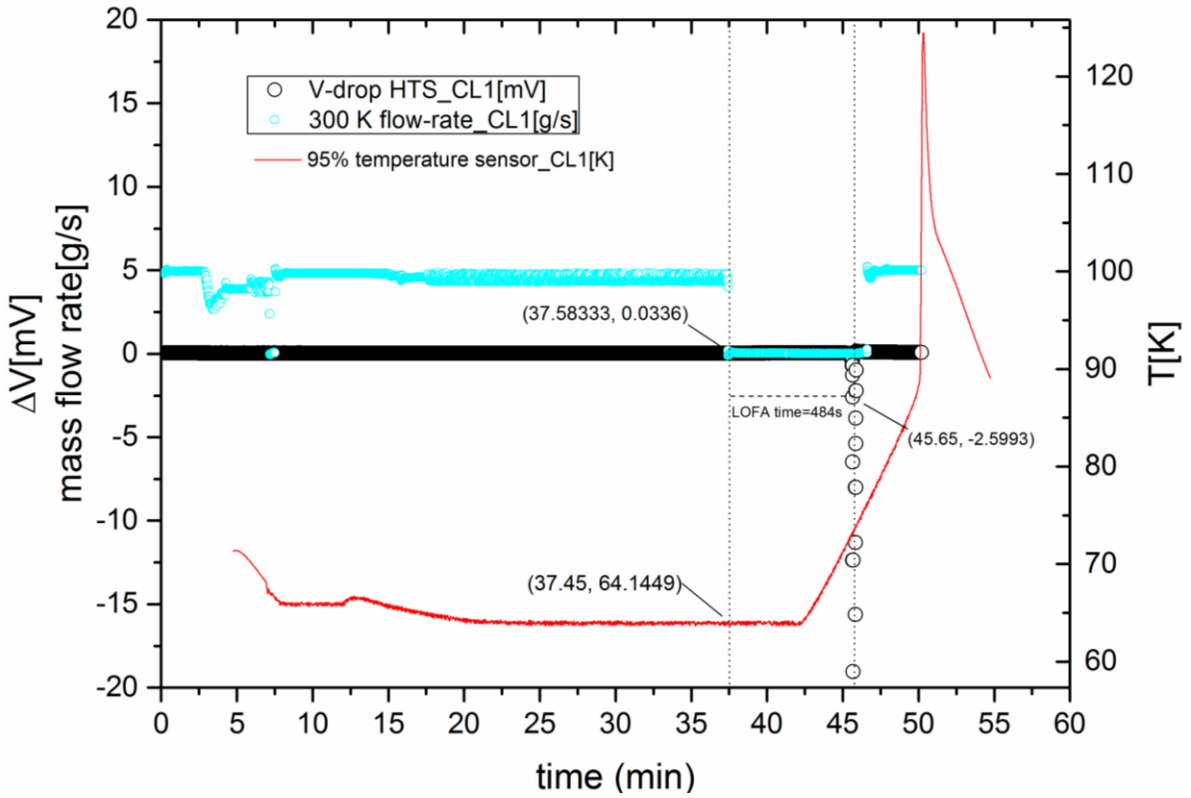

Figure 9 Minimum LOFA time for CL1. Data set: V-drop HTS=MAG-HTS-CL1-ME-005:ET; 300K flow-rate=MAG-HTS-CL1-MF-001:FT and 95%temperature sensor=MAG-HTS-CL1-MT-007:TT.

Unfortunately, the minimum LOFA time for CL2 cannot be determined taking into account the voltage drop over HTS (ME004B and ME005 traces) due to missing data, see Figure 10. Thus the signal ME004A corresponding to the voltage drop over the shunt was used and it follows from Figure 11 that the minimum LOFA time for CL2 is 447 s.

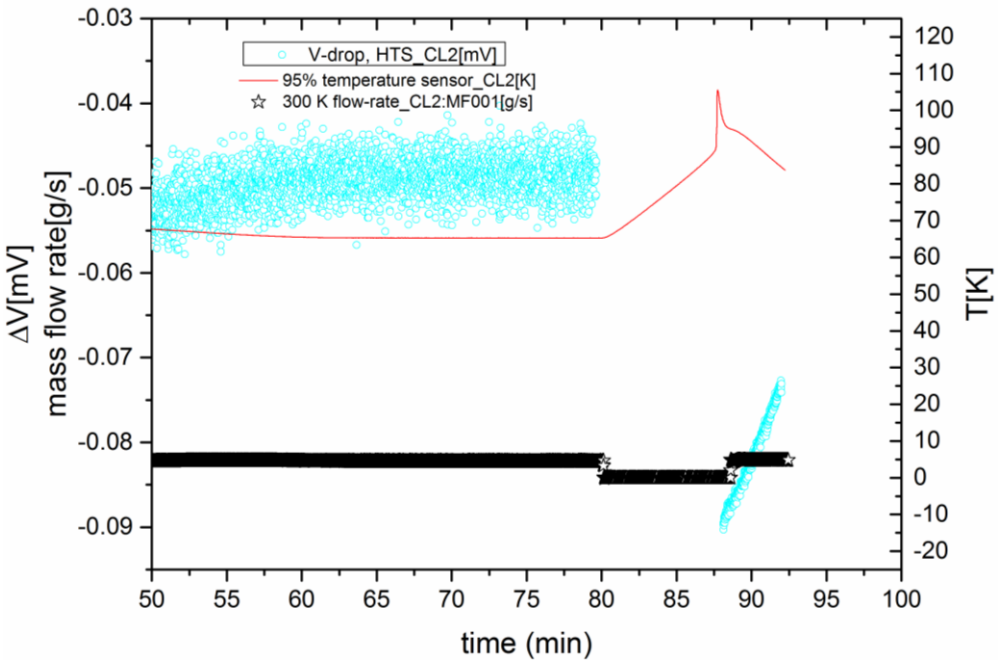

Figure 10 Minimum LOFA time for CL2: the discontinuity in the pressure drop over HTS does not allow the estimation of the minimum LOFA time for CL2. Data set: V-drop HTS=MAG-HTS-CL2-ME-005:ET; 300K flow-rate=MAG-HTS-CL2-MF-001:FT and 95%temperature sensor=MAG-HTS-CL2-MT-007:TT.

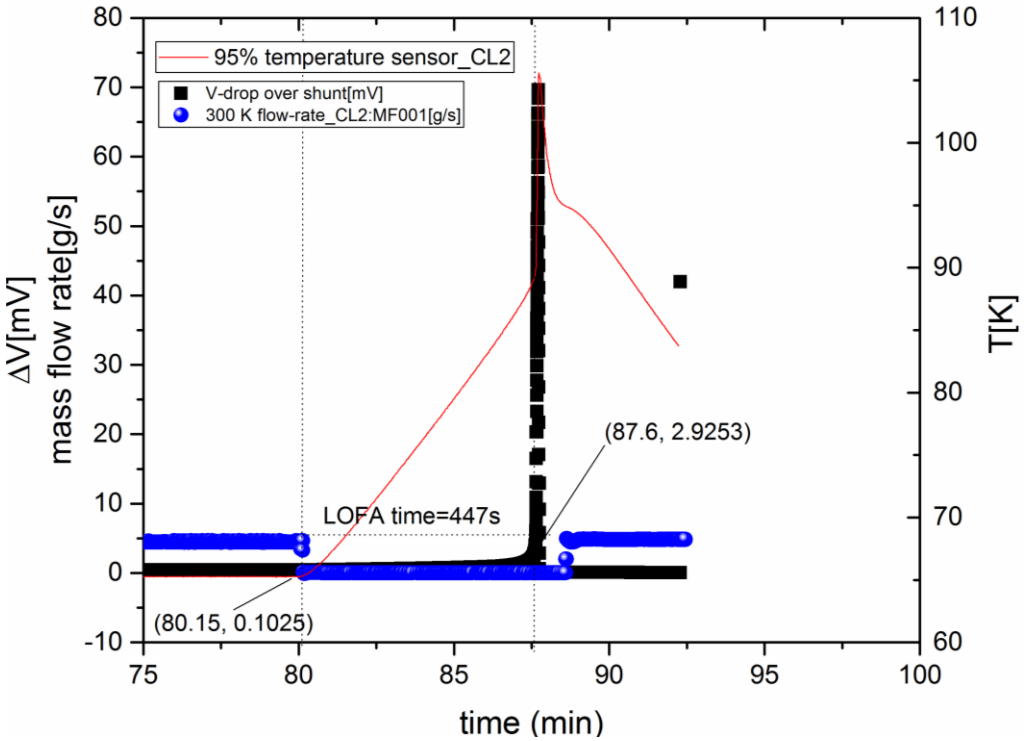

Figure 11 Minimum LOFA time estimated by means of ME004 signal (i.e. the voltage drop over shunt).

As reported in Table 1, the experimental minimum LOFA time for both current leads is higher than ITER requirement (400 s).

Table 1 *Comparison between the minimum LOFA time experimental results (as obtained from the analysis at ASIPP* **[3]** *and at CERN) and the ITER requirement*

Parameter	ITER Requirement	CL1		CL2	
		ASIPP	CERN	ASIPP	CERN
Minimum LOFA time (s)	400	457	484	490	447

2.5 Minimum HTS overheating time constant

The minimum overheating time, i.e. the time from start of quench detection at 3 mV to the time when the current is switched off is 16 s for CL1 and 10 s for CL2.

As shown in Figure 12 and Figure 13, to obtain the OHT, the original voltage data (black curves) were shifted in time (blue curves) because the two systems for the acquisition of the voltages (QDS system) and of the temperatures and currents (CODAC system) are not synchronized during the measurements.

In Table 2 such values are compared with the ITER specifics: the OHT for CL2 is 5 s lower than the expected value (15 s).

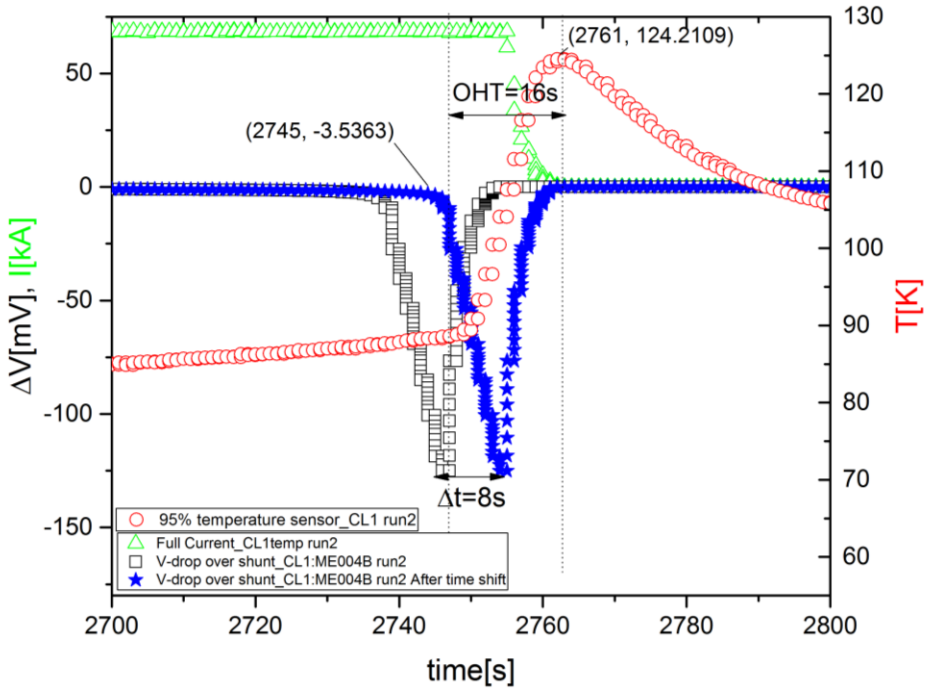

Figure 12 Minimum overheating time for CL1.

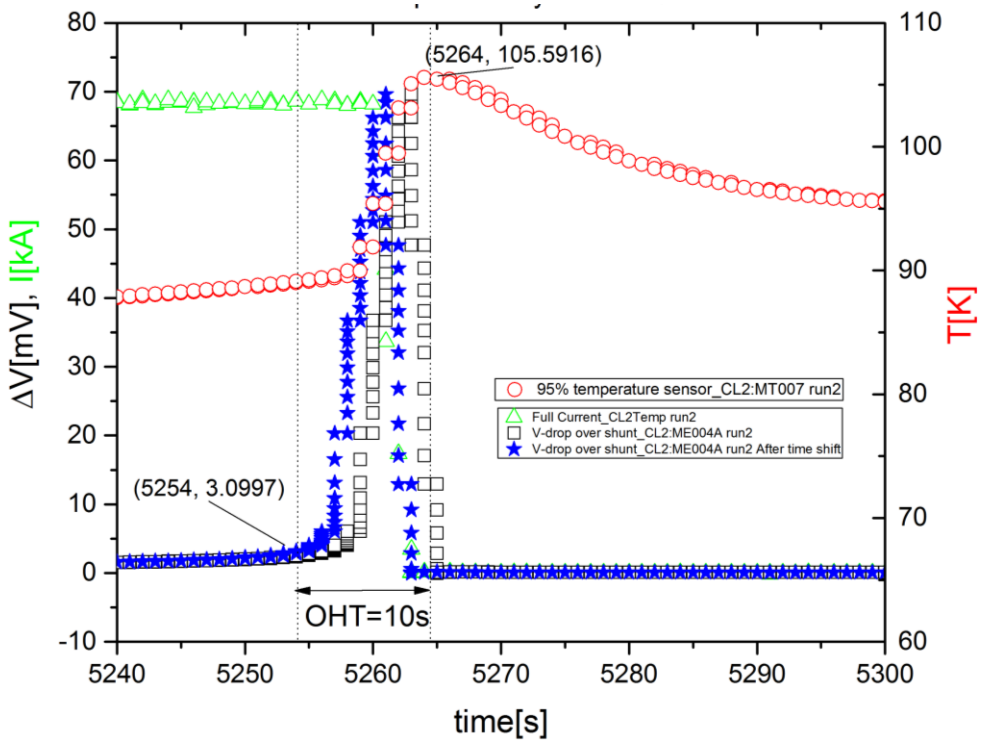

Figure 13 Minimum overheating time for CL2.

Table 2 *Comparison between the minimum Overheating time experimental results and the ITER requirement.*

Parameter	**ITER Requirement**	**CL1**	**CL2**
		CERN	
Minimum overheating time (s)*	15	16	10

*the hot spot temperature is the maximum temperature recorded, i.e. 100 K. From the data, 200K was never reached.

3. STEADY STATE (CASE 4.1)

In this section the main results on the steady state tests are presented and discussed. As reported in Figure 1, these tests were performed on the 13th of July 2015 for both the leads (CL1 and CL2) and the technical details of the data acquisition are reported in ref. [1].

The main goal of this section is to check if the parameters as the mass flow rate, the pressure and voltage drop are, according to prediction, sufficiently stable to be considered in the steady state regime.

3.1 Mass flow rate in HEX section

In Figure 14 the measurements of the mass flow rate of the HEX are shown for both the leads.

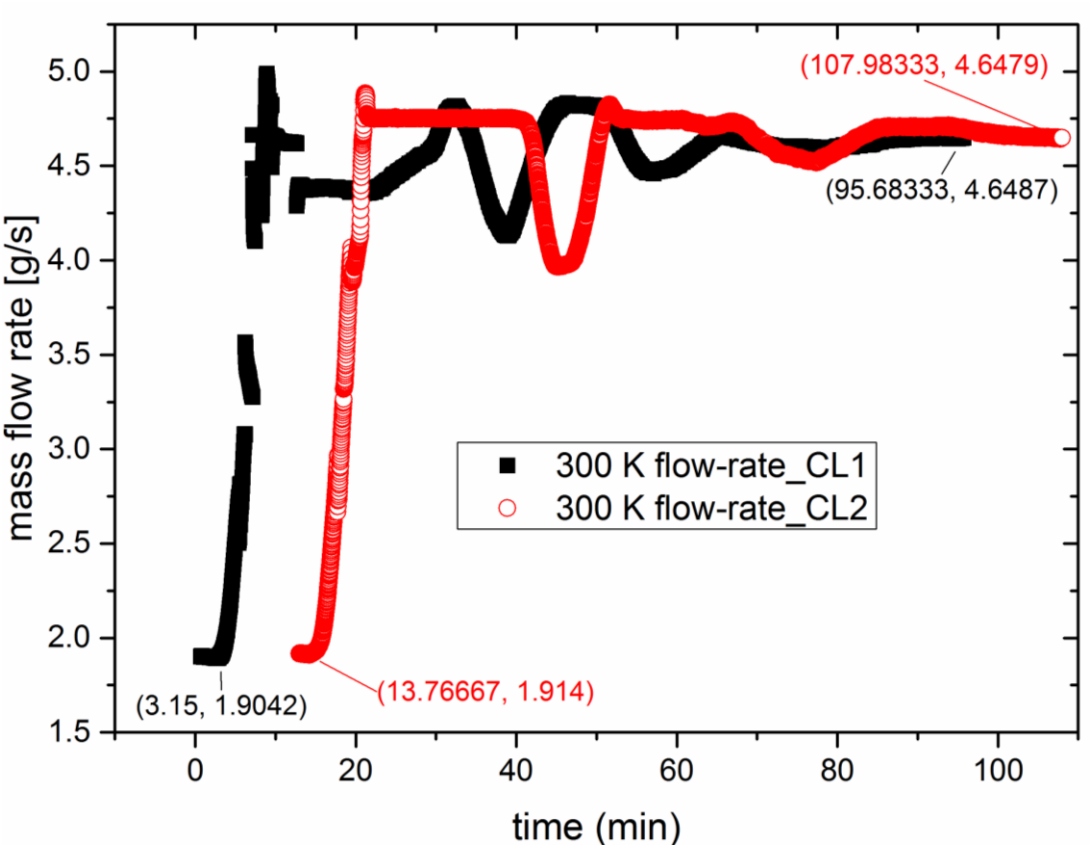

Figure 14 Mass flow rate in the HEX for CL1 (black curve) and CL2 (red curve). Data set: MAG-HTS-CL2-MF-001:FT for CL2 and MAG-HTS-CL1-MF-001:FT for CL1.

To check the stability of such data the error bars have been added in the flat region (i.e. starting at the 80th minute), Figure 15. The error bar comes from the precision of the flow meters (+/- 0.05 g/s) as communicated by the team in Hefei.

Looking at Table 3 it is possible to conclude that the results obtained in this test analysis are in very good agreement to those obtained from the 2D and 3D full model [4]**.**

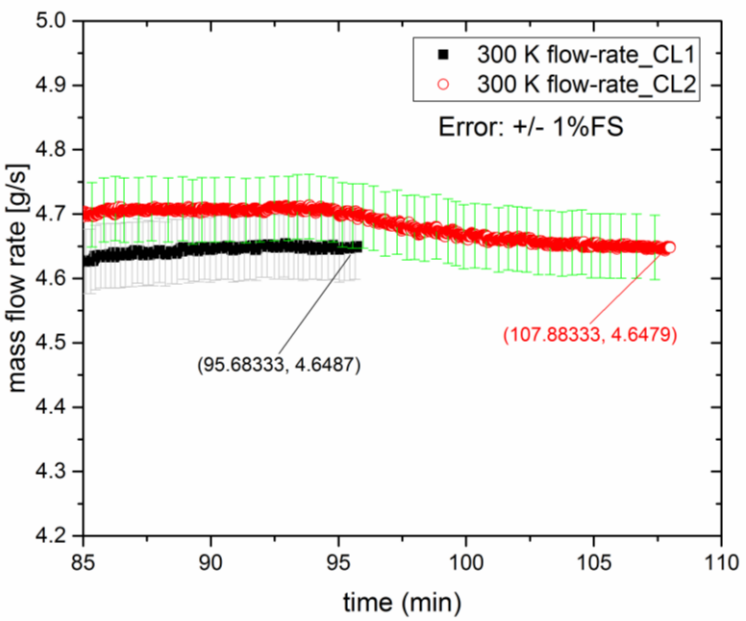

Figure 15 Steady state region for the mass flow rate in the HEX for both the CLs. Accuracy of +/-1%FS (FS=5 g/s).

Table 3 *Mass flow rate in HEX: comparison between experimental, 3D FE full model* **[4]** *and specification values.*

	3D Full model	IO Specification	CL1 (CERN) Experimental	CL2 (CERN) Experimental
Mass flow rate in HEX (g/s)	4.5	<4.8	4.65	4.65

3.2 Pressure drop in 50 K GHe circuit in HEX

In Figure 16 the measurements of pressure drop at room temperature (300 K) and in nominal cryogenic conditions (50 K) are plotted for both the CLs. The steady state region, as in the previous case (i.e. for the mass flow rate in Figure 14), has been reached after 80 minute the start of the current ramp.

Subtracting to the 50 K inlet supply pressure (around 4.5 bar) the 300 K exit pressure (around 3.5 bar), it was found that in the steady state regime the pressure drops in the 50 K circuit in HEX are 0.11 and 0.12 MPa for CL1 and CL2 respectively, see Figure 17.

Comparing these values with those predicted by the 3D FE model [4], see Table 4, it is possible to conclude that **the experimental values fully match the simulated values as well as the ITER specification**.

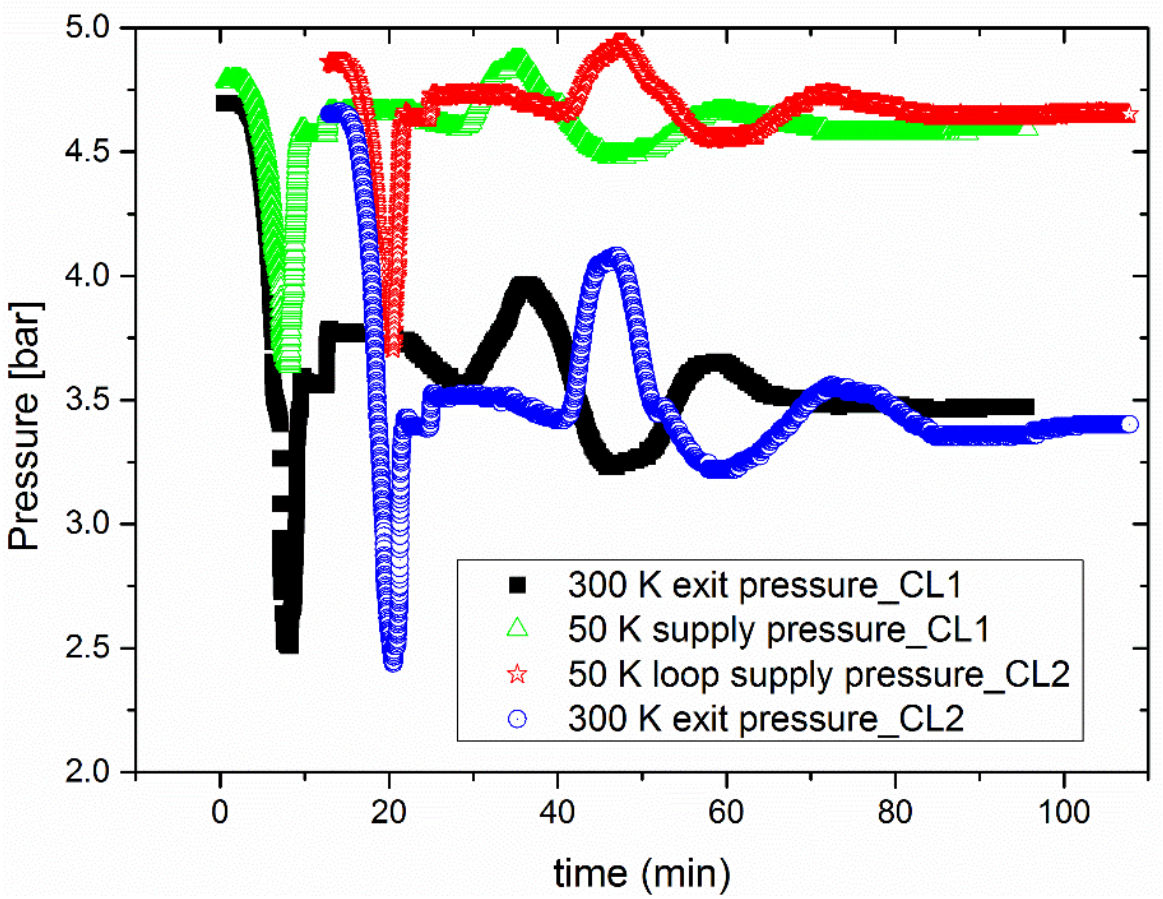

Figure 16 Pressure measurements at 300K and 50K for both the CLs. Data set: MAG-HTS-CL1:MP001-PT & MAG-HTS-CL1:MP002-PT ➔ for CL1; MAG-HTS-CL2:MP001-PT & MAG-HTS-CL2:MP002-PT ➔ for CL2.

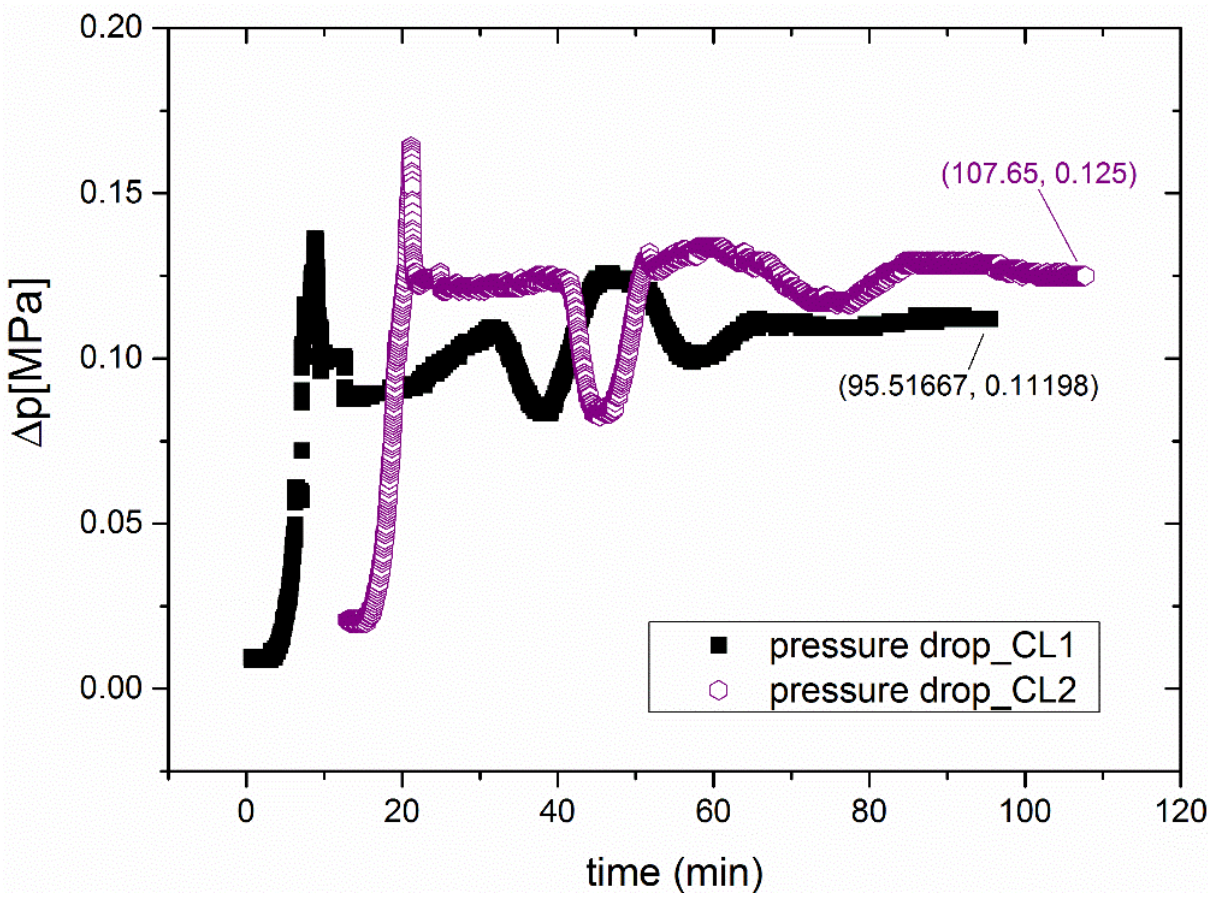

Figure 17 Pressure drop in HEX for CL1 (black curve) and CL2 (violet curve).

Table 4 *Maximum pressure drop in 50K circuit in HEX: comparison between experimental, 3D FE full model* **[4]** *and specification values.*

	3D Full model	IO Specification	CL1 (CERN) Experimental	CL2 (CERN) Experimental
Max pressure drop in 50K circuit in HEX [MPa]	0.12	<0.2	0.11	0.12

3.3 Voltage drop over HEX

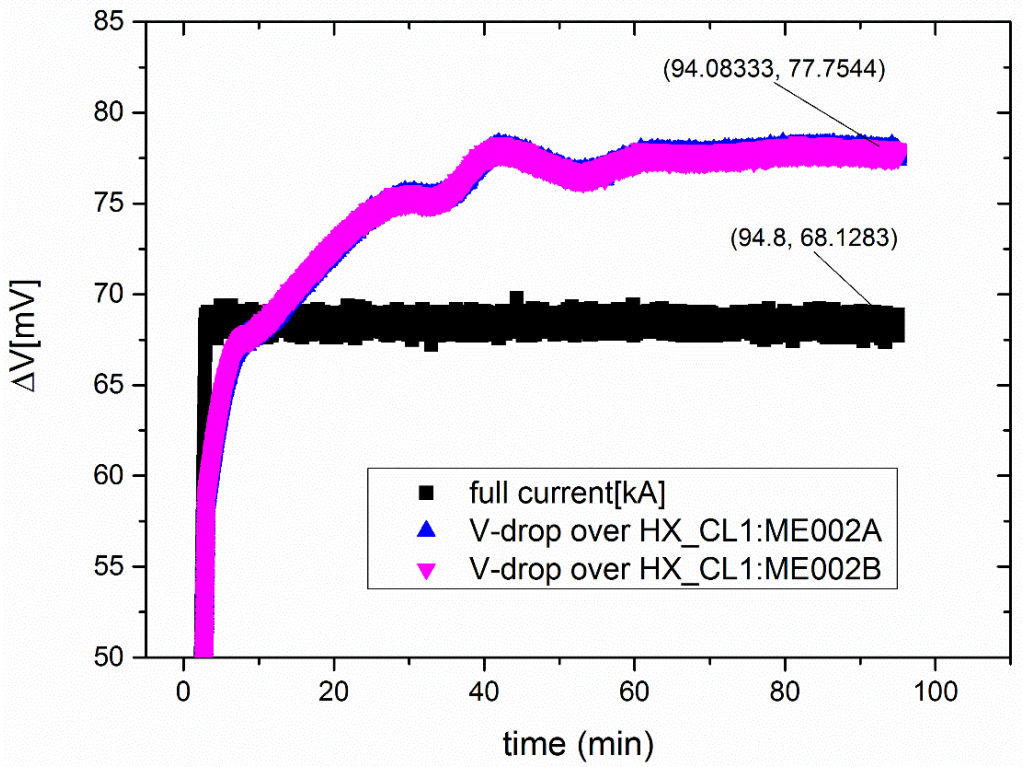

Figure 18 Voltage drops for CL1. Data set: MAG-HTS-CL1:ME002A-ET & MAG-HTS-CL1:ME002B-ET.

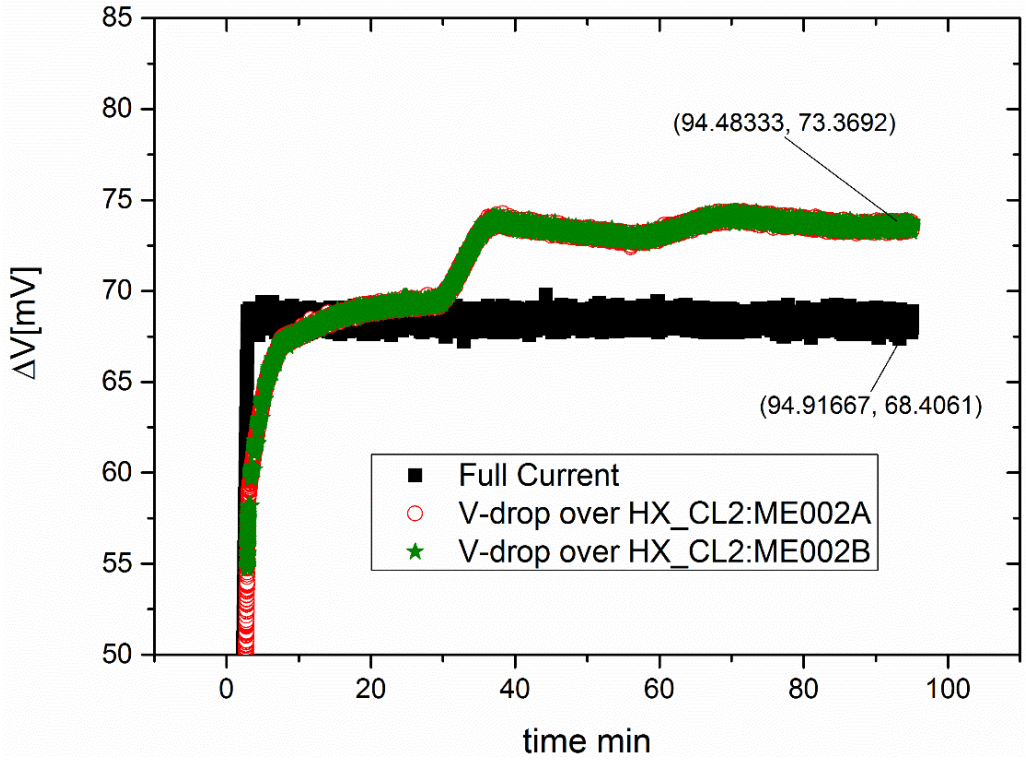

Figure 19 Voltage drop in CL2. Data set: MAG-HTS-CL2:ME002A-ET & MAG-HTS-CL2:ME002B-ET.

In Figure 18 and Figure 19 the voltage drops over HEX for CL1 and CL2 are reported. In the same plots the nominal current is shown.

Two voltage taps were used for each current leads (ME002A and ME002B) and it was found that in the steady state regime the voltage drops are 77.75 and 73.37 mV for CL1 and CL2 respectively.

4. UNDER/OVER CURRENT (CASES 6.1, 6.2, 6.3, 6.4, 6.5)

In this section the main results on the under/over current tests are presented and discussed. As reported in Figure 1 and summarized in Table 5 these tests were performed on the 9th and on the 11th of July 2015 for both the leads (CL1 and CL2) and the technical details of the data acquisition are reported in ref. [1].

Table 5 Summary of the under/over current tests

CASE	CURRENT [kA]	DATE	
6.1	75	11.07.2015	Over current
6.2	64	09.07.2015	Under current
6.3	60	09.07.2015	Under current
6.4	55	09.07.2015	Under current
6.5	50	11.07.2015	Under current

4.1 Voltage drop over HEX

In Figure 20 and Figure 21 the voltage drops over HEX for CL1 and CL2 are reported.

As expected in the over current case (case 6.1, 75 kA, see Table 5) the voltage drop is higher than for the under current cases (i.e. below 68 kA: from 6.2 to 6.5 cases, see Table 5). By the way, as shown hereafter, it should be noticed that the 75 kA case never reached steady state due to the ~5g/s flow limitation in the flow controller. It follows that the reliability of the over current values is lower with respect to those of the under current cases as well as of the steady state.

For the case 6.3 (60 kA) for both the lead: at ~7000 s the voltage drop goes to zero. From the data it appears that LOFA tests were performed as shown in Figure 22 and Figure 23 for CL1 and CL2 respectively.

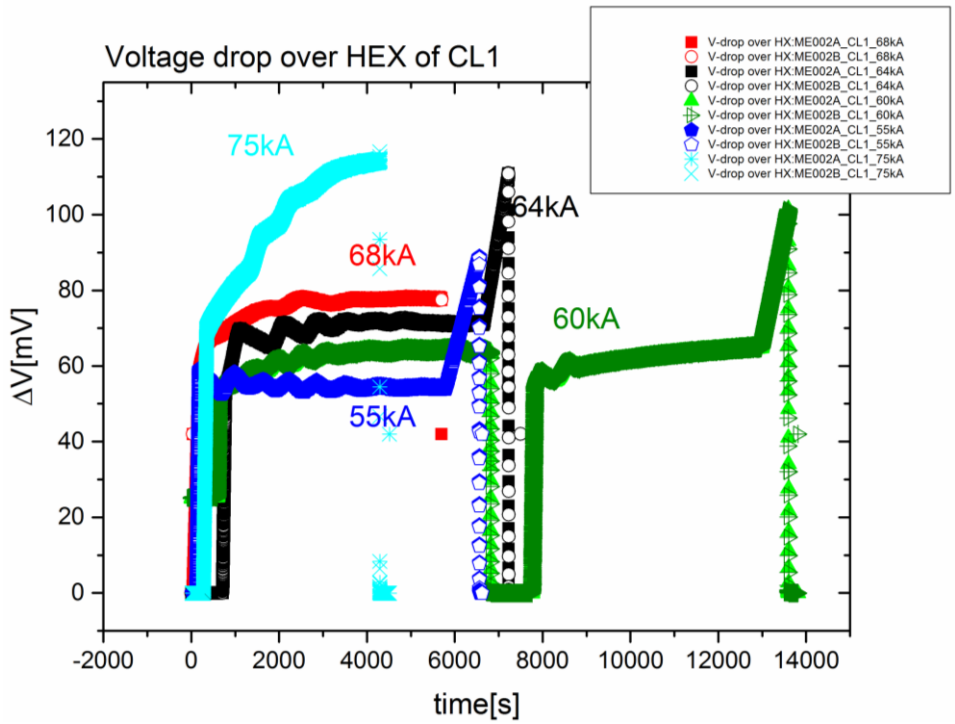

Figure 20 Voltage drops over HEX for CL1 at different currents. It should be noticed that HEX didn't reached steady state condition when operated at 75 kA.

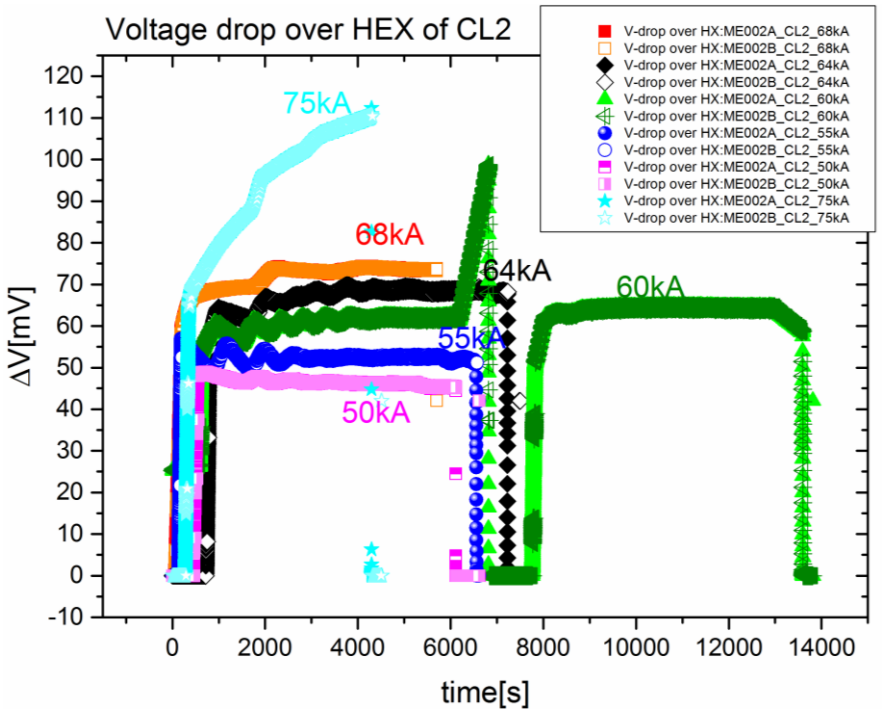

Figure 21 Voltage drops over HEX of CL2 for different currents. It should be noticed that HEX didn't reached steady state condition when operated at 75 kA.

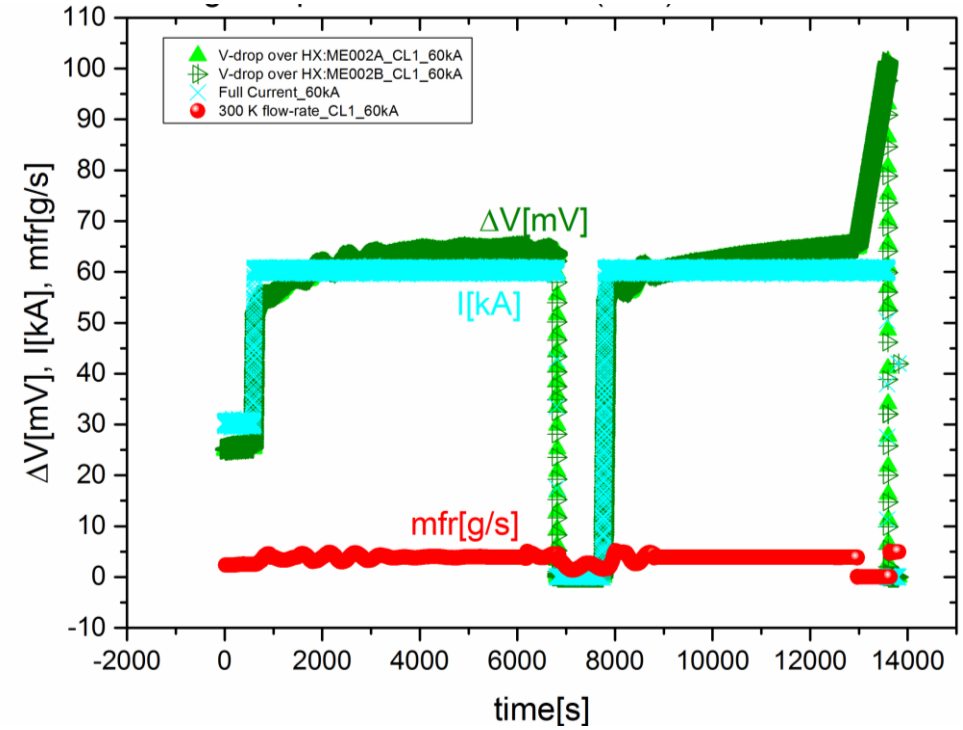

Figure 22 Comparison between Voltage drop and mass flow rate for the over current case at 60kA.

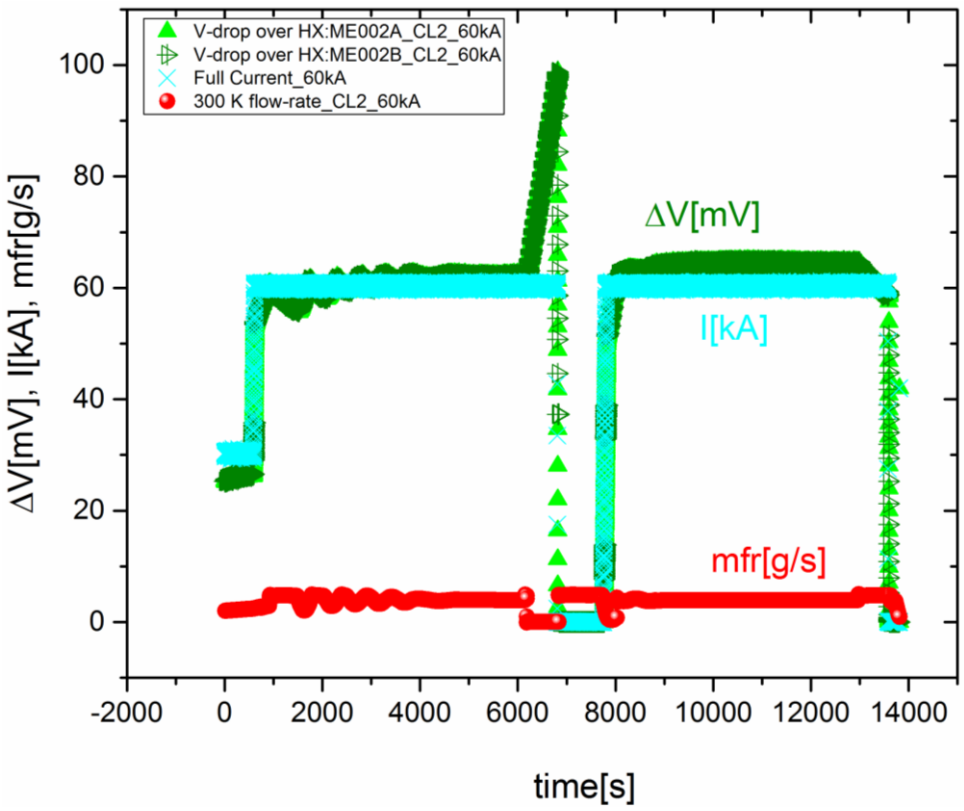

Figure 23 Comparison between Voltage drop and mass flow rate for the over current case at 60kA.

4.2 Mass flow rate in HEX

In Figure 24 and Figure 25 the mass flow rate in HEX for CL1 and CL2 are plotted respectively. The instrumental error on the mass flow is 0.05 g/s.

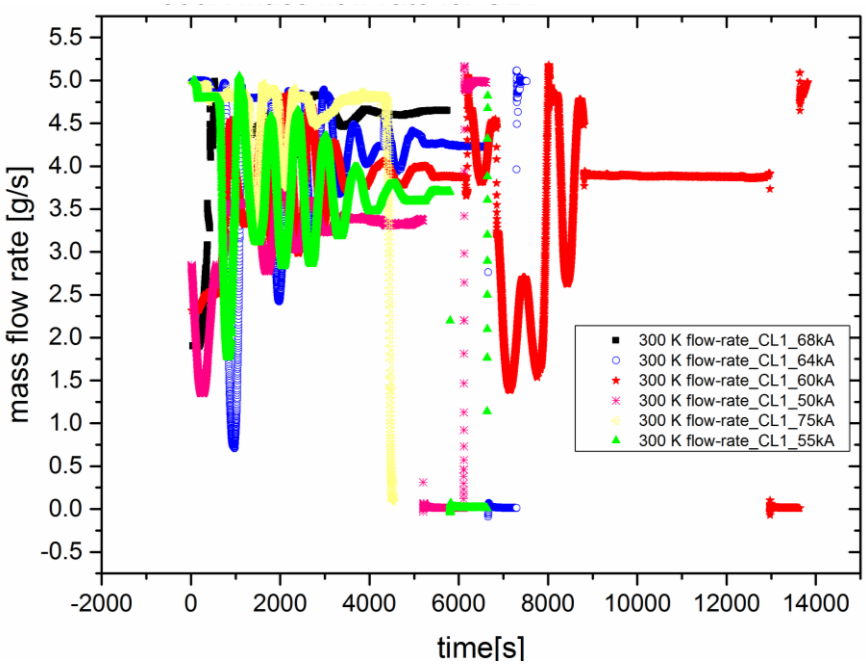

Figure 24 Mass flow rates as a function of time in HEX of CL1 for different currents. The mass flow rate for the 75 kA is lower than 5g/s due to the limitation in the flow-controller.

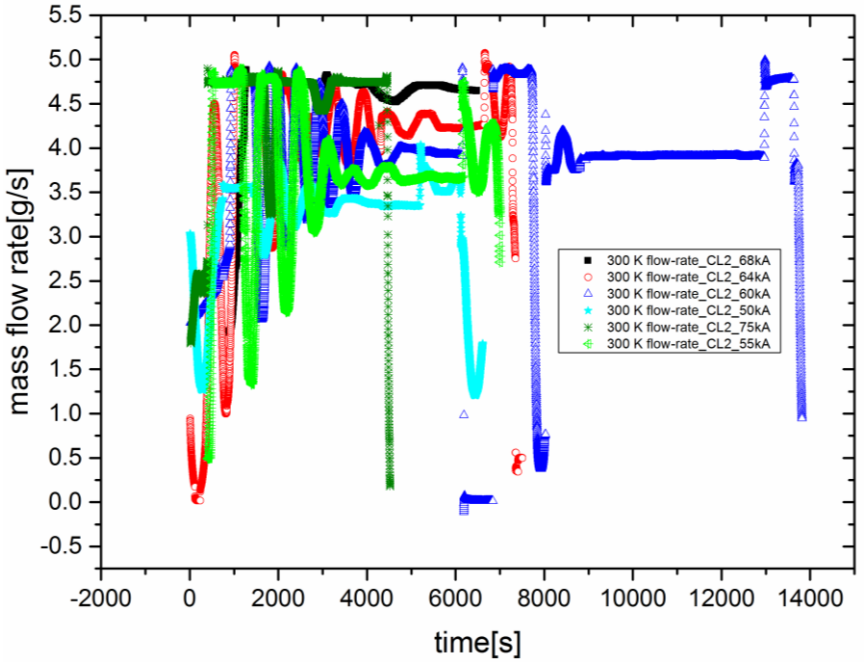

Figure 25 Mass flow rates as a function of time in HEX of CL2 for different currents. The mass flow rate for the 75 kA is lower than 5g/s due to the limitation in the flow-controller.

In Figure 26 and Figure 27 the magnifications up to 6000 s are reported to investigate the mass flow rate value in the stable region: as expected, taking as reference the nominal value of 68 kA with a mass flow rate of 4.6+/-0.5 g/s, it was found that in the under current cases (from 6.2 to 6.5, see Table 5) the mass flow rate is lower while in the over current case (i.e. case 6.1) the mass flow rate is higher with respect to that one at 68 kA.

Such trend is shown in Figure 28 where the mass flow rate for both the leads is plotted as a function of current and a very good agreement between the two data sets has been found.

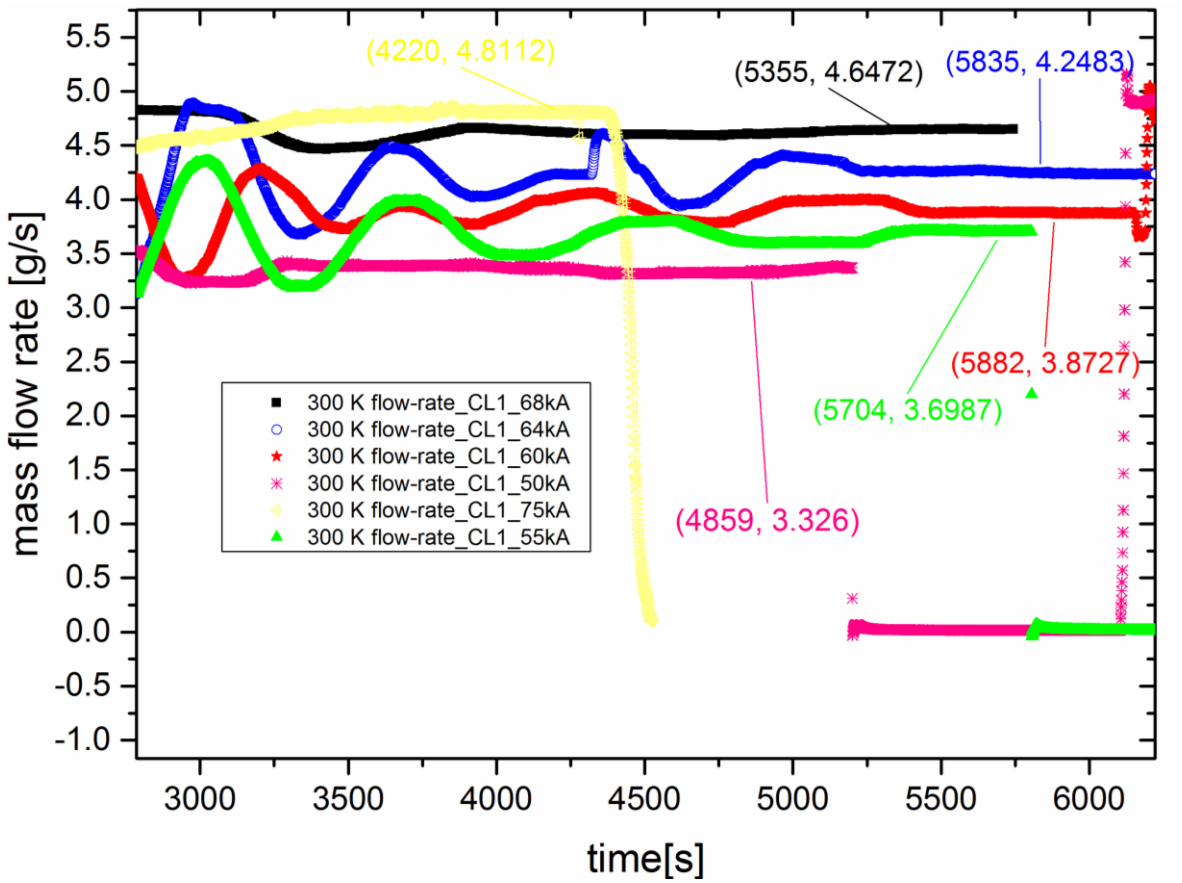

Figure 26 Mass flow rate in HEX of CL1 in the stable region at different currents.

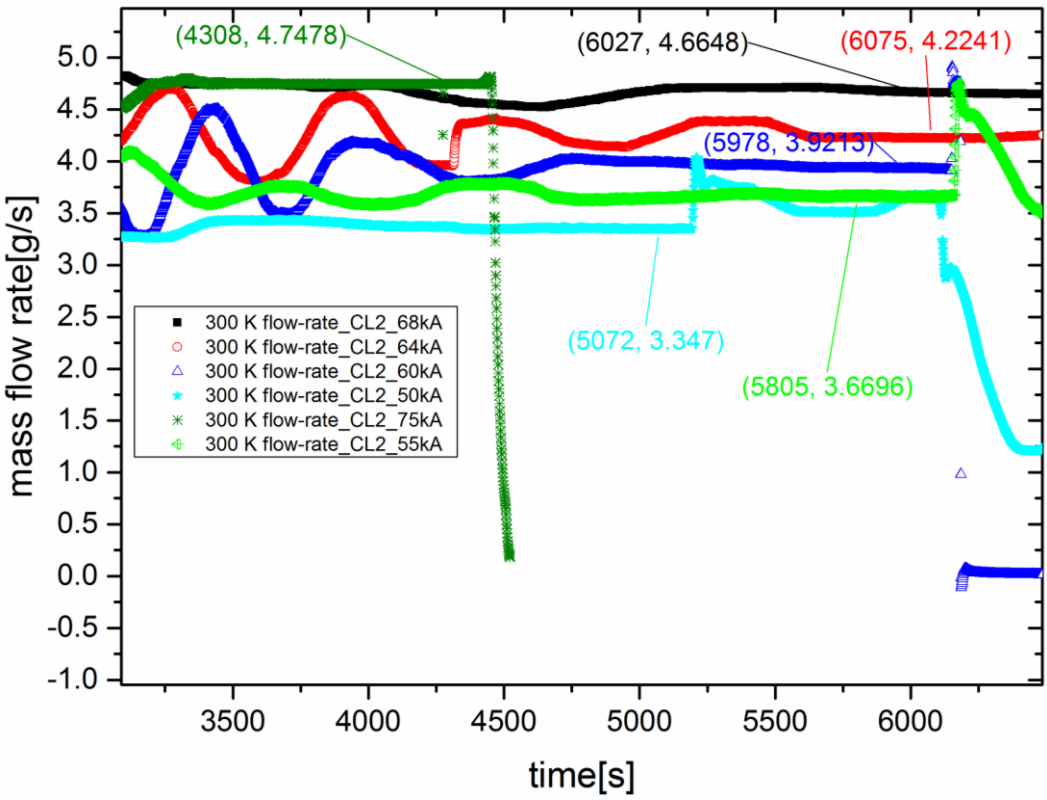

Figure 27 Mass flow rate in HEX of CL2 in the stable region at different currents.

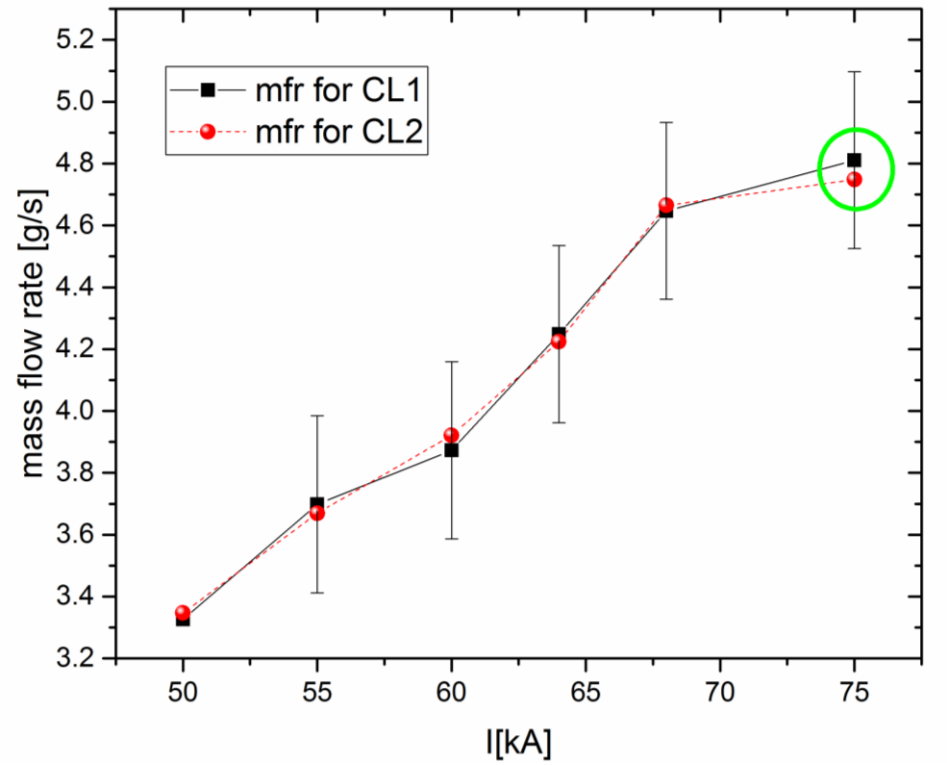

Figure 28 Mass flow rate (mfr) as a function of current for CL1 (black curve) and CL2 (red curve). The 75 kA value is signed with the green circle because it did not reach steady state conditions.

As shown in Figure 29, where the ratio between the mass flow rate and the current (mfr/I) is plotted as a function of the current (in the range from 45 kA to 80 kA), the current of the HEX is well optimized for both the CLs.

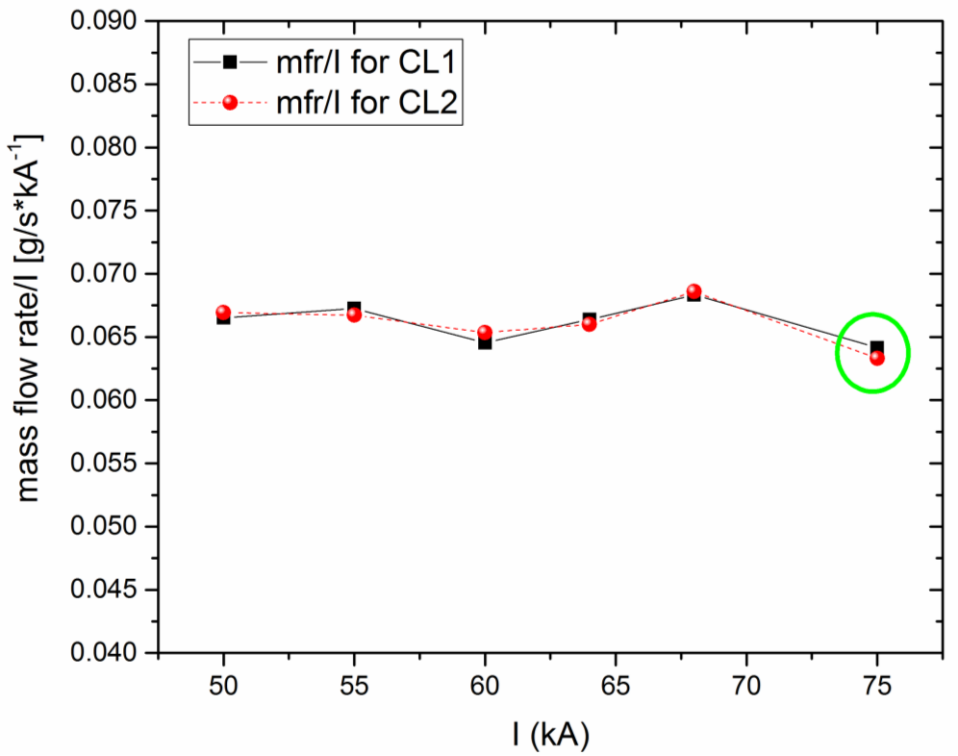

Figure 29 Mass flow rate/I as a function of the current. The 75 kA value is signed with the green circle because it did not reach steady state conditions.

4.3 Pressure drop in 50K GHe circuit in HEX

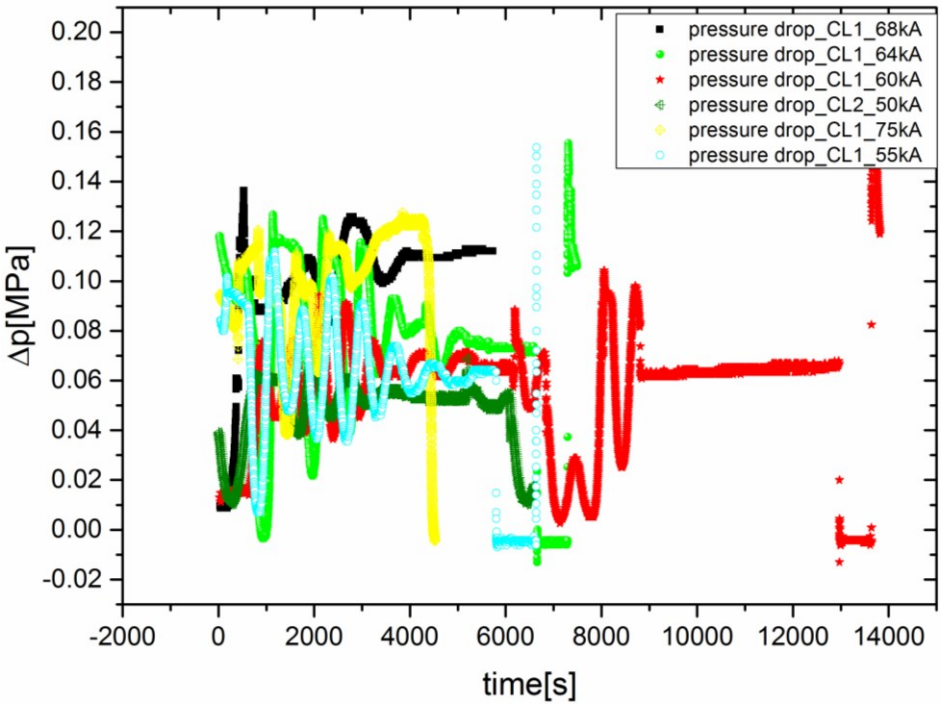

Figure 30 Pressure drops in 50 K GHe circuit in HEX for CL1 at different currents.

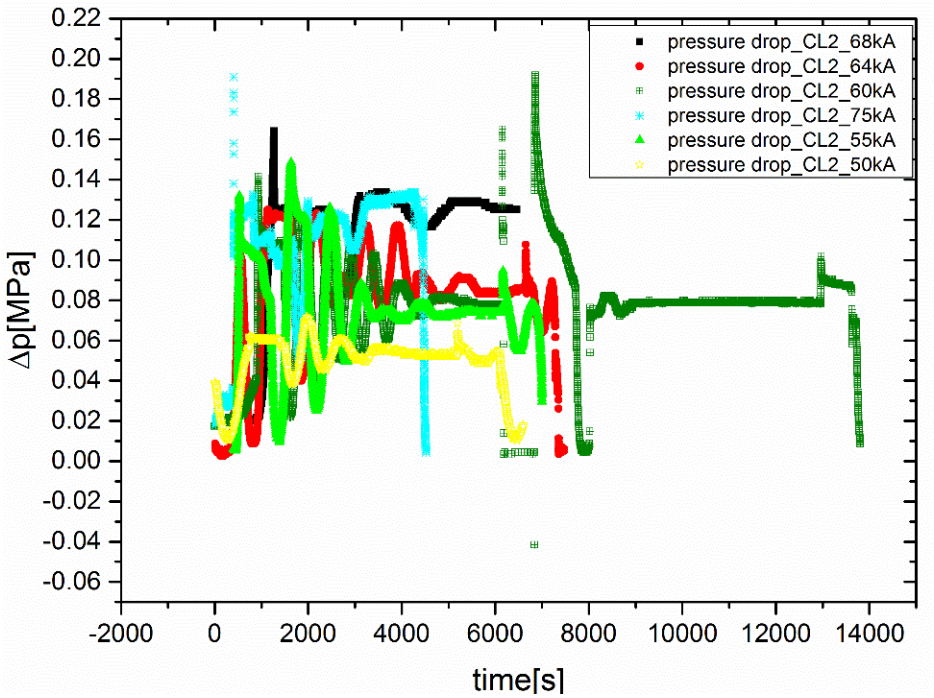

Figure 31 Pressure drops in 50 K GHe circuit in HEX for CL2 at different currents.

In Figure 30 and in Figure 31 the pressure drops in 50 K GHe circuit in HEX for both the leads at different currents are shown. They were obtained as explained in Subsection 3.2.

Due to the instability during the measurements some magnification in the range between 3000 and 6000 s (where the values seem to be more stable) has been done, see Figure 32 and Figure 33.

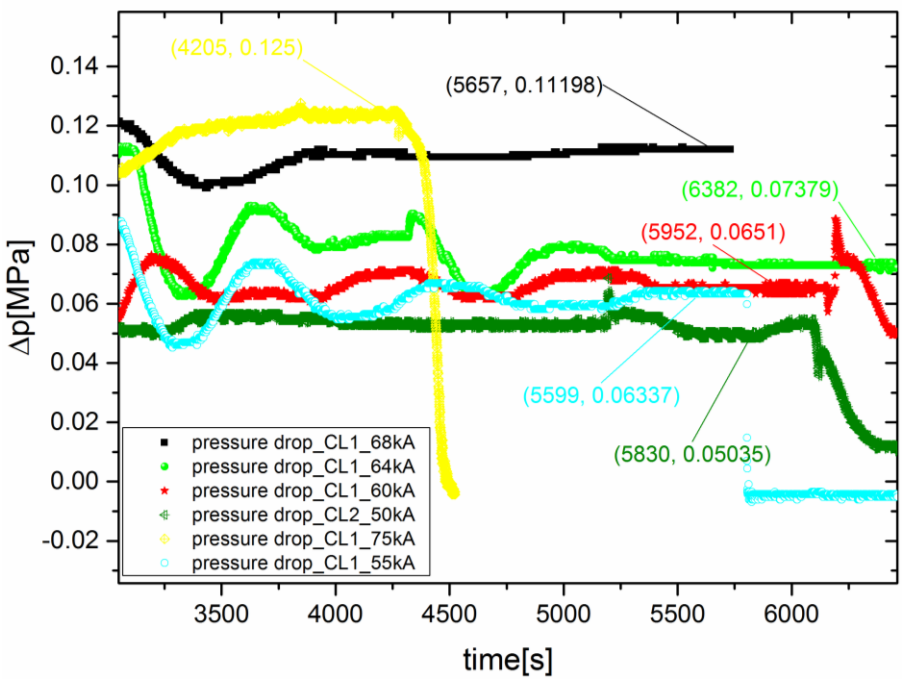

Figure 32 Pressure drops in HEX at different currents for CL1 in the stable region.

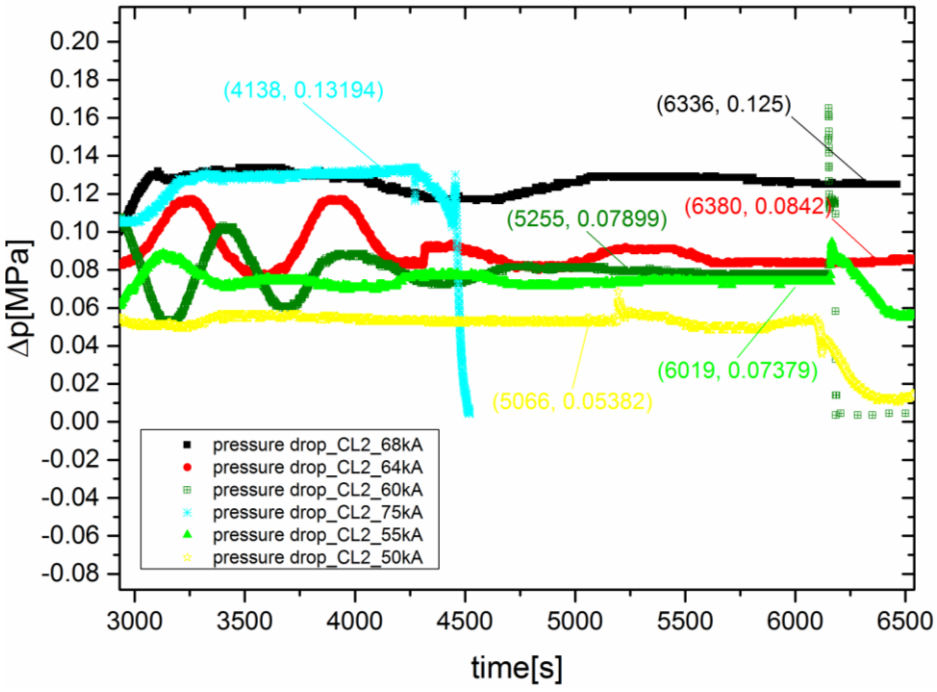

Figure 33 Pressure drops in HEX at different currents for CL2 in the stable region.

In such a way the dependence of the pressure drops as a function of current can be obtained and in Figure 34 it is shown that **the pressure drop is higher for higher current, i.e. higher flows, confirming the expected trend**.

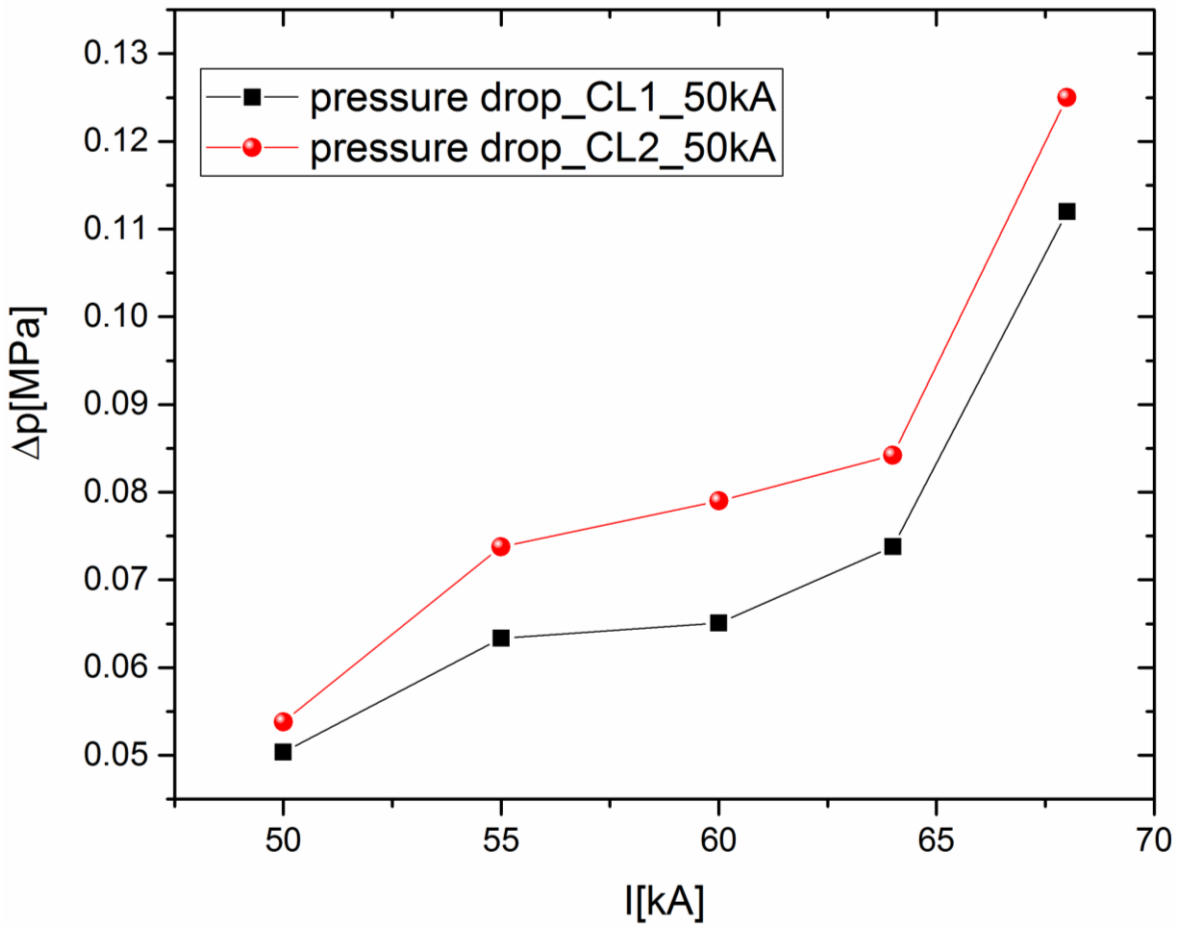

Figure 34 Pressure drop in 50 K GHe circuit in HEX as a function of the current for CL1 (black curve) and CL2 (red curve).

The pressure drop as a function of the mass flow rate and of the current is shown in Figure 35.

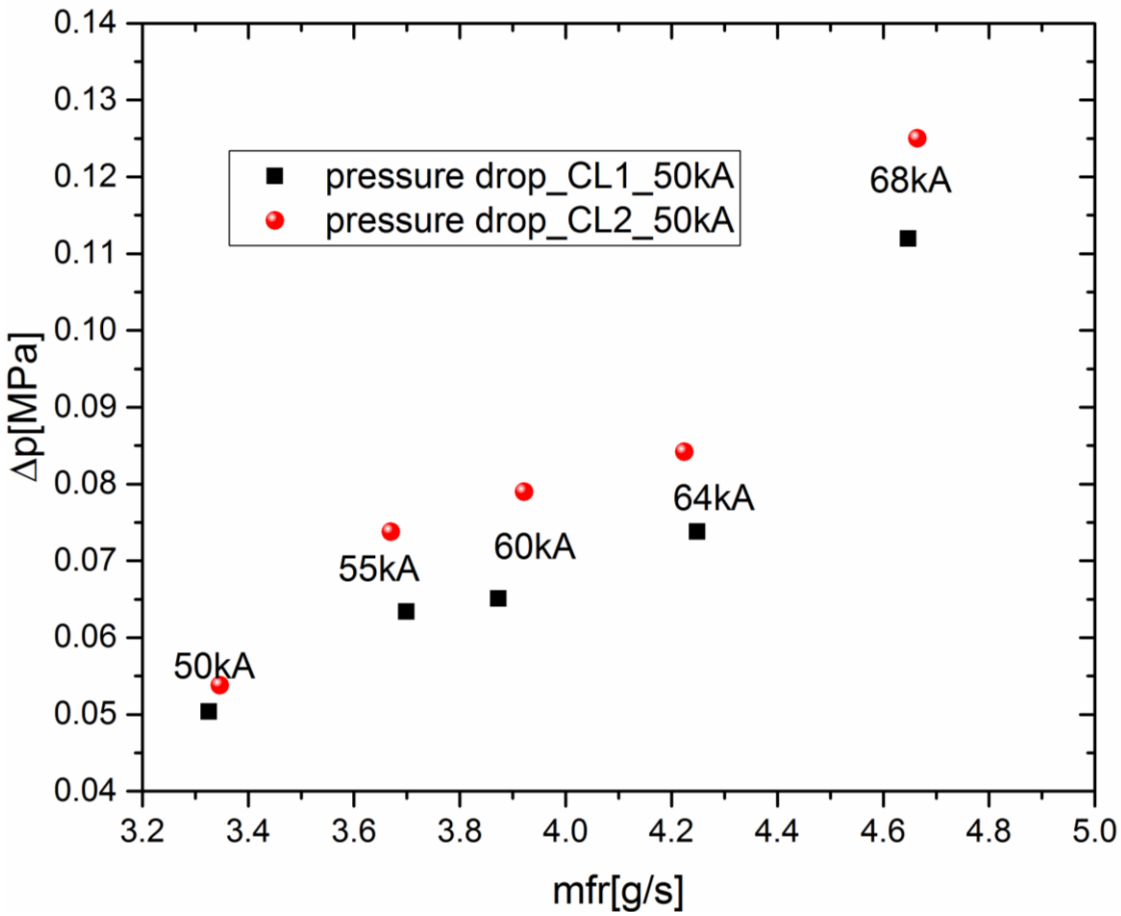

Figure 35 Pressure drop in 50 K GHe circuit in HEX as a function of the mass flow rate for CL1 (in black) and for CL2 (in red).

4.4 HTS warm end temperature

In Figure 36 and Figure 37 the HTS warm end temperature for both the leads are reported and **the values in steady state are in good agreement with the ITER requirement (65 K)**.

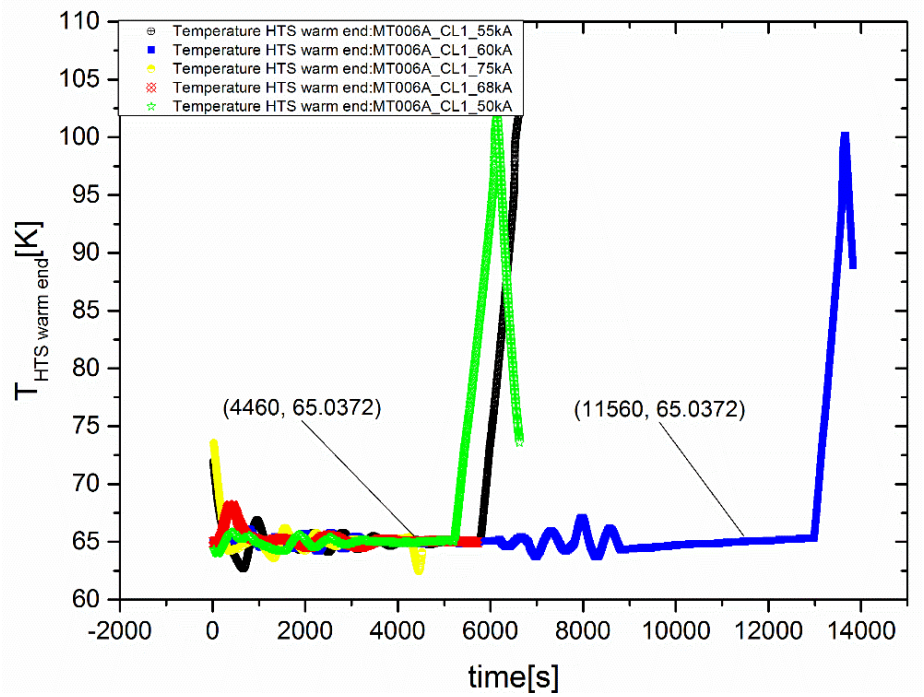

Figure 36 HTS temperature warm end for CL1.

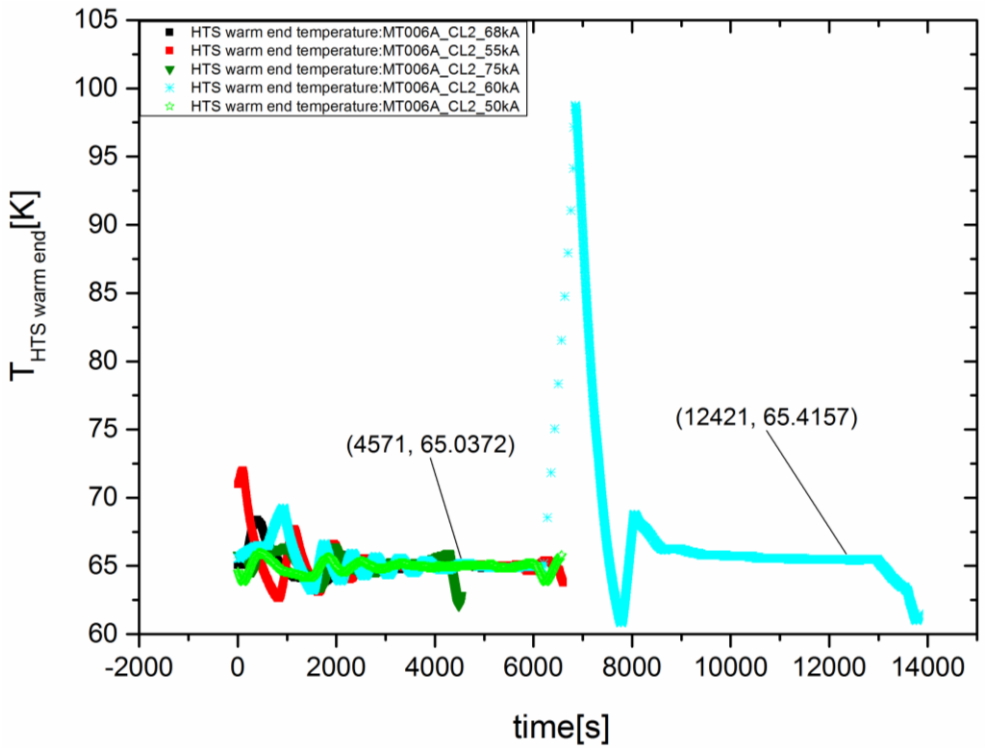

Figure 37 HTS temperature warm end for CL2.

4.5 LOFA time for under/over current

From Figure 38 to Figure 49 the minimum LOFA time is calculated for each case and for both the CLs. In Figure 50 the minimum LOFA time as a function of the current is shown: as expected for higher current the LOFA time decreases from 891 s at 50 kA to 129 s at 75 kA.

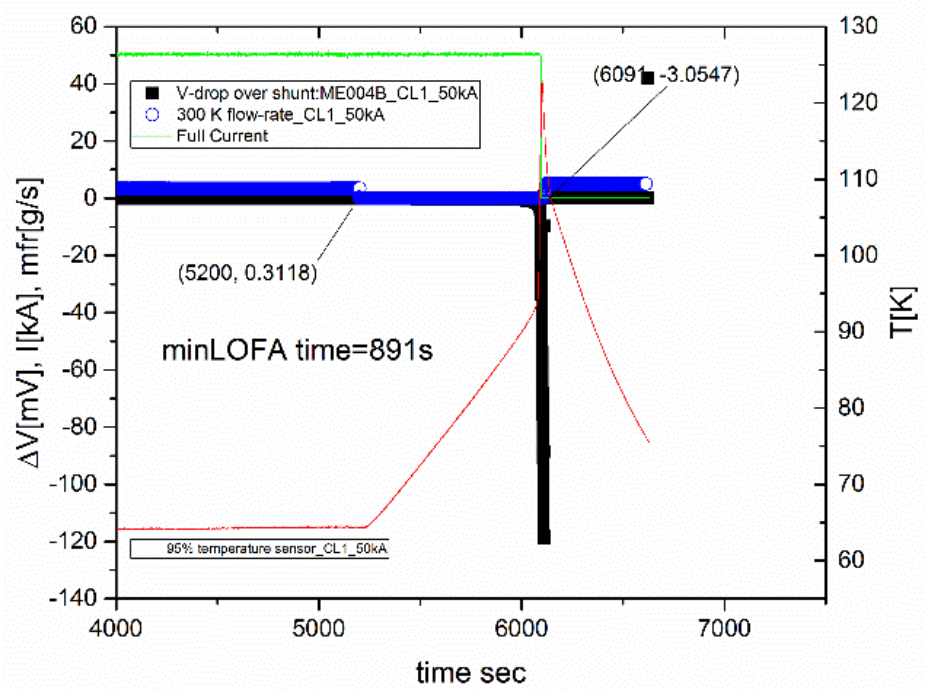

Figure 38 Minimum LOFA time for CL1 at 50 kA. Due to the lack of ME005 data set (V-drop over HTS) the ME004B data set (V-drop over shunt) have been used.

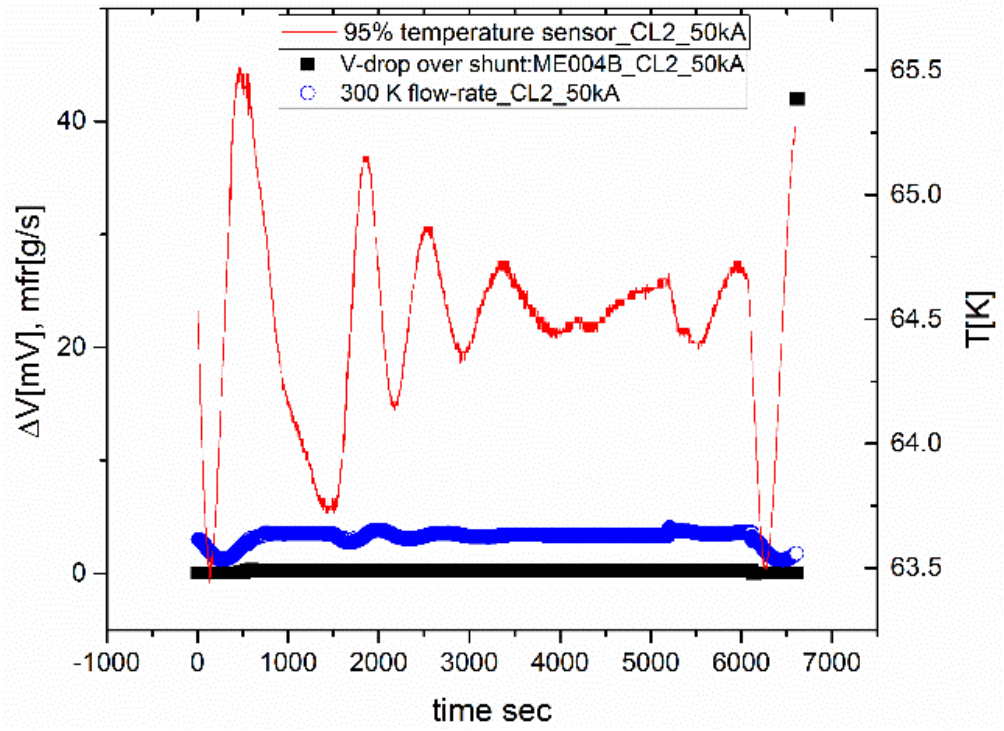

Figure 39 The minimum LOFA time for CL2 at 50 kA cannot be determined due to the fact that the mass flow rate curve is not complete. N.B. the temperature sensor MT007 (95% temperature sensor) doesn't work properly.

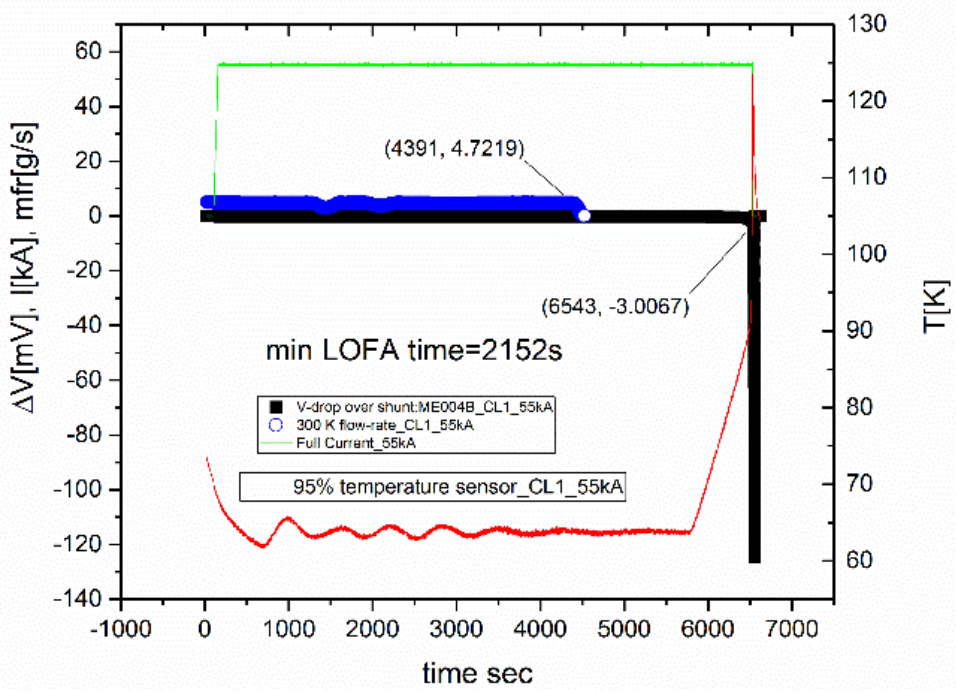

Figure 40 Minimum LOFA time for CL1 at 55 kA. The value obtained (2152s) seems to be too high probably due to the fact that the mass flow rate curve is not complete.

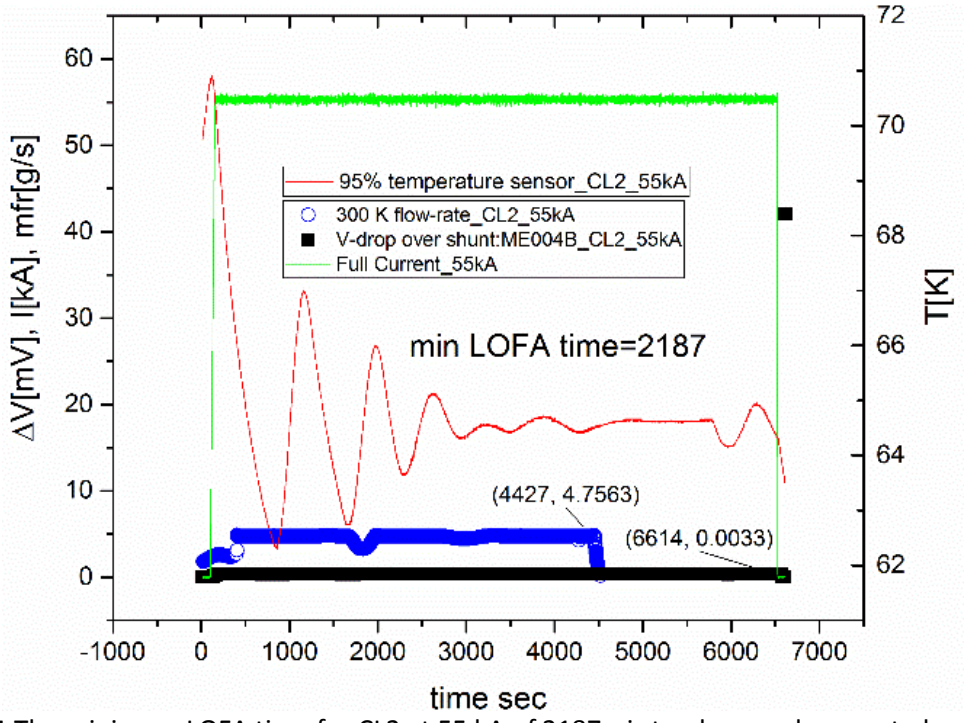

Figure 41 The minimum LOFA time for CL2 at 55 kA of 2187 s is too long and seems to be unreal probably due to the fact that the mass flow rate curve is not complete. N.B. the temperature sensor MT007 doesn't work properly.

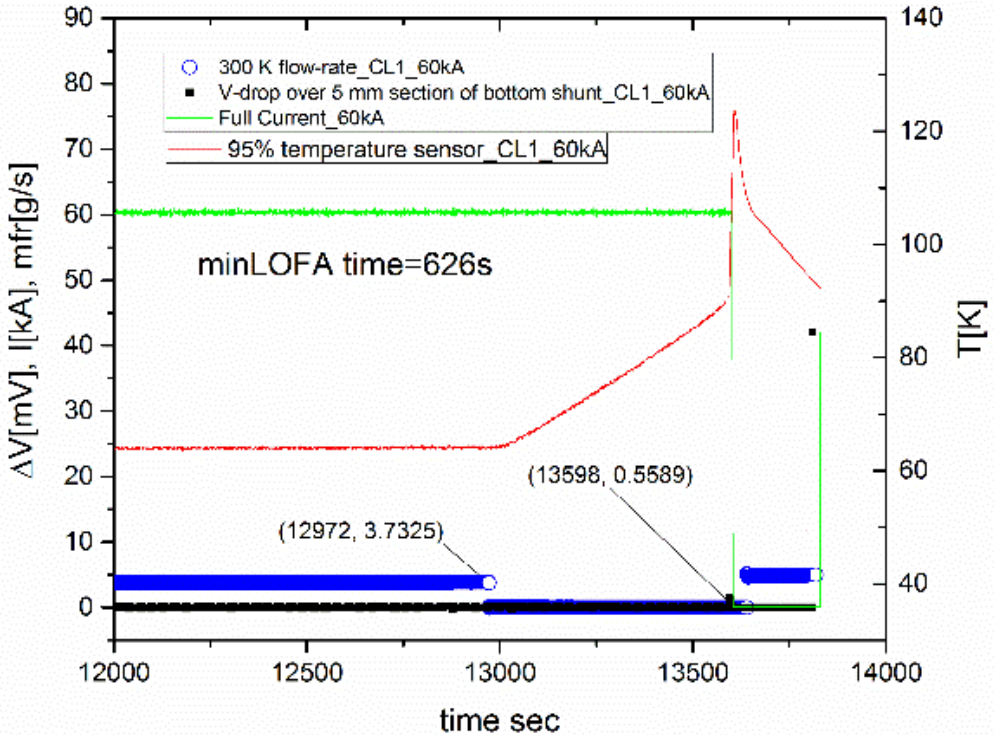

Figure 42 Minimum LOFA time for CL1 at 60 kA. Due to the lack of ME005 data set (V-drop over HTS) the ME004B data set (V-drop over shunt) have been used to determine the minimum LOFA time.

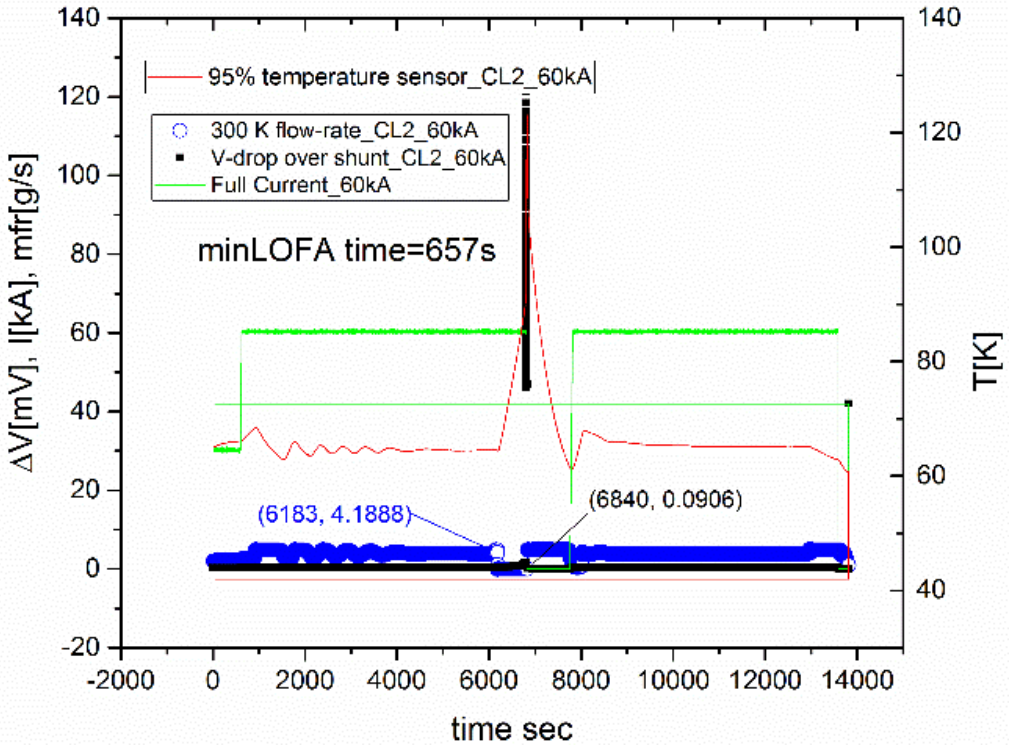

Figure 43 Minimum LOFA time for CL2 at 60 kA. Due to the lack of ME005 data set (V-drop over HTS) the ME004B data set (V-drop over shunt) have been used to determine the minimum LOFA time.

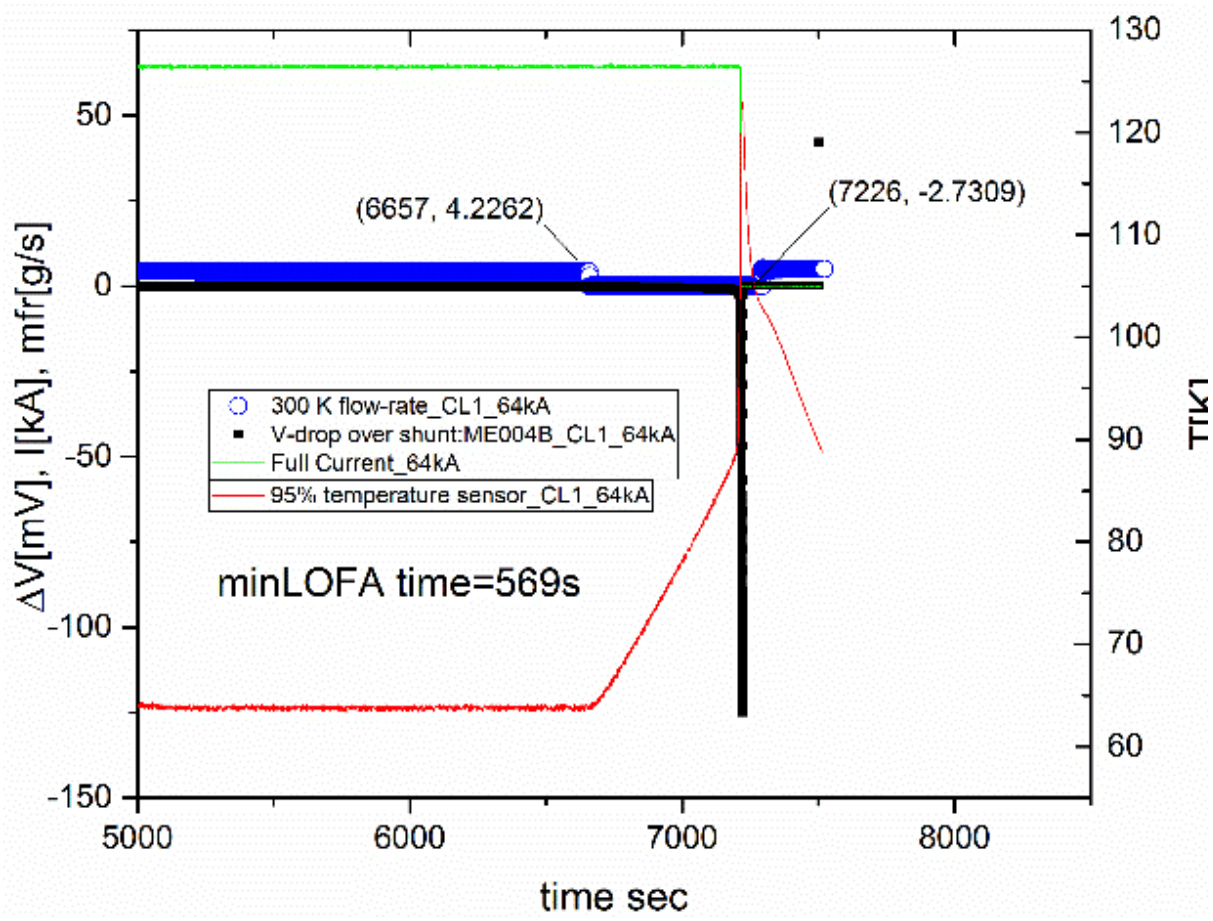

Figure 44 Minimum LOFA time for CL1 at 64 kA. Due to the lack of ME005 data set (V-drop over HTS) the ME004B data set (V-drop over shunt) have been used.

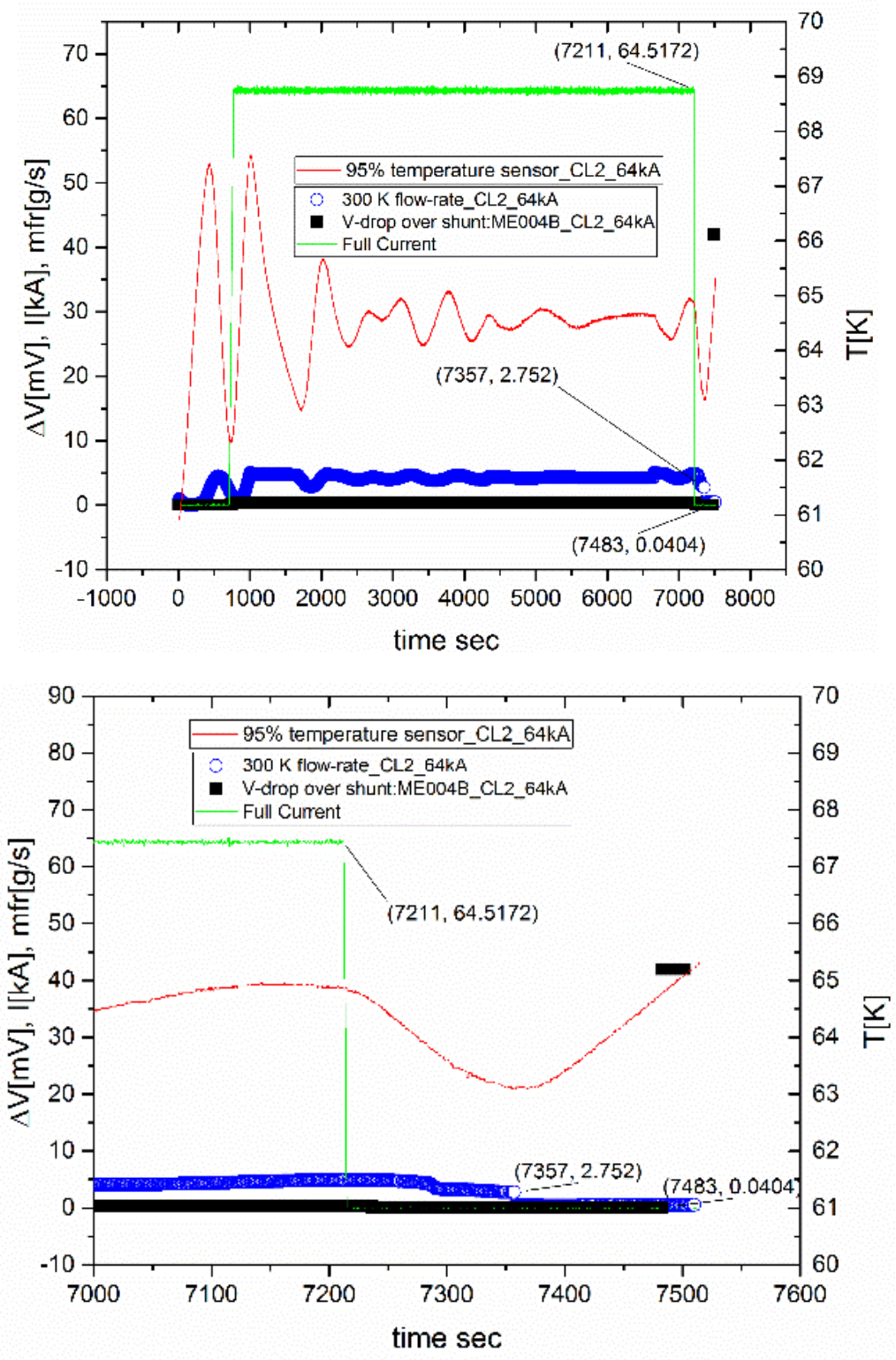

Figure 45 From these data sets it was not possible to estimate the minimum LOFA time for CL2 at 64 kA.

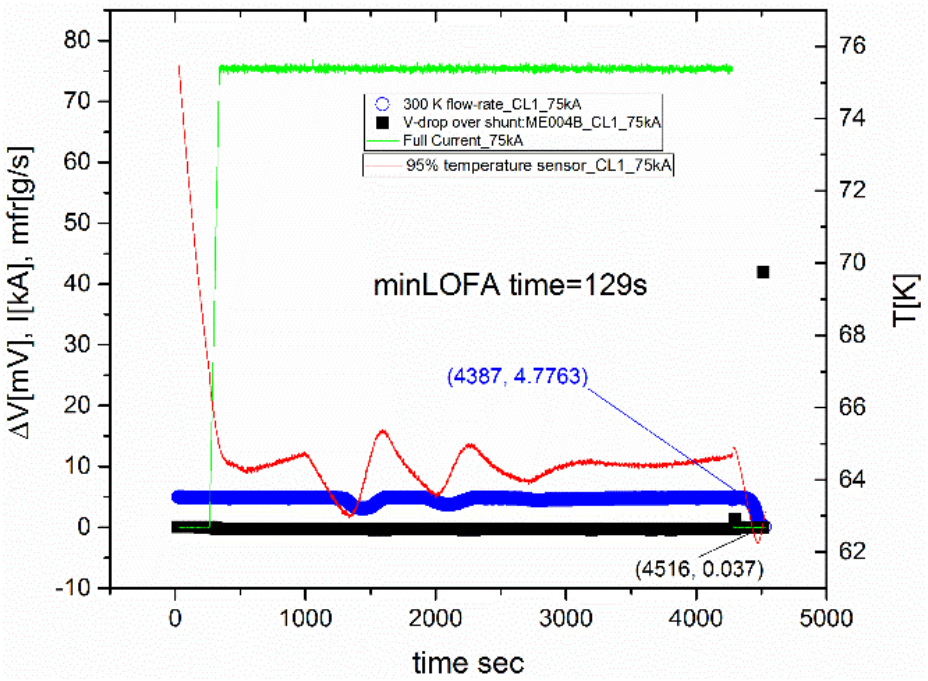

Figure 46 The minimum LOFA time for CL1 at 75 kA could be not very precise because, unfortunately, the mass flow rate curve is not complete due to the limitation imposed by the flow-controller. N.B. the temperature sensor MT007 doesn't work properly.

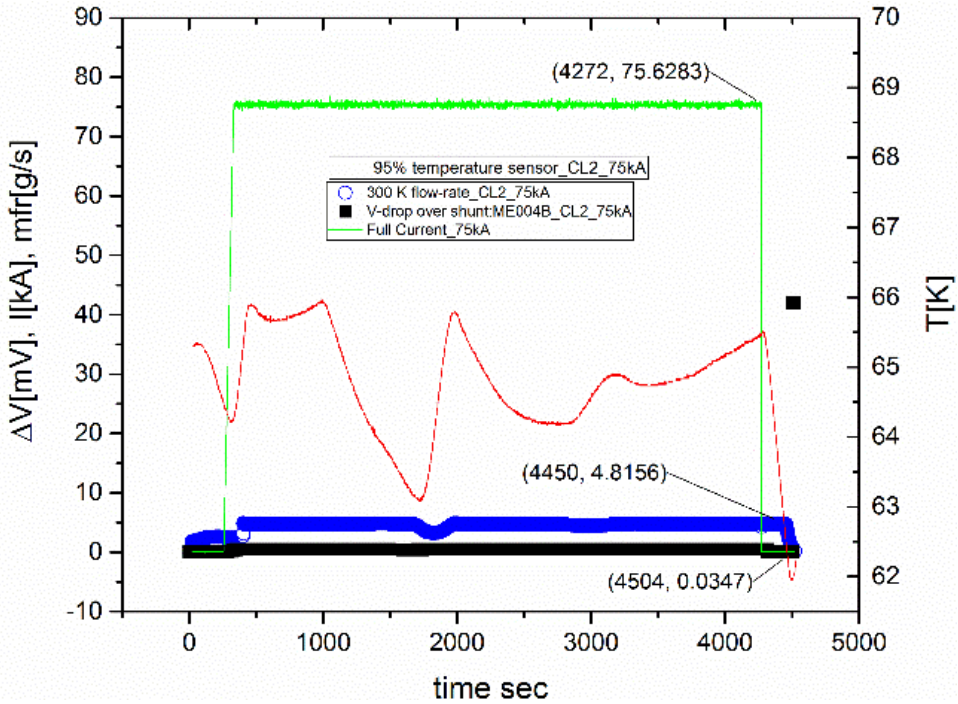

Figure 47 The minimum LOFA time for CL2 at 75 kA could be not very precise because, unfortunately, the mass flow rate curve is not complete. N.B. the temperature sensor MT007 doesn't work properly.

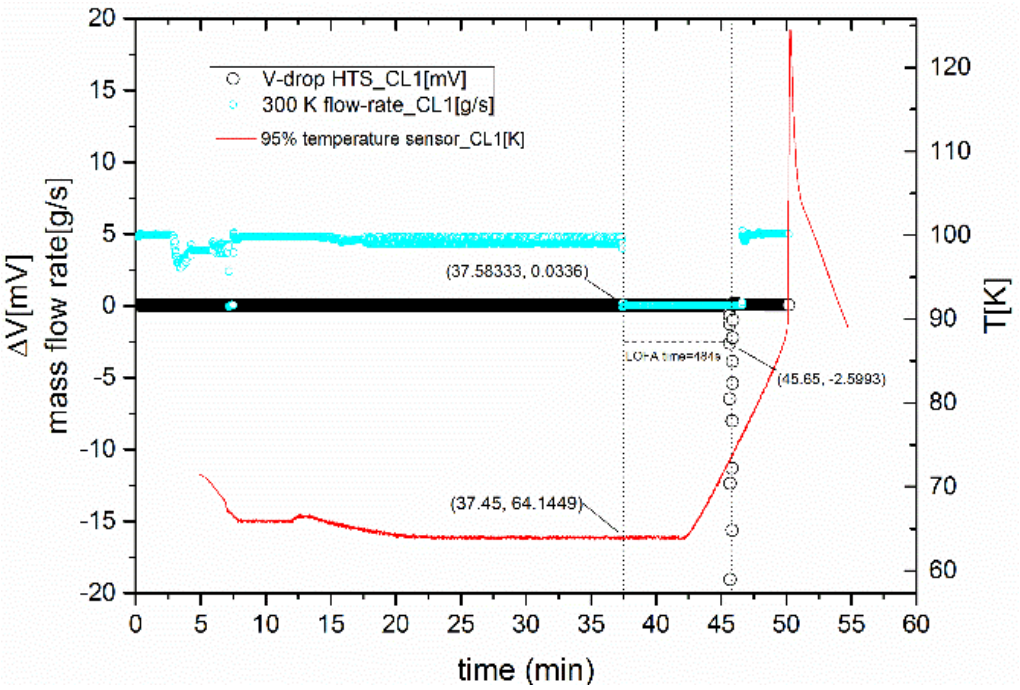

Figure 48 Minimum LOFA time for CL1 at nominal condition (68 kA).

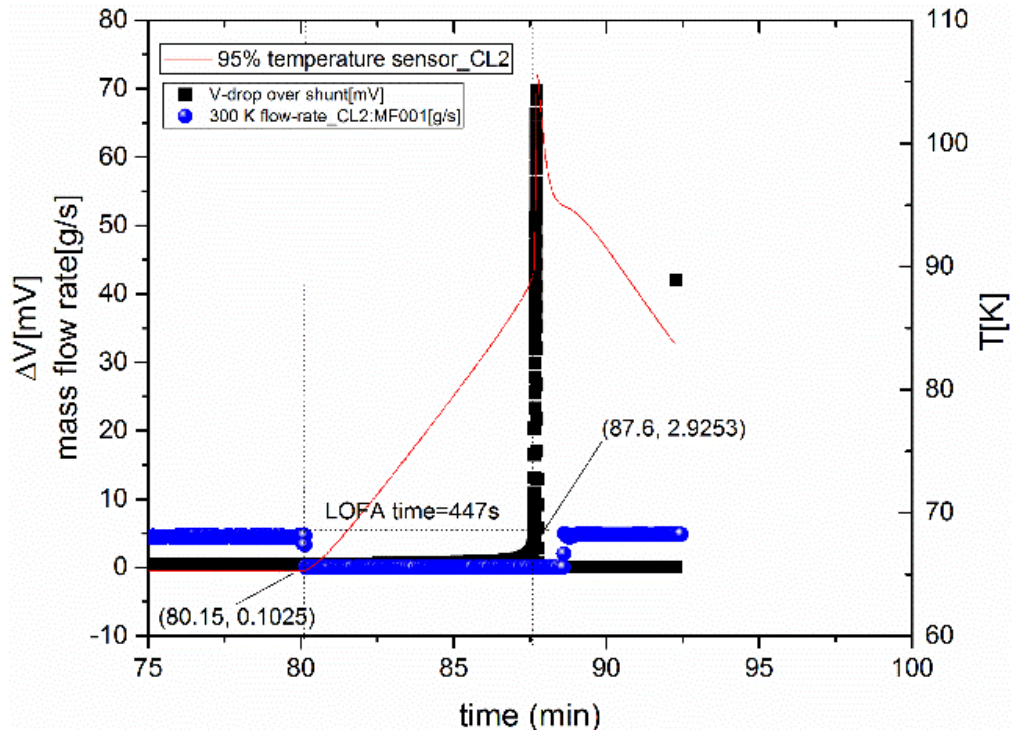

Figure 49 Minimum LOFA time for CL2 at nominal condition (68 kA).

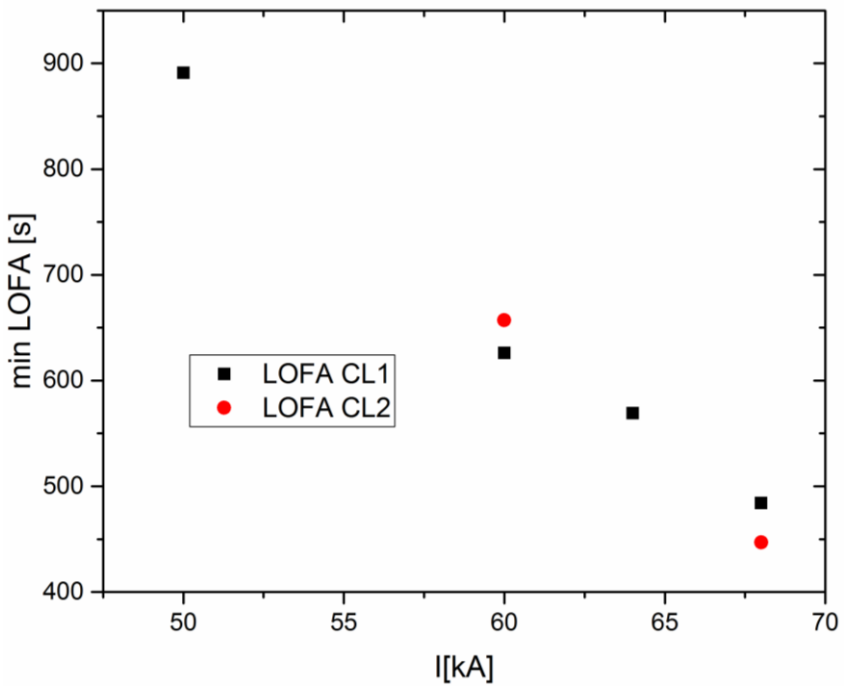

Figure 50 Minimum LOFA time as a function of the current for both the current leads (CL1 in black and CL2 in red).

4.6 Current

In Figure 51 the all currents in the different under/over current cases for CL1 and CL2 are represented.

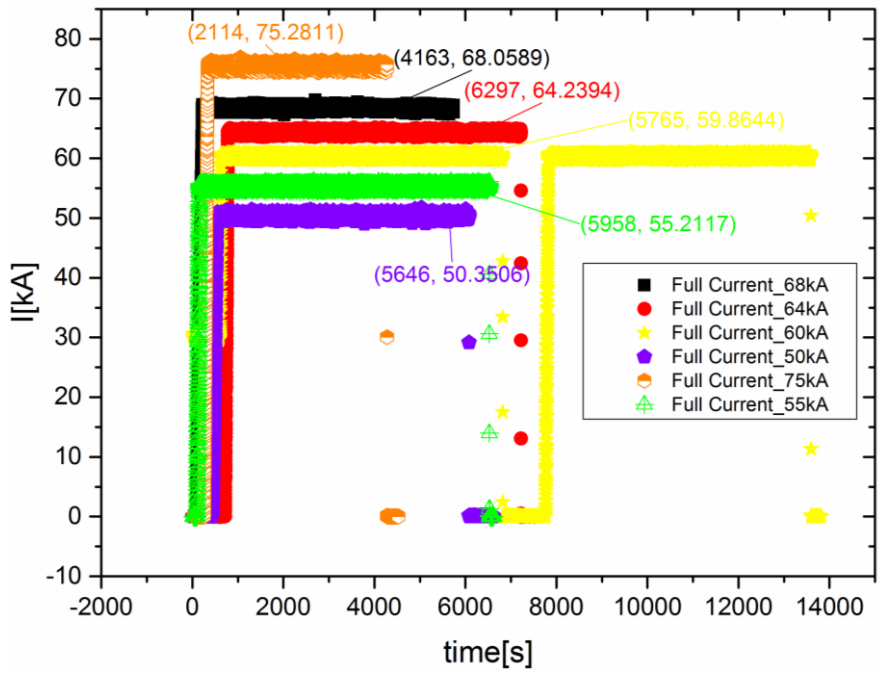

Figure 51 Current for the under/over current cases.

4.7 Summary under/over current analysis

In Figure 52 the voltage drops at different currents is plotted as a function of the mass flow rate for both the CLs.

As expected, for currents below the nominal value (i.e. 68 kA) the mass flow rate is lower than the 4.65 g/s found in Section 3.1 while for currents above the nominal value the mass flow rate is higher.

N.B. The values of the voltage drops and of the mass flow rates are taken at the same time for each case.

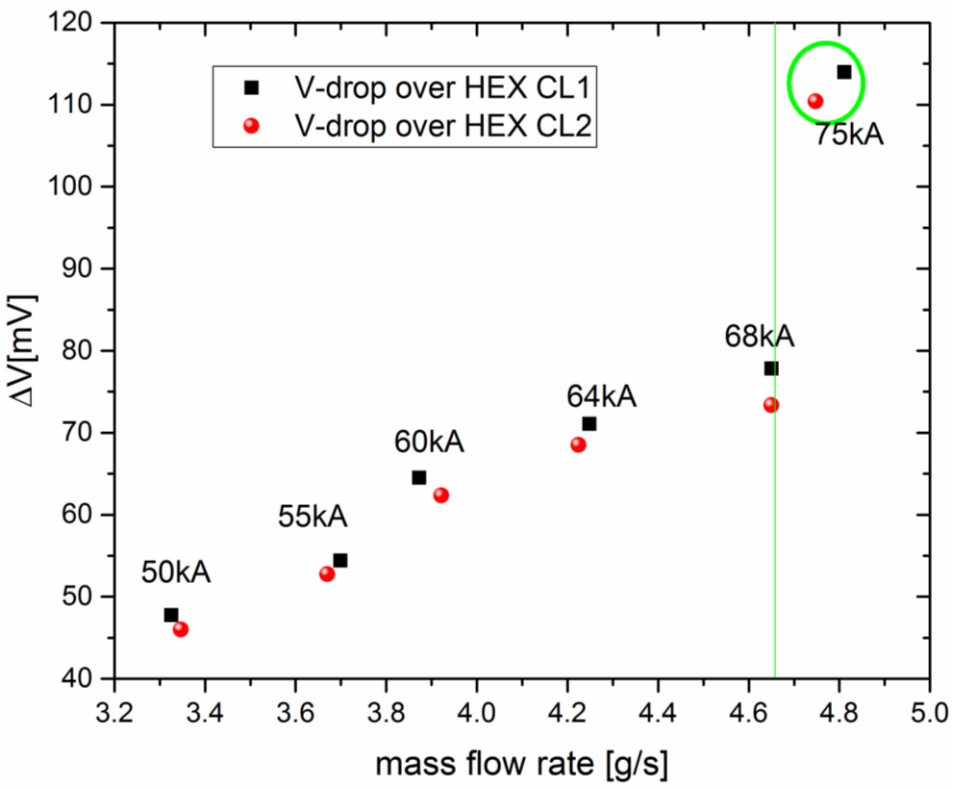

Figure 52 Voltage drop over HEX as a function of mass flow rate and current. The 75 kA value is signed with the green circle because it did not reach steady state conditions.

In Figure 53 the voltage drops over HEX as function of the current is shown.

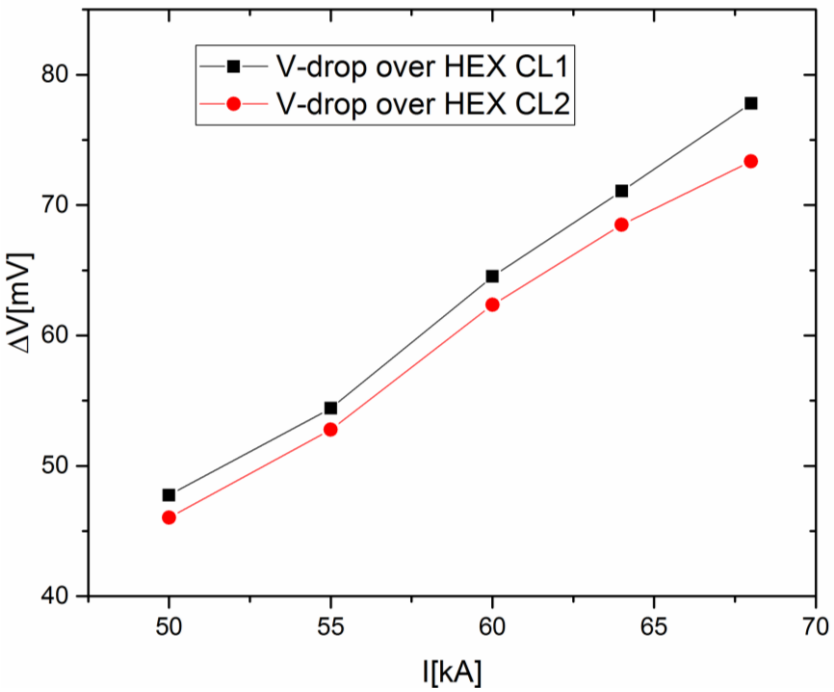

Figure 53 Voltage drop over HEX as a function of the current for both the current leads (for CL1 in red and CL2 in black).

4 STAND BY (CASES 2.2 and 3.2)

In this section the main results on the stand by tests are presented and discussed. As reported in Figure 1 these tests were performed on the 5th and on the 9th of July 2015 for CL2 and CL1 respectively and the technical details of the data acquisition are reported in ref. [1].

4.1 Current

In Figure 54 the full current as a function of time in the stand by regime for both the leads is shown.

As shown in Figure 55, the small fluctuation of the full current in the stand-by mode (about +/- 0.15 kA) can be considered negligible if compared with that one in the steady state regime.

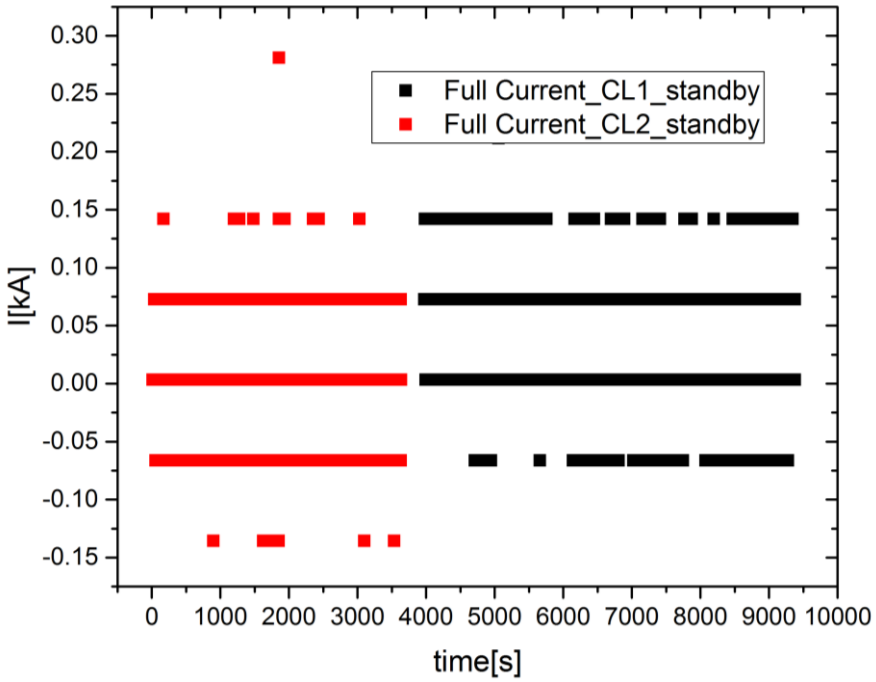

Figure 54 Full current in the stand by regime for CL1 (in black) and for CL2 (in red).

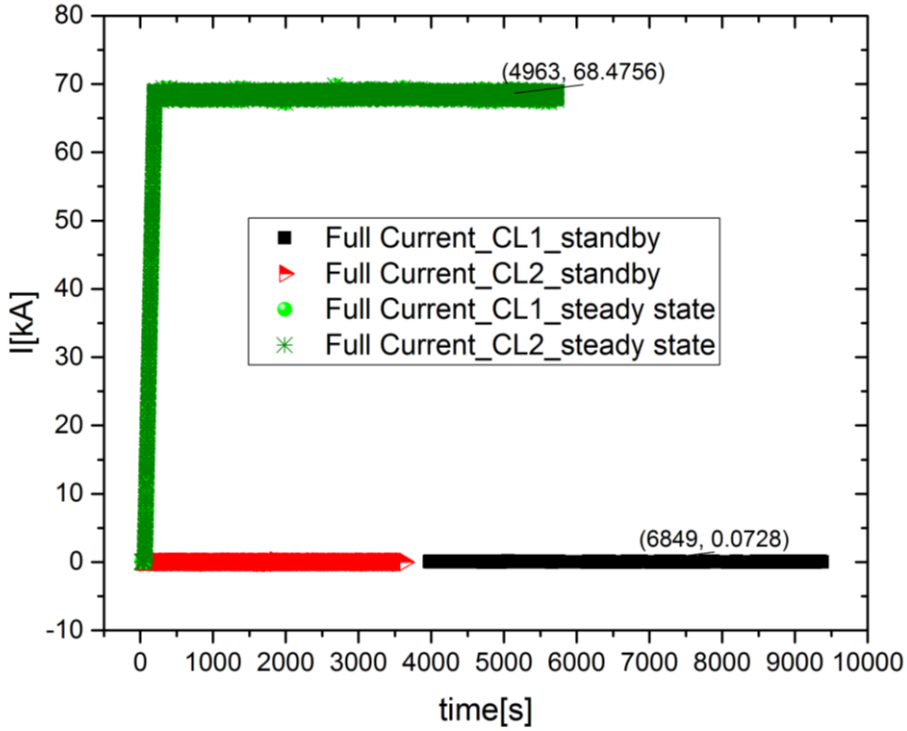

Figure 55 Comparison full current in stand by and in the steady state regime.

4.2 Mass flow rate

In Figure 56 the measurements of the mass flow rate over HEX in stand by regime for both the leads are shown.

Some instability issues occurred during the mass flow rate measurement in CL2 and thus it was not possible to estimate its value; on the other hand it was found for CL1 that in stand by mode **the mass flow rate decreases by a factor 3.43 g/s with respect to the value found in the steady state regime** (i.e. the mass flow rate in stand by state is 1.22 g/s).

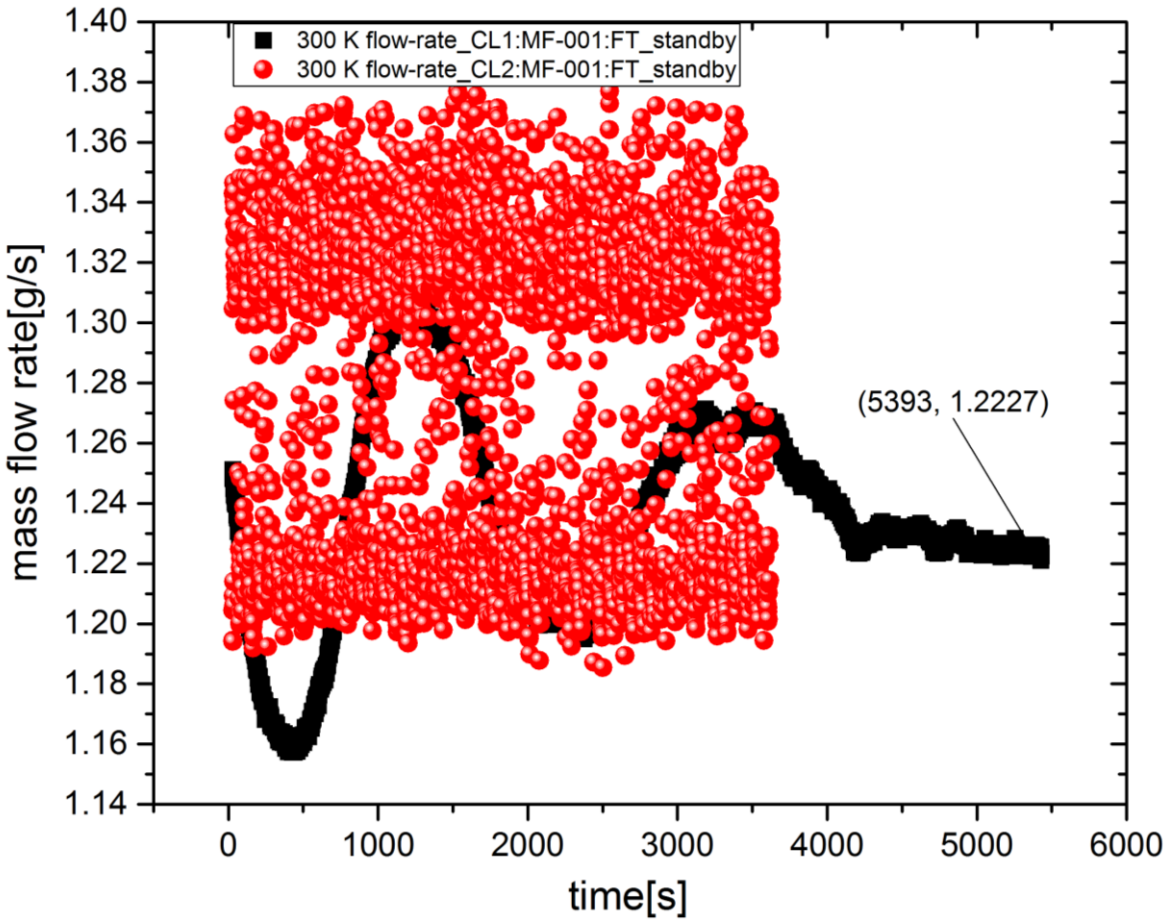

Figure 56 Mass flow rate in HEX for CL1 (black curve) and CL2 (red curve) in stand by regime (case 3.2).

4.3 Pressure drops over HEX

In Figure 57 the measurements of pressure drop at room temperature (300 K) and at 50 K are shown for both the CLs. Also in this case the result on CL2 seems to reflect instability during the data acquisition.

To obtain the pressure drop over CL1 HEX in stand-by mode the 50 K supply pressure was subtracted to the 300 K exit pressure and the result is shown in Figure 58.

Comparing the pressure drops over CL1 HEX in stand by and steady state mode, see Figure 59, a **difference of 0.11 MPa has been found, that means, in steady state regime the pressure drop over HEX is about two times that in stand-by**.

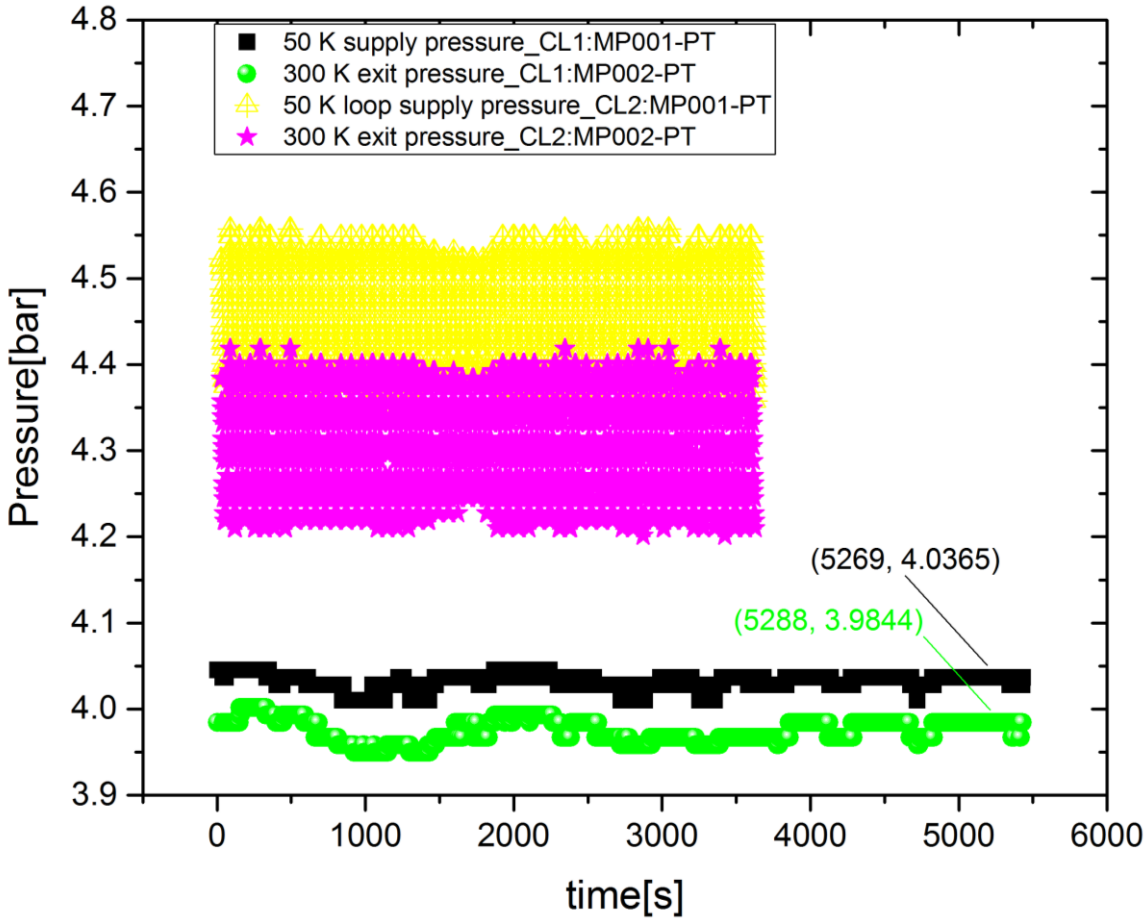

Figure 57 Inlet and exit pressure measurements at 300 K and 50 K in stand-by mode for both the CLs.

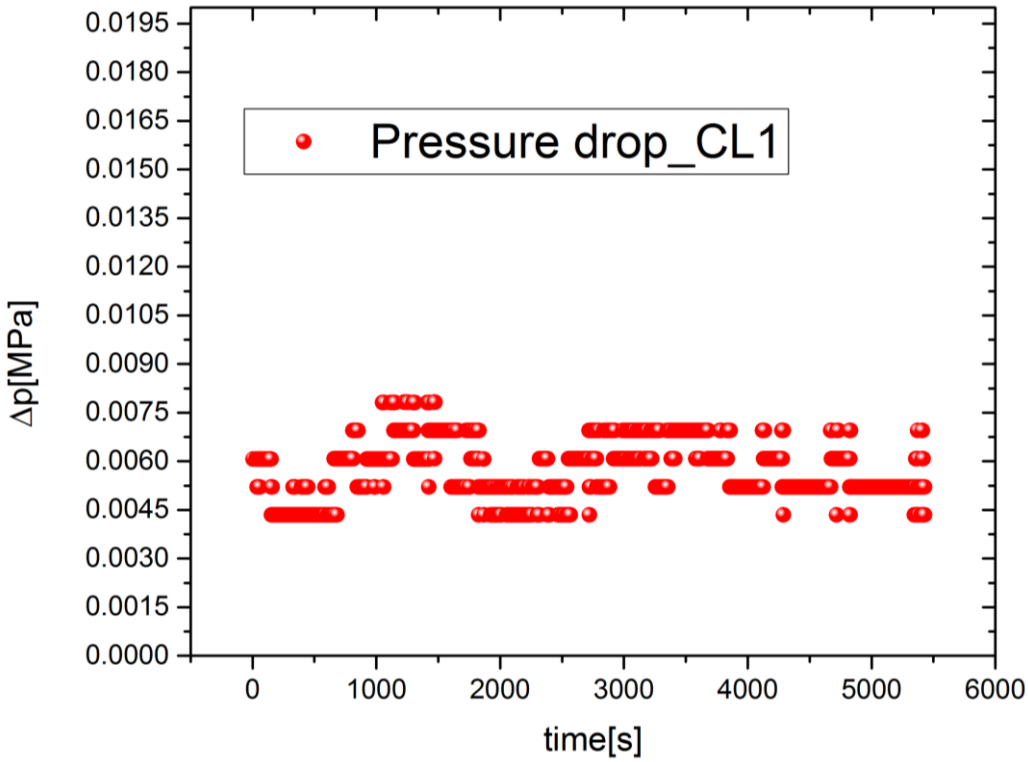

Figure 58 Pressure drop in 50 K circuit in HEX for CL1 in stand-by mode.

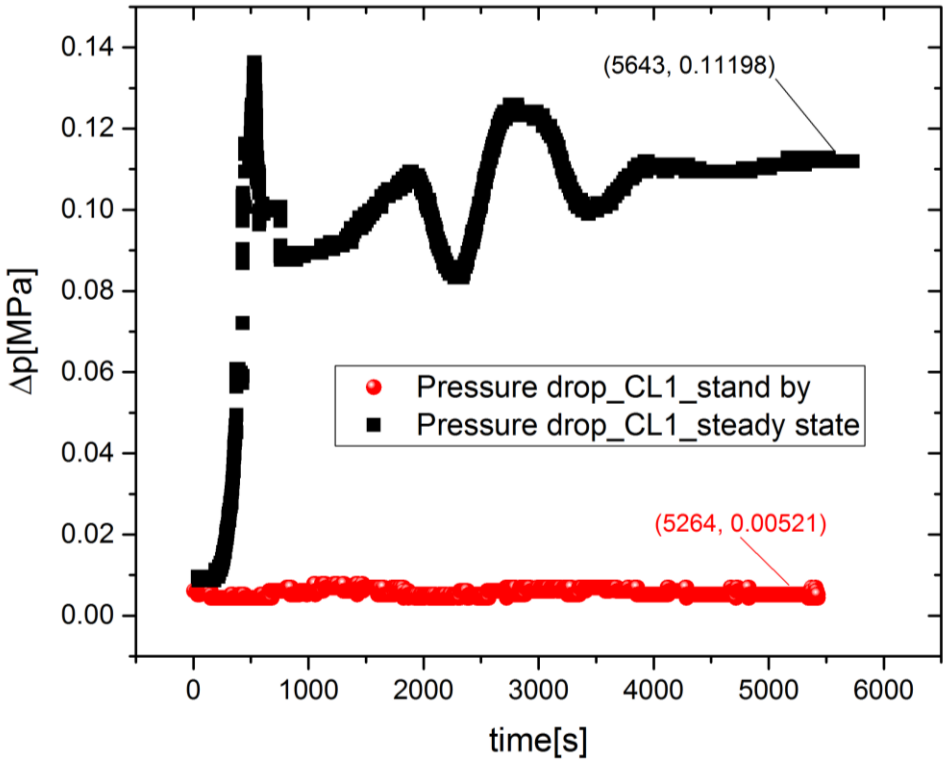

Figure 59 Comparison of pressure drops in 50 K circuit in CL1 HEX for the stand by and steady state regimes.

4.4 HTS warm end temperature

As shown in Figure 60 in stand by regime the HTS warm end for both the leads is 80 K, i.e. 15.1 K higher than the same temperature measured during the steady state tests.

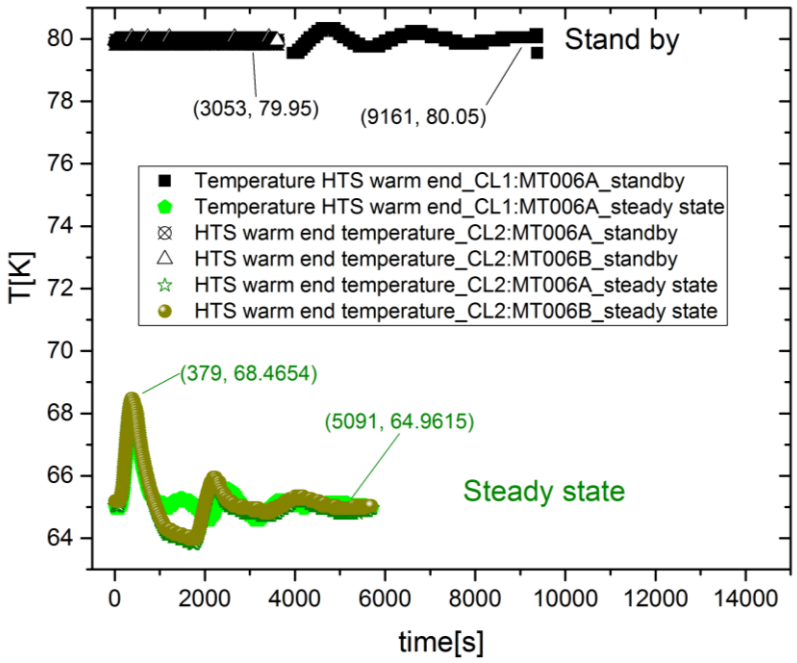

Figure 60 Comparison of HTS warm temperature in both the CLs between the stand by and the steady state regime.

5 OVER COOLING (CASES 5.10, 5.11)

In this section the main results on the over cooling tests are presented and discussed. As reported in Figure 1 these tests were performed on the 11th of July 2015 for both the leads (CL1 and CL2) and the technical details of the data acquisition are reported in ref. [1].

In Table 6 the main characteristics of this two overcooling cases (5.10 and 5.11) are reported.

Table 6 *Main characteristics of the overcooling tests.*

CASE	HEX inlet T (K)	HTS top T (K)	HEX inlet pressure (bara)	5K inlet pressure (bara)	5K inlet T (K)
5.10	45	60	4	>3	<5
5.11	45	65	4	>3	<5

5.1 Pressure drop in 50K GHe circuit in HEX

In Figure 61 the measurements of pressure at 300 K and 50 K are plotted for both the leads in the two overcooling cases under study.

As shown in Figure 62, subtracting to the 50 K pressure the 300 K pressure, the pressure drops in the 50 K circuit in HEX have been found to be lower than the ITER requirements (see Table 4 for comparison).

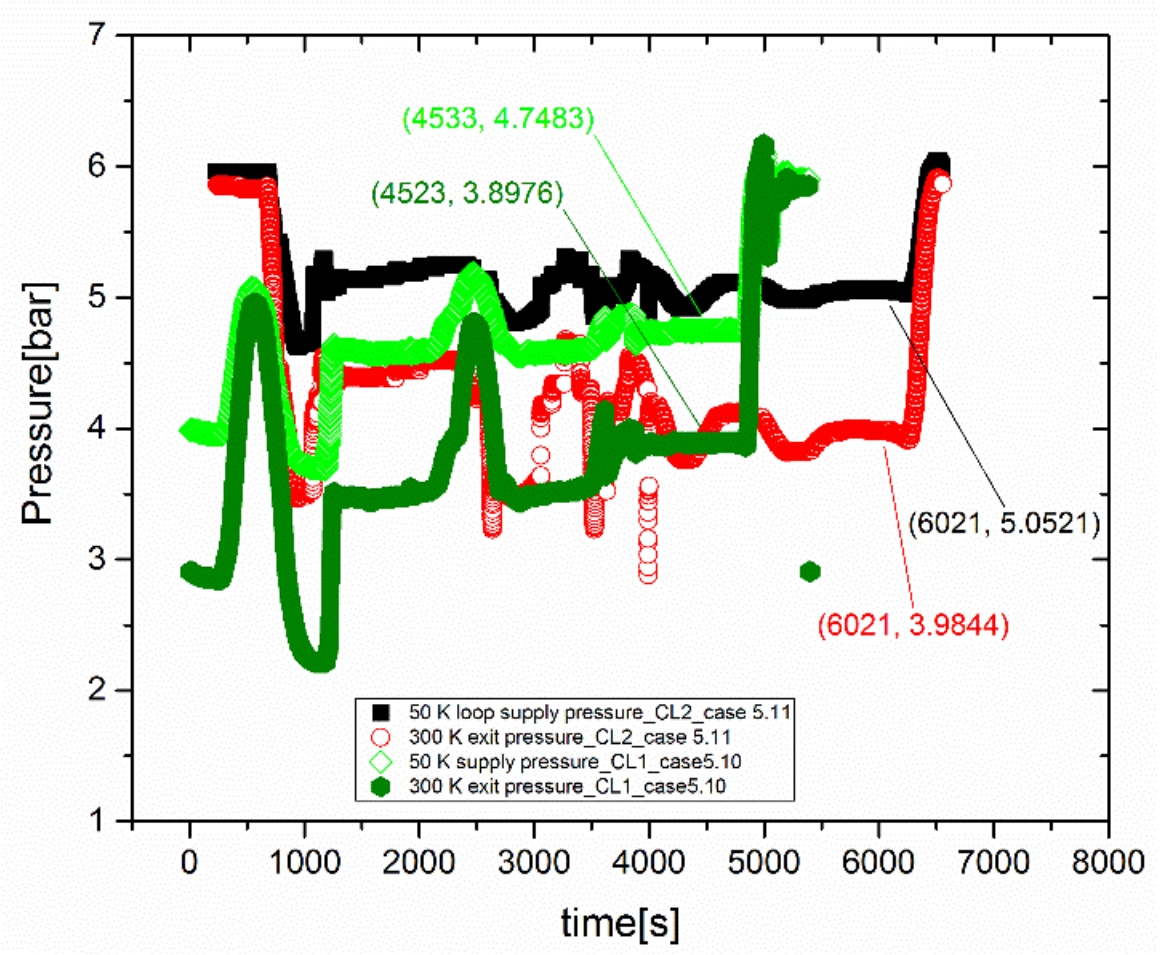

Figure 61 Pressure measurements for both the leads in the two overcooling cases (5.10 and 5.11).

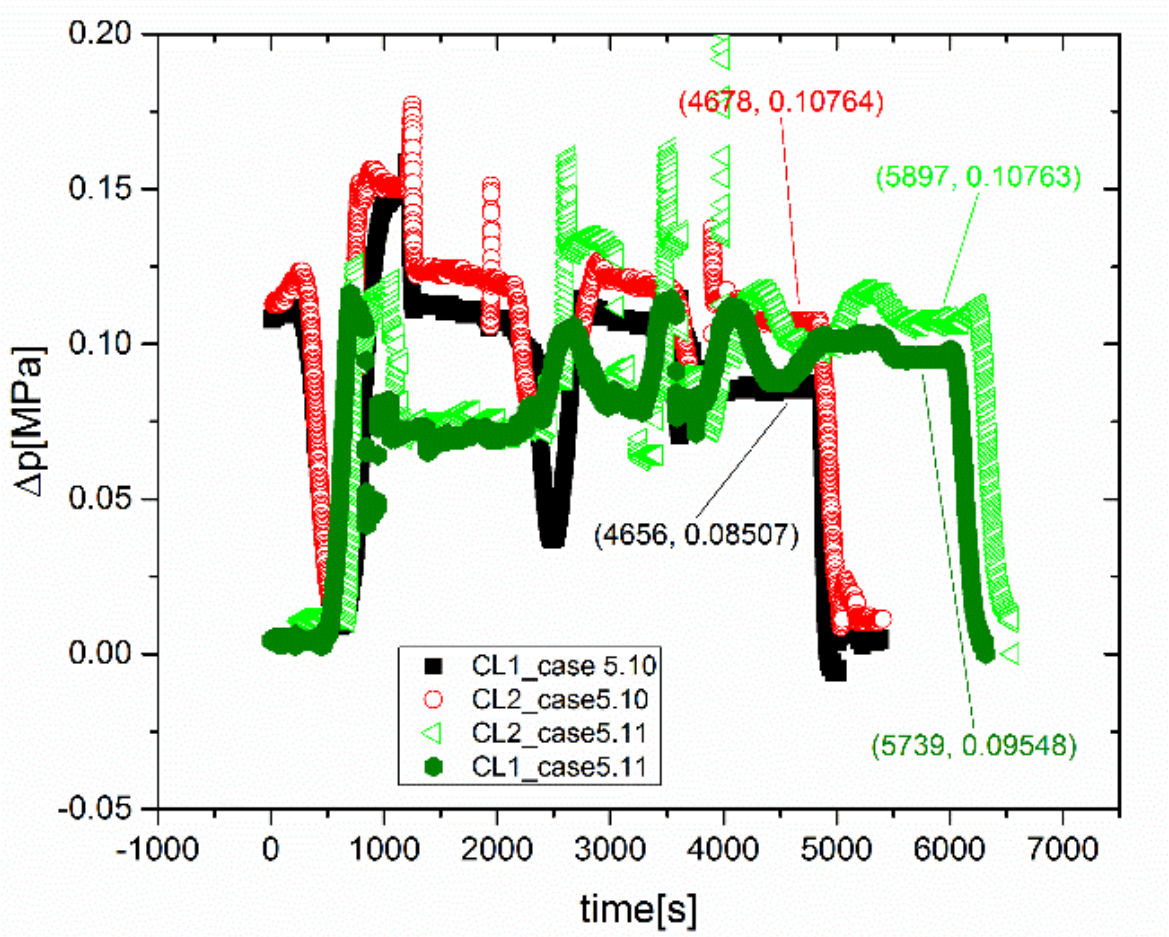

Figure 62 Pressure drops in 50K circuit in HEX for both the overcooling cases and for both the leads.

5.2 HTS warm end temperature and mass flow rate in HEX

The HTS warm end and the mass flow rate in the HEX for both the leads are shown in Figure 63 for the case 5.10 and in Figure 64 for the case 5.11.

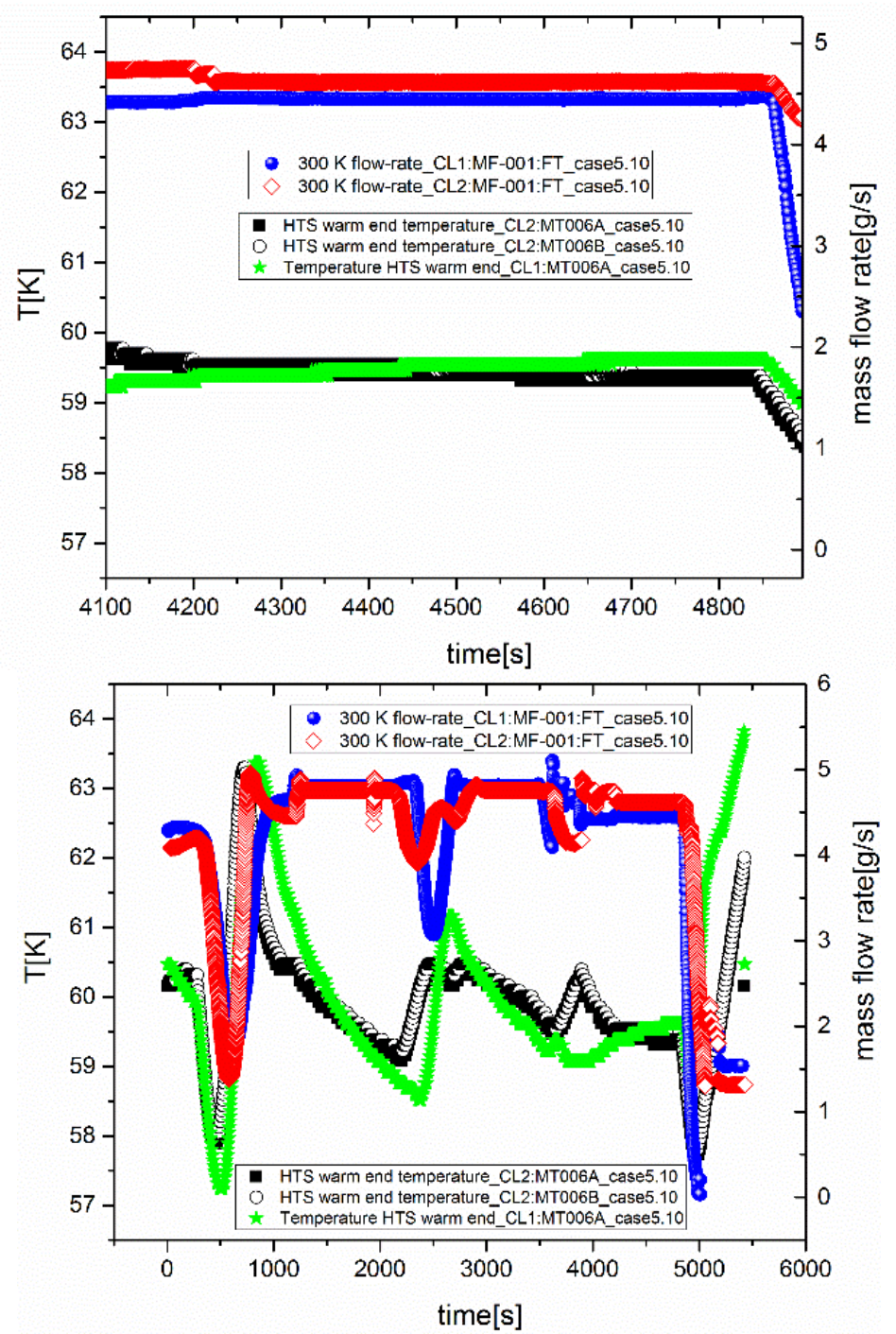

Figure 63 HTS warm end and mass flow rate for both the leads in the case 5.10. Magnification of the stable region on the bottom.

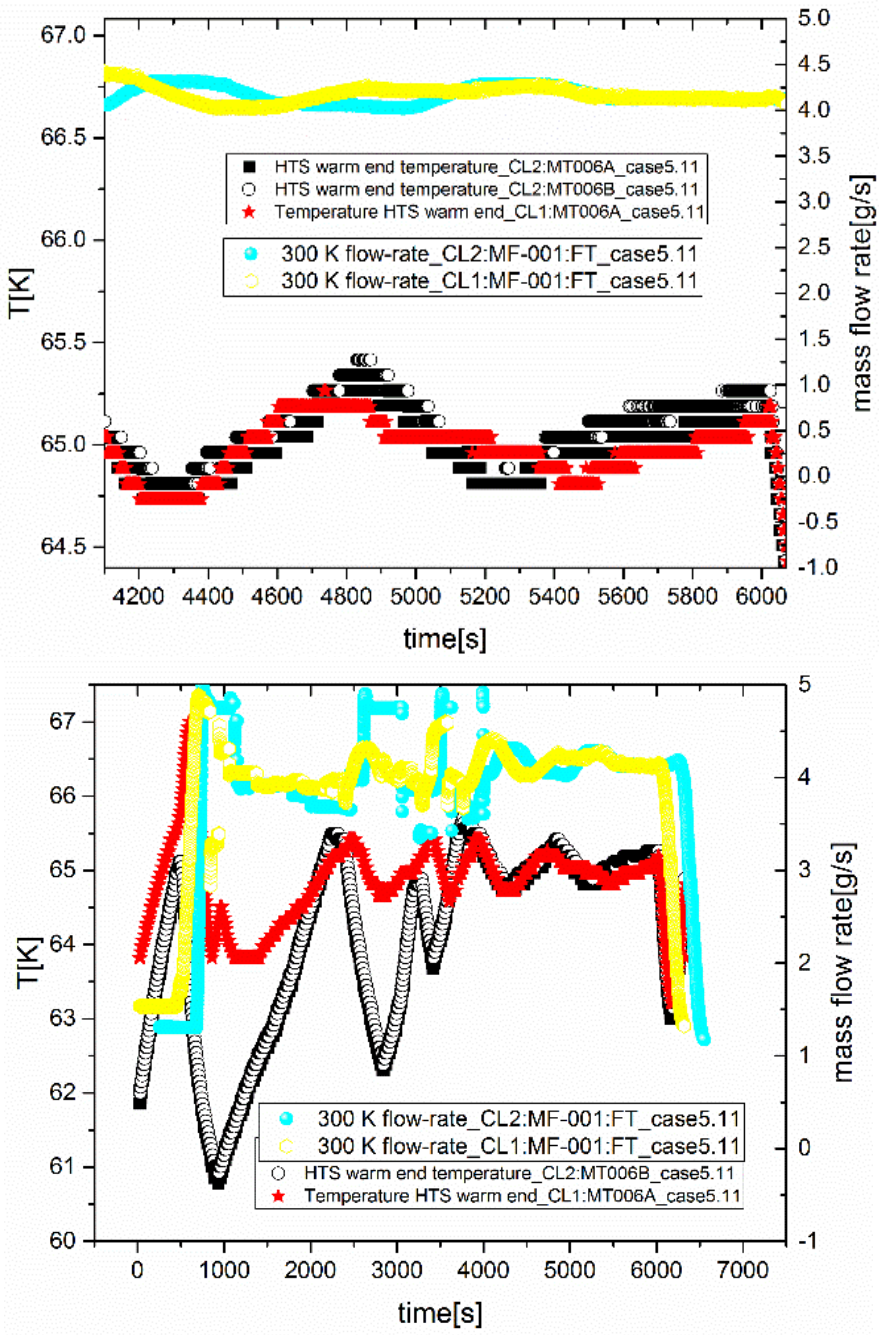

Figure 64 HTS warm end and mass flow rate for both the leads in the case 5.11. Magnification of the stable region on the bottom.

5.3 Voltage drop over HEX only case 5.11

To compare the effect of the overcooling on the voltage drop as well as on the mass flow rate the case 5.11 has been studied (unfortunately no data of voltage drop are available for the case 5.10).

Taking into account at the same time the voltage drop and the mass flow rate values from Figure 65 and Figure 66 then the voltage drops as a function of the mass flow rate for the case 5.11 is compared to the nominal value as shown in Figure 67.

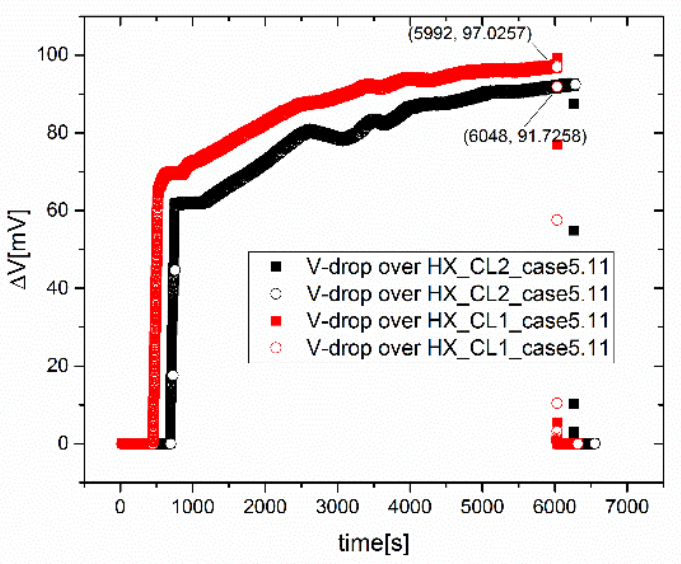

Figure 65 Voltage drop for the case 5.11.

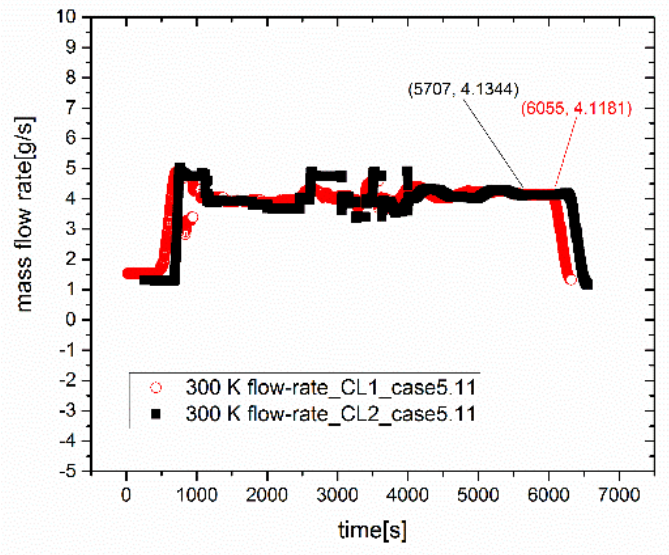

Figure 66 Mass flow rate for the case 5.11.

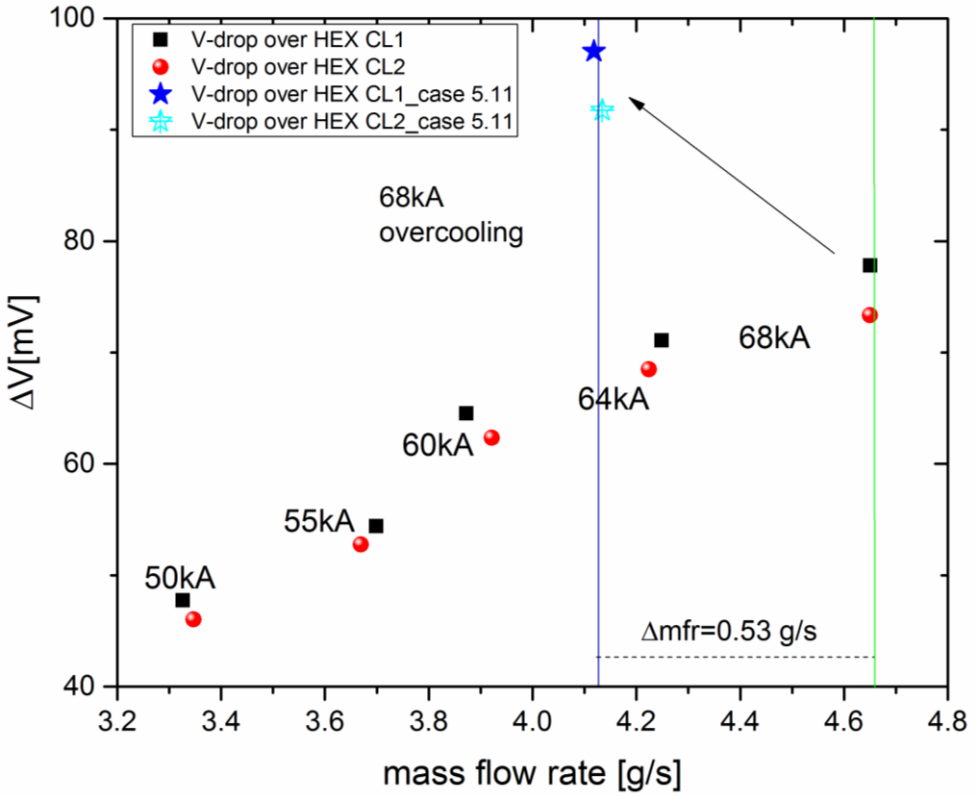

Figure 67 Voltage drop as a function of the mass flow rate for the case 5.11 and comparison with the nominal value (i.e. 68kA).

6 TEMPERATURE PROFILE

In this section the comparison between the simulated temperature profile and the measurements on TF prototype will be reported.

The 3D FE thermo-hydraulic and electrical model described in reference [4] has been used to get the temperature profile for the TF CLs. In such model the terminal is not included and it will be introduced in the next 3D FE model.

6.1 Experimental data

In Figure 68 the position of the temperature sensors mounted on TF CLs during the test procedure in Hefei (ASIPP) is shown.

In Figure 69 the broken sensors are reported on the PID and in Table 7 the list of CERNOX sensors with issues as presented by P. Bauer during the weekly meeting on 4th of November 2015 **[5]** is shown.

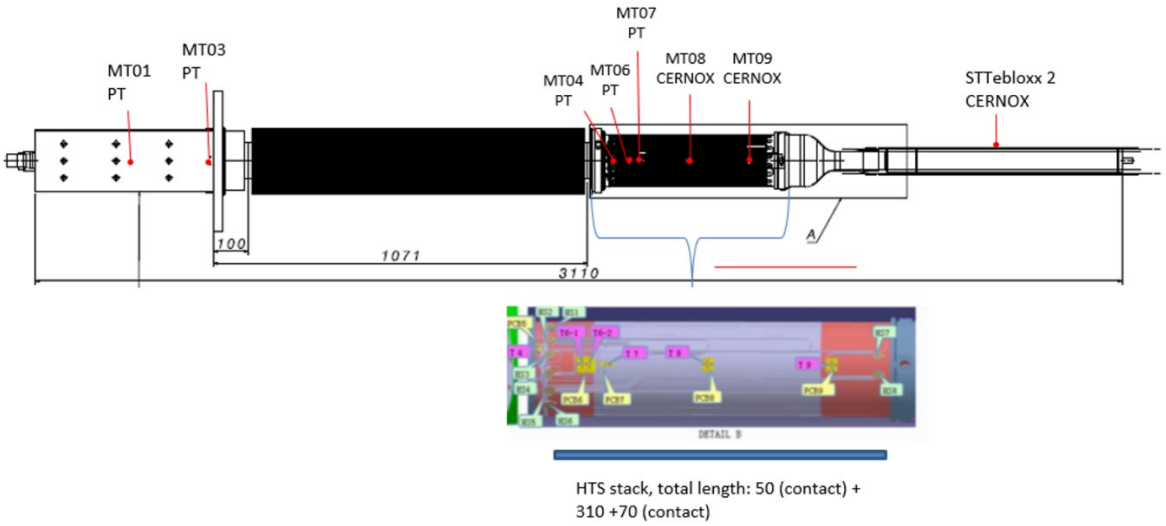

Figure 68 Position of the temperature sensors on the TF prototype **[2]**.

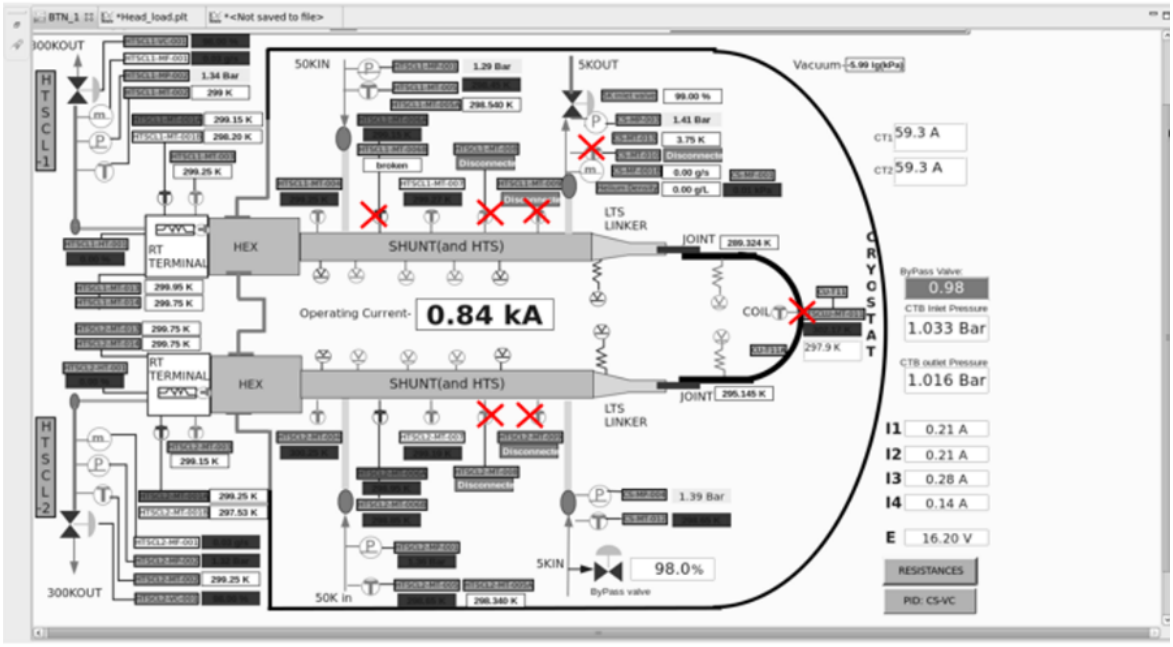

Figure 69 PID: the broken CERNOX sensors are marked with red cross **[2]**.

Table 7 *List of CERNOX sensors with issues* **[2]**.

MAG-HTS-CL1:MT008B-TT	CL1	Temp sensor middle of shunt	bypass for e-bloxx	unexpected current effects, mostly not usable
MAG-HTS-CL1:MT009B-TT	CL1	Temp sensor bottom of shunt	bypass for e-bloxx	unexpected current effects, mostly not usable
MAG-HTS-CS:MT010B-TT	CL1	5 K exit temperature	bypass for e-bloxx	only exploitable after July 11th, use MT010-TT instead
MAG-HTS-CL1:MT006B-TT	CL1	Temperature HTS warm end		broken
MAG-HTS-CL1:MT008-TT	CL1	Temperature sensor middle of shunt	use channel B instead (ebloxx problem)	not working after July5th cool-down,
MAG-HTS-CL1:MT009-TT	CL1	Temperature sensor bottom of shunt	use channel B instead (ebloxx problem)	not working after July5th cool-down,
MAG-HTS-CL2:MT008B-TT	CL2	Temp sensor middle of shunt	bypass for e-bloxx	unexpected current effects, mostly not usable
MAG-HTS-CL2:MT009B-TT	CL2	Temp sensor bottom of shunt	bypass for e-bloxx	unexpected current effects, mostly not usable
MAG-HTS-CLU:MT011-TT	U-bend	Temp sensor U-bend		Not working most of the time

From Figure 70 to Figure 73 the results for the sensors MT006, MT004, MT009B and MT003 are reported. The temperature values marked in each graph will be used in section 1.3 to perform the comparison with the simulated temperature profile.

It should be noticed that although in Table 7 it was stressed that the sensor MT009B could have some issue due to unexpected current effects, such sensor is used in the present study because it shows reasonable values (see later on the good agreement with the simulated temperature profile, see Figure 75).

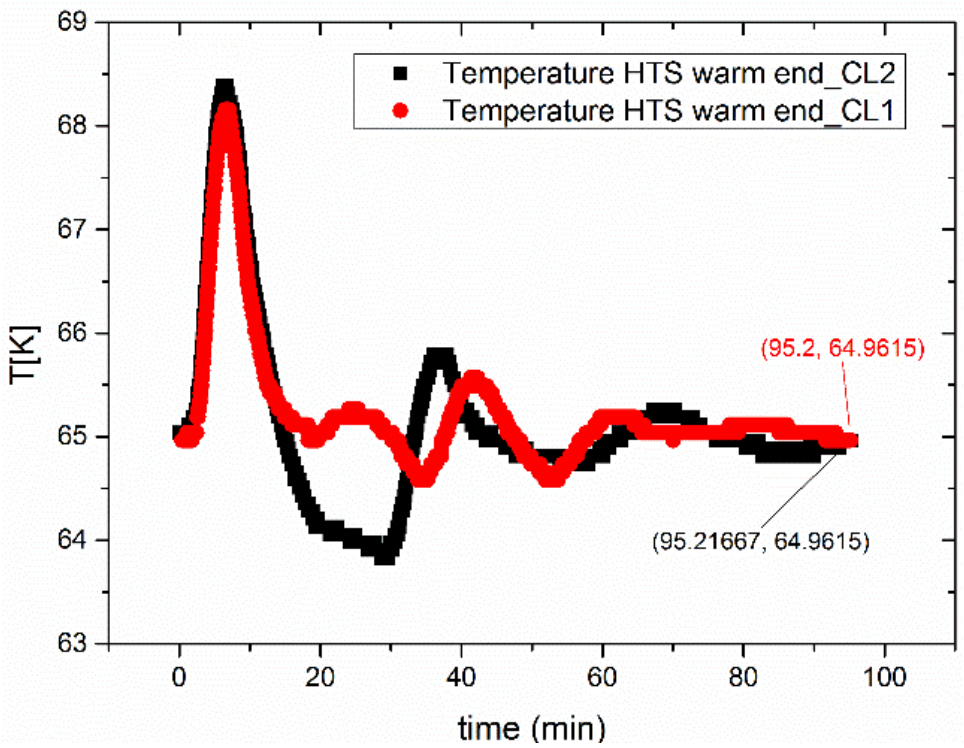

Figure 70 MT006: temperature at the HTS warm end.

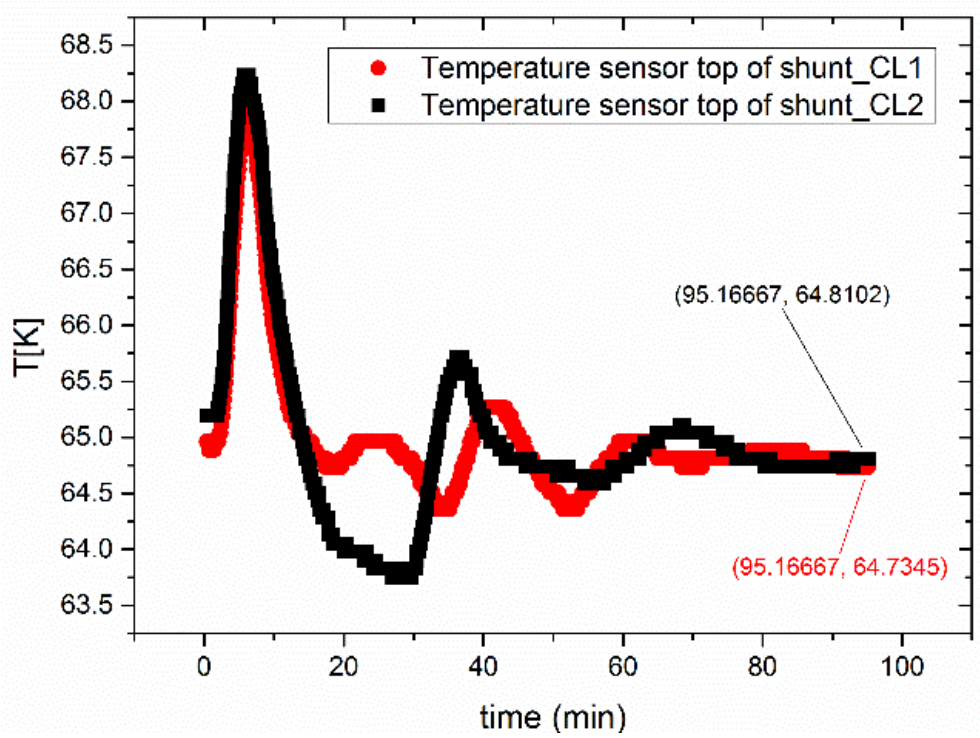

Figure 71 MT004: temperature at the top of shunt.

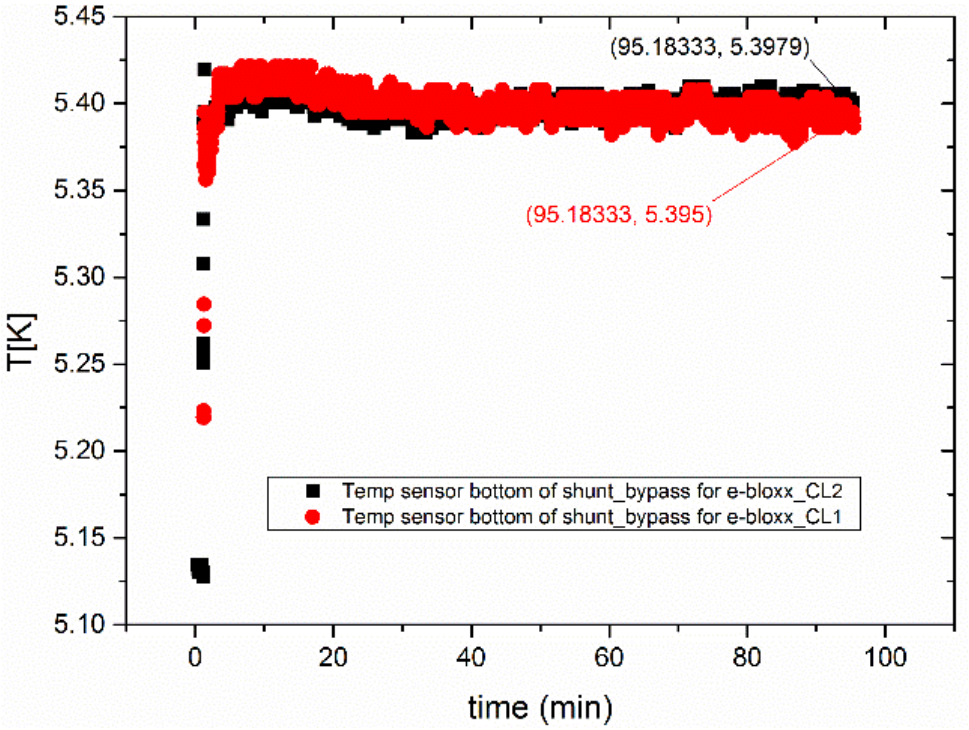

Figure 72 MT009B: temperature at the bottom of shunt.

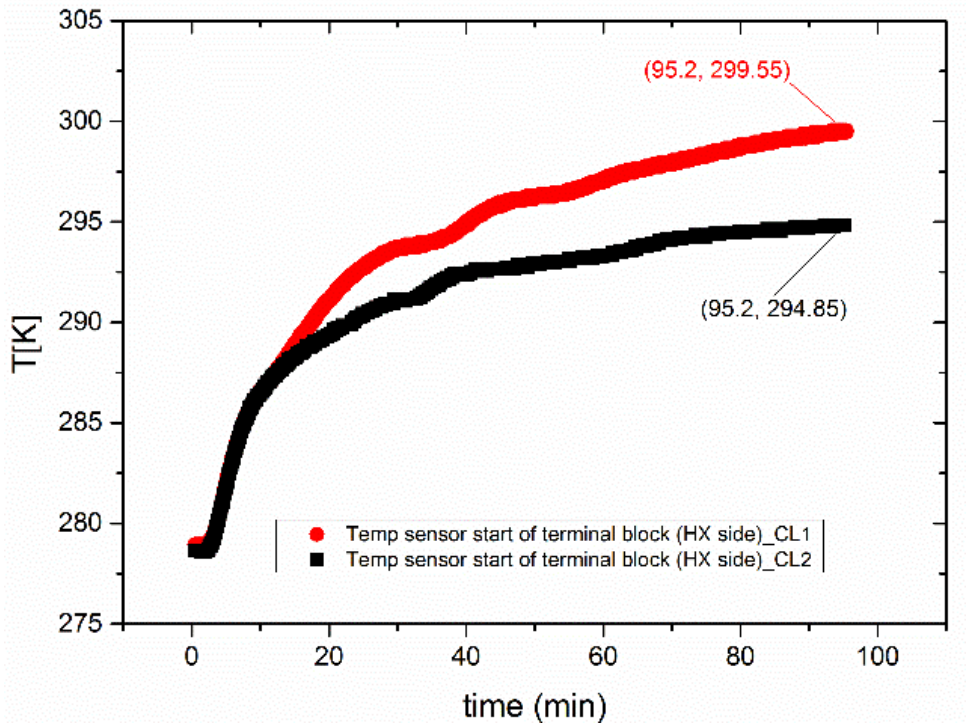

Figure 73 MT003: temperature at the beginning of terminal block (HEX side)

N.B. All these temperature data are extracted from the steady state test (Case 4.1).

6.2 3D FE thermo-hydraulic and electrical model

The 3D FE thermo-hydraulic and electrical modelling performed on a complete 68 kA ITER HTS current lead is described in details in ref. [4].

In Figure 74 the position of the CERNOX sensors on the 3D model are shown and in

Table 8 their main characteristics are summarized.

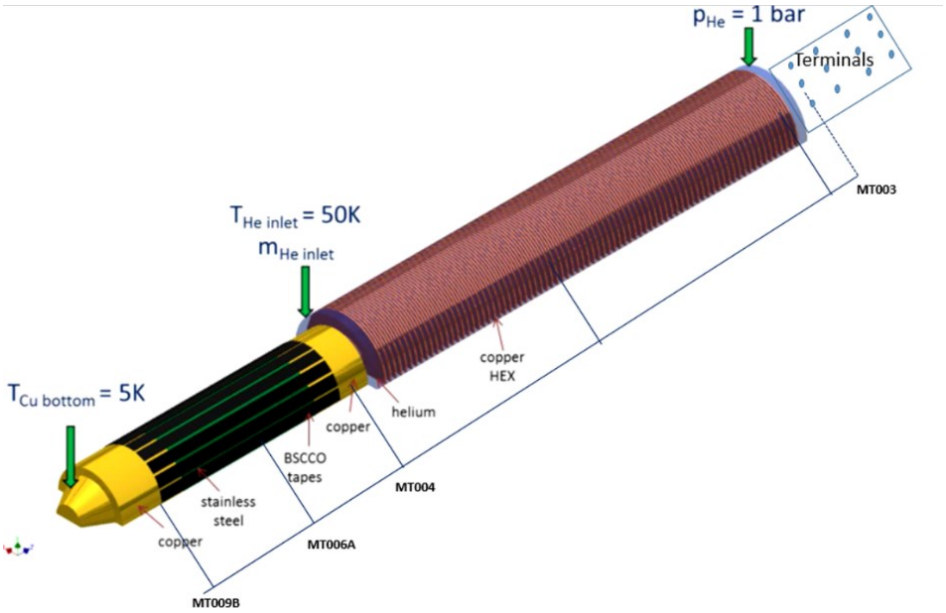

Figure 74 Position of the temperature sensors on the 3D model of TF HTS CL. The simulation does not take into account the terminals (in blue).

Table 8 *CERNOX sensors selected for the comparison with the numerical result*

Sensor	Position [m]	Time [min]	T_{CL1}[K]	T_{CL2}[K]
MT006 Temperature HTS warm end	-0.05	95.2	64.9615	64.9615
MT004 Temperature sensor top of shunt	0	95.17	64.7345	64.8102
MT009B Temperature sensor bottom of shunt	-0.5	95.18	5.395	5.3979
MT003 Temperature sensor start of terminal block (HX side)	1.1	95.2	299.55	294.85

6.3 Comparison between experimental and simulated data

The temperature profile along the TF HTS current lead at nominal current (68kA) has been obtained from the 3D thermo-hydraulic and electrical model in which the RRR of Cu was fixed at 185 and the He mass flow rate at 4.5g/s.

As shown in Figure 75 **the experimental values acquired with the 4 temperature sensors** (see Table 8) **are in perfect agreement with the calculated temperature profile**.

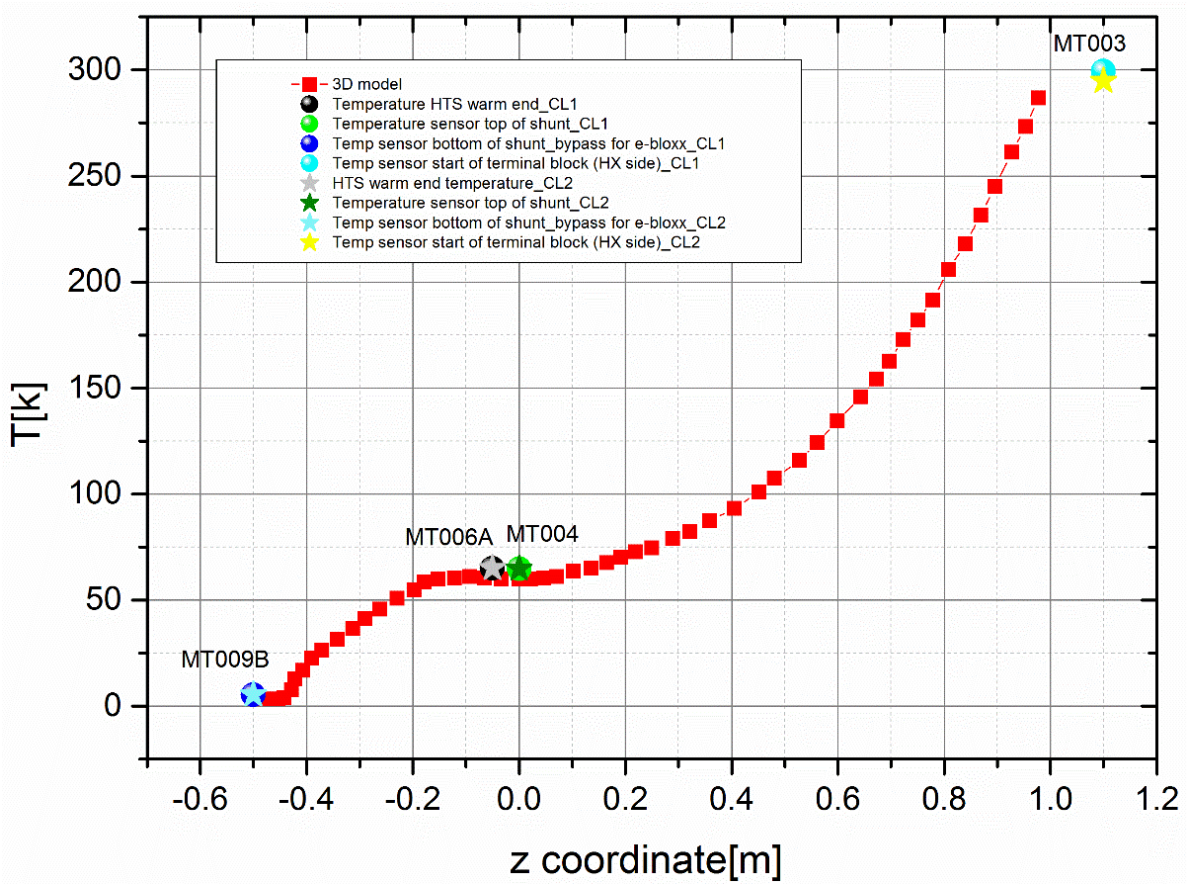

Figure 75 Comparison between the theoretical (from the 3D model) and experimental temperature profile for the TF HTS prototypes.

The MT003 sensor corresponding to that mounted on the terminal has to be checked with the temperature profile obtained from the new 3D model that will include the terminal. We can already conclude that the detected terminal temperature already follows the trend of the temperature profile shown in Figure 75.

7 JOINT RESISTANCES (CASE 10.1)

In this section the joint resistances are extrapolated from a linear fit of the V-I curves.

The positions of the voltage taps mounted on the prototype during the joint resistance measurements are shown in Figure 76 while the linear fits are presented from Figure 77 to Figure 84.

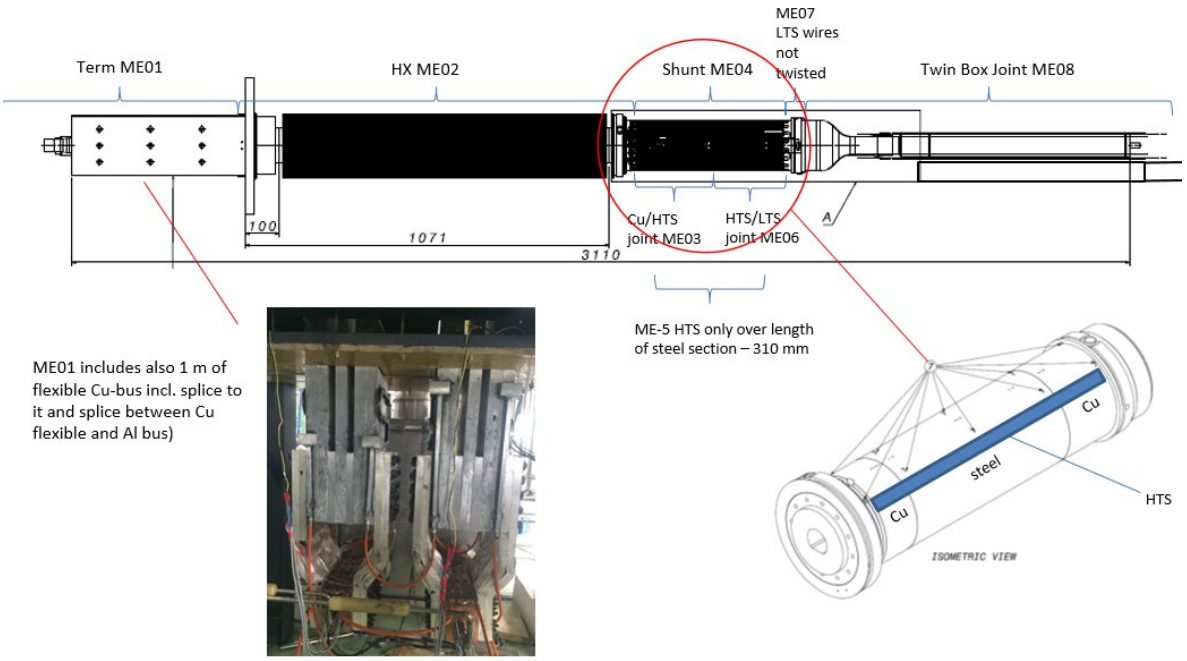

Figure 76 Voltage tap (Quench detection). Courtesy of P. Bauer **[5]**.

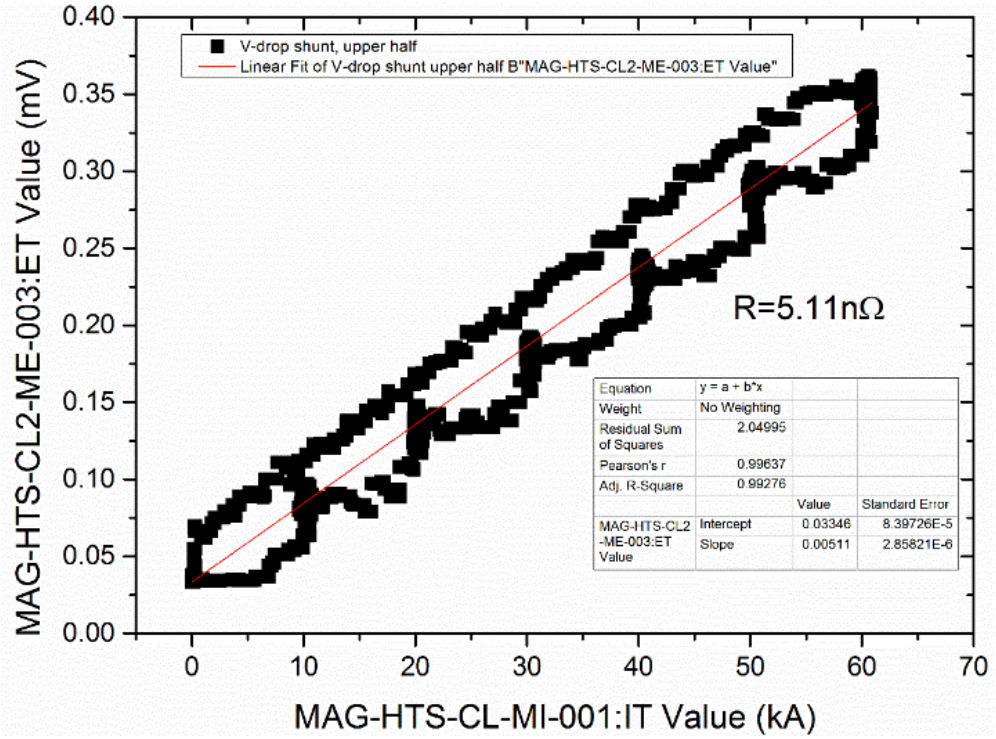

Figure 77 V-I characteristic to obtain the resistance on the upper half of the shunt, i.e. $R_{65K\ Cu\text{-}HTS}$ (ME003), for CL2.

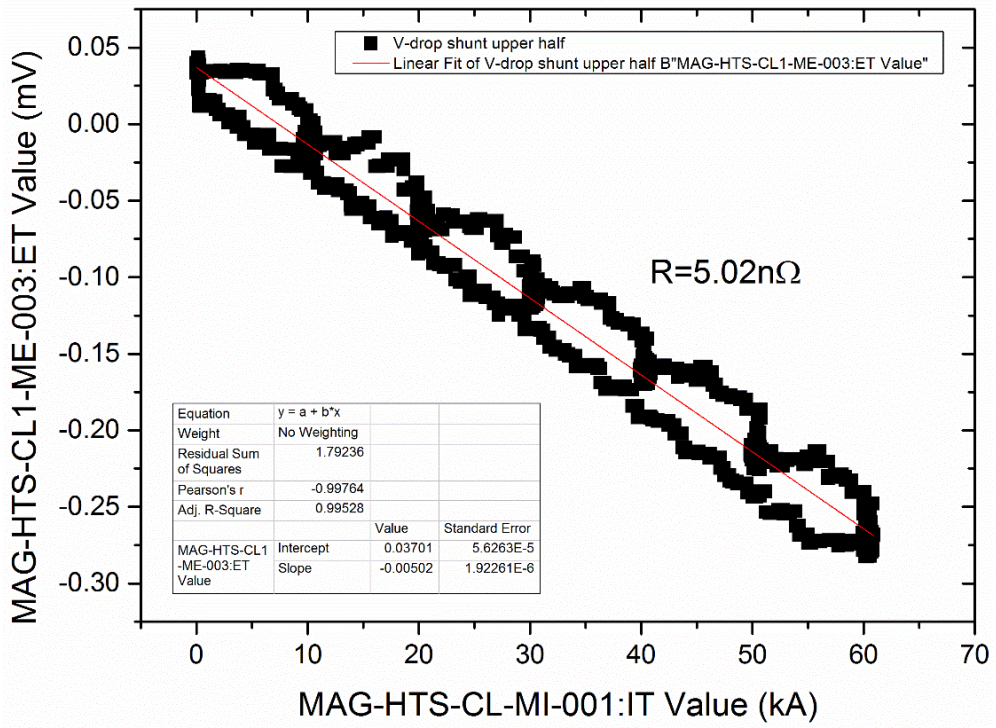

Figure 78 V-I characteristic to obtain the resistance on the upper half of the shunt, i.e. $R_{65K\ Cu\text{-}HTS}$ (ME003), for CL1.

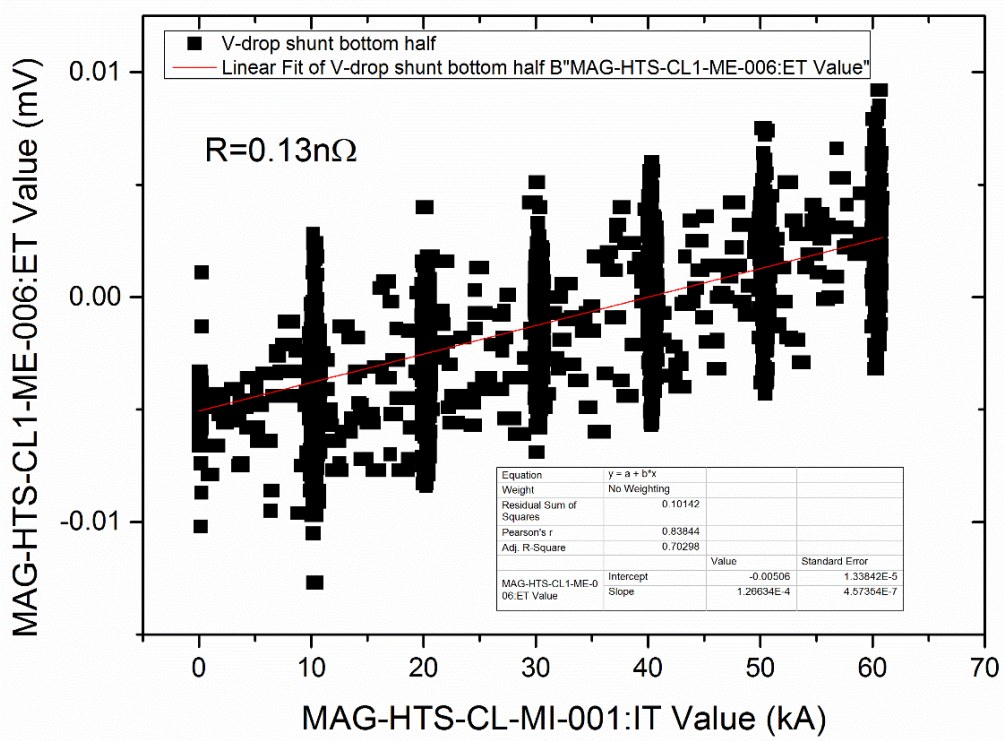

Figure 79 V-I characteristic to obtain the resistance on the bottom half of the shunt, i.e. $R_{HTS-LTS}$ (ME006), for CL1.

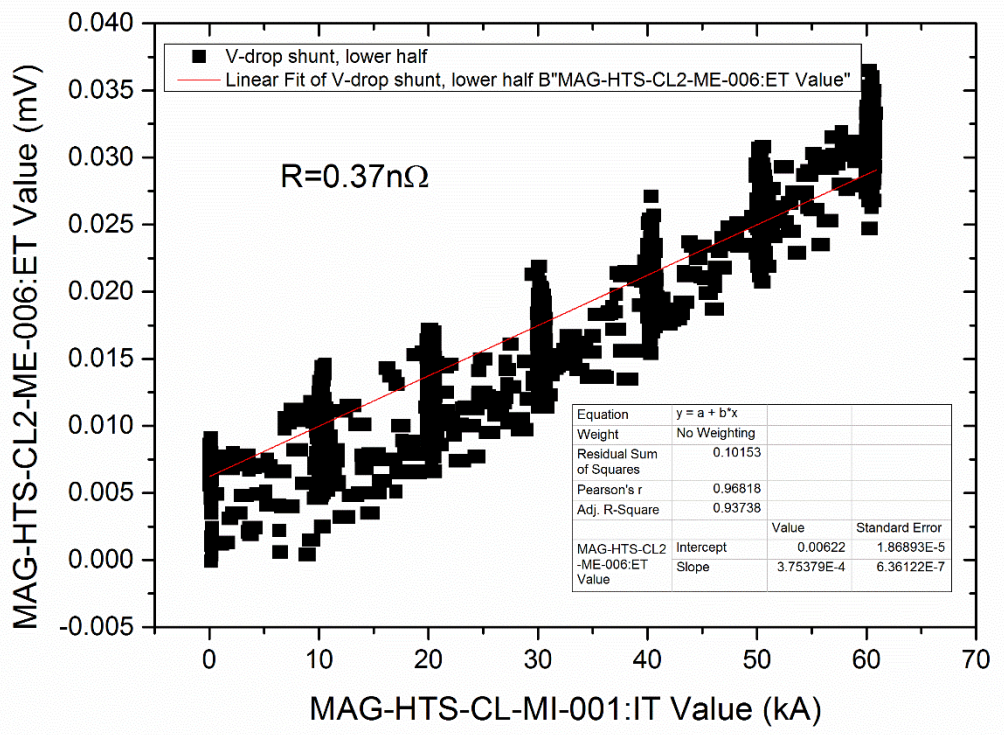

Figure 80 V-I characteristic to obtain the resistance on the bottom half of the shunt, i.e. $R_{HTS-LTS}$ (ME006), for CL2.

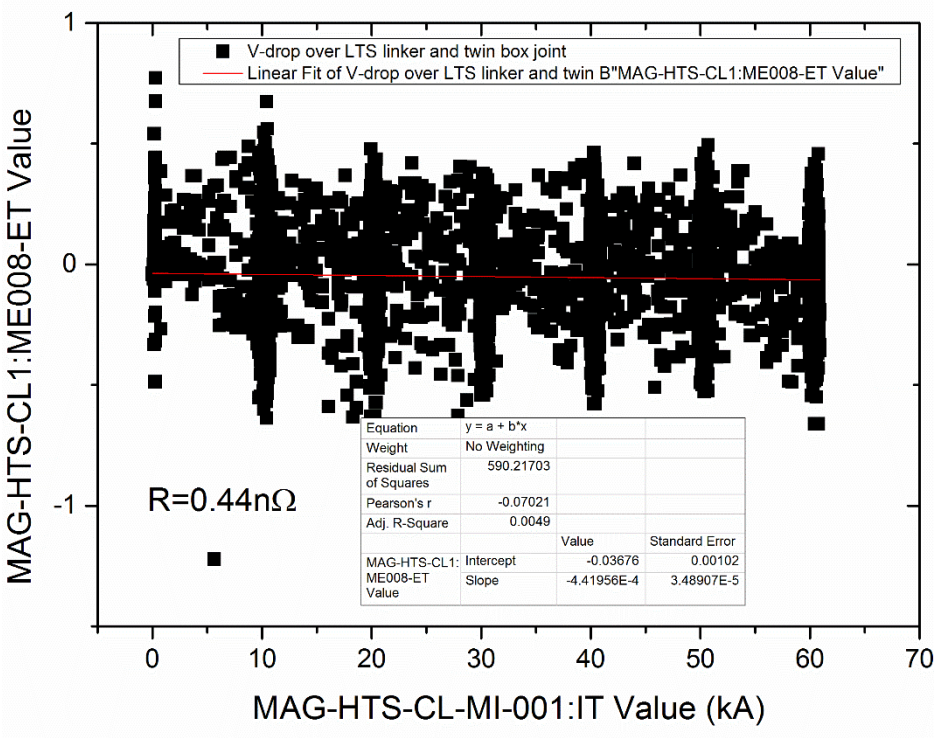

Figure 81 V-I characteristic to obtain the resistance over LTS linker and twi box joint, i.e. $R_{TWIN\ BOX\ (LTS\text{-}LTS)}$ (ME008), for CL1.

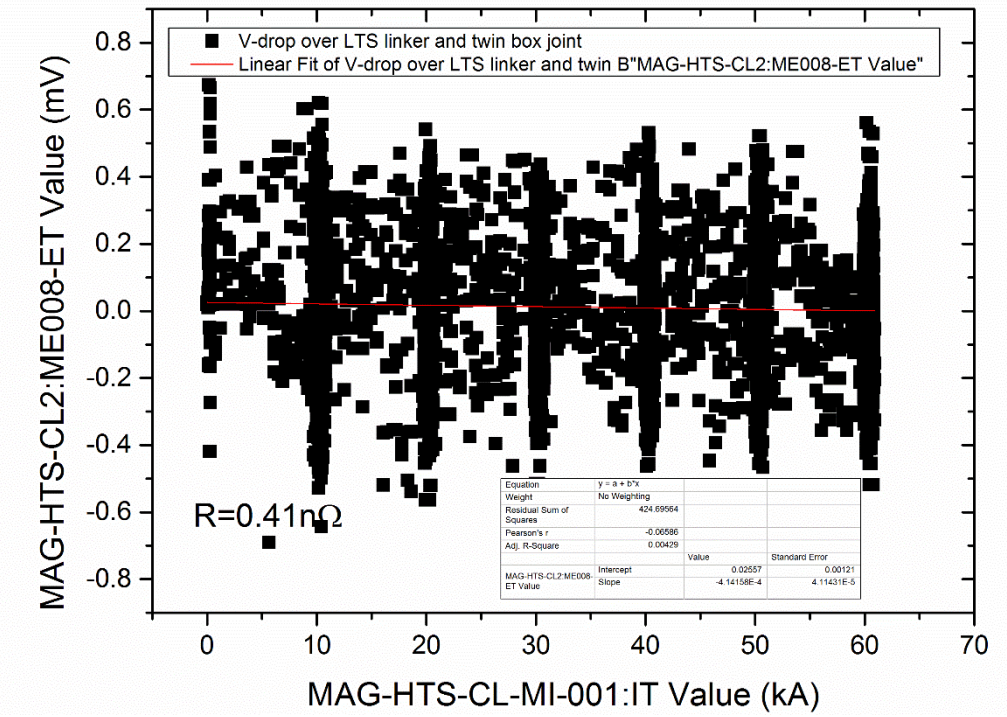

Figure 82 V-I characteristic to obtain the resistance over LTS linker and twi box joint, i.e. $R_{TWIN\ BOX\ (LTS\text{-}LTS)}$ (ME008), for CL2.

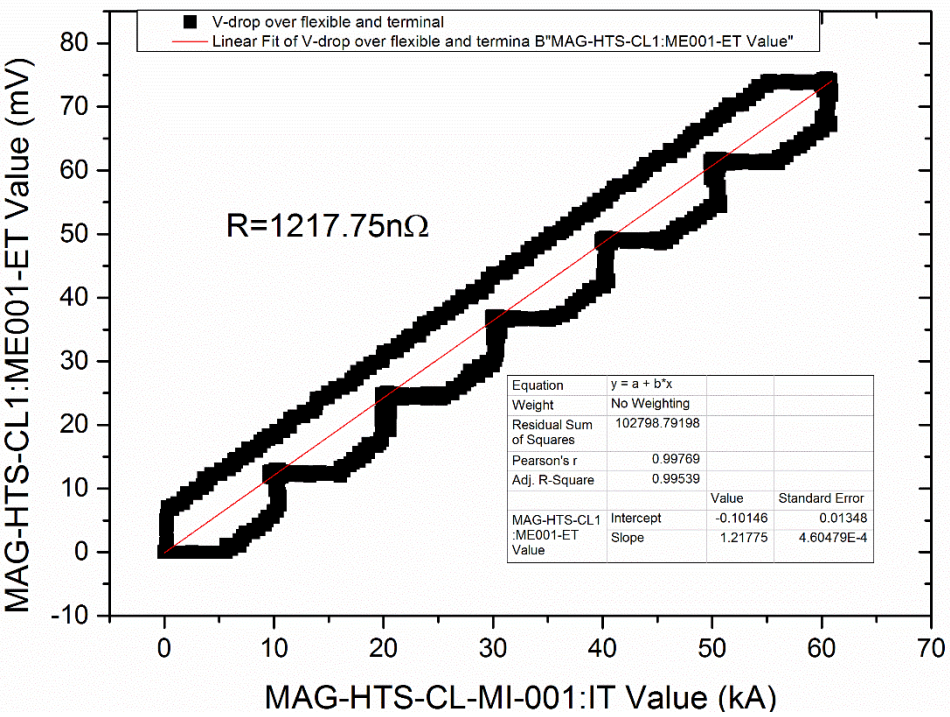

Figure 83 V-I characteristic to obtain the resistance over flexible and terminal for CL1.

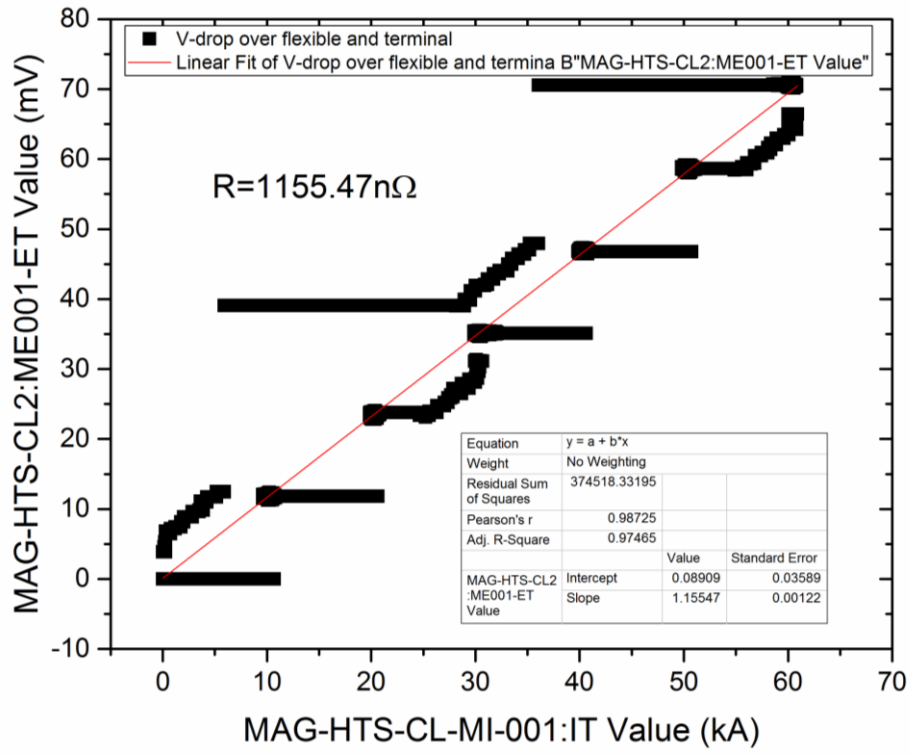

Figure 84 V-I characteristic to obtain the resistance over flexible and terminal for CL2.

The hysteretic like behaviour that occur in Figure 77, Figure 78 and Figure 83 are expected due or to the different clocks used to perform the current and voltage measurement (QDS and CODAC system, see slide #9 in ref. [2] for further details on the two systems) or to the inductive voltage. To investigate on such behaviour the comparison between the current and voltage data as a function of time has been performed and the results are shown below (from Figure 85 to Figure 108).

A. Upper half of the shunt (ME003) for CL1: $R_{65K\ Cu\text{-}HTS}$

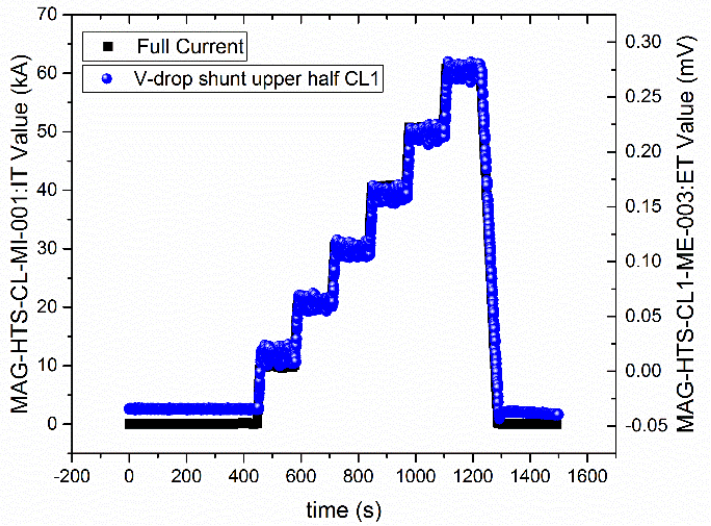

Figure 85 V(t) and I(t) curves for the upper half of the shunt as a function of time for CL1.

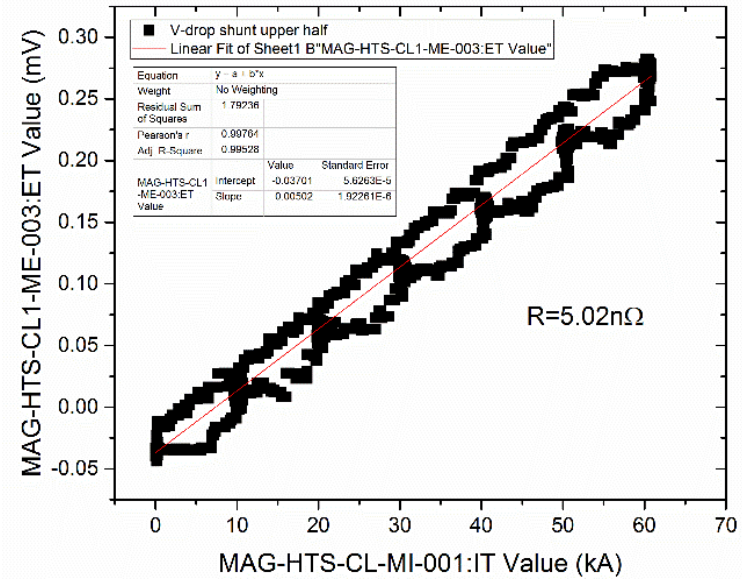

Figure 86 V-I characteristic curve to obtain the resistance on the upper half of the shunt for CL1 before shifting the time of the two data sets (i.e. V(t) and I(t)).

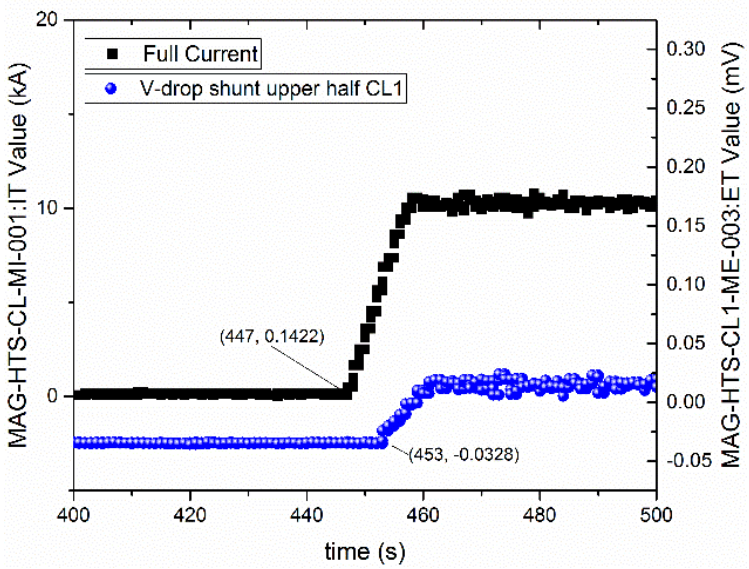

Figure 87 Magnification of the V(t) and I(t) curves for the upper half of the shunt of CL1 to estimate the time shift between CODAC and QDS acquisition systems (6 s).

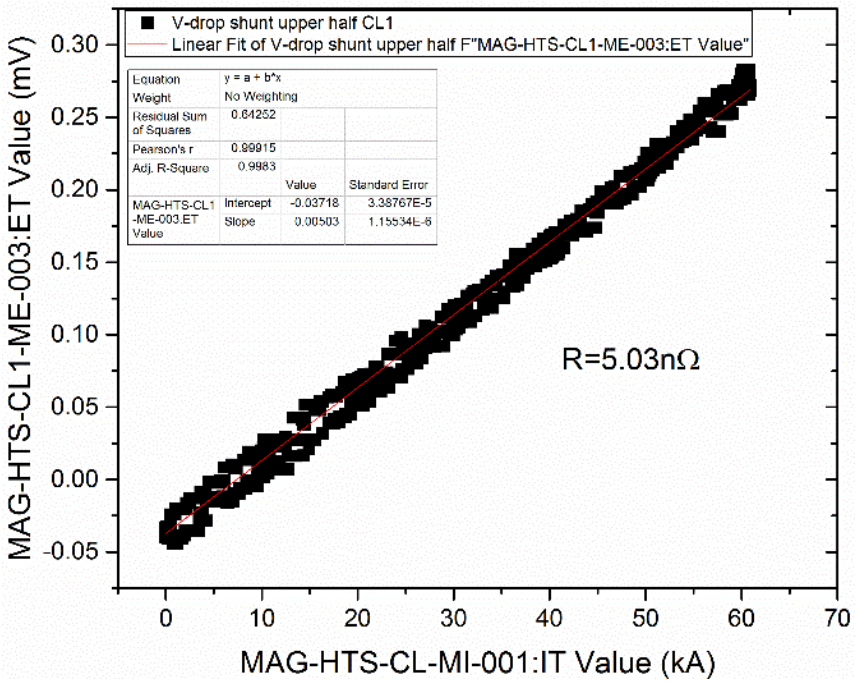

Figure 88 V-I characteristic curve to obtain the resistance on the upper half of the shunt for CL1 after shifting the time of the two data sets (i.e. V(t) and I(t)).

The difference between the resistance values found before and after the shift in time is only 0.01 nΩ.

B. Upper half of the shunt (ME003) for CL2: $R_{65K\ Cu\text{-}HTS}$

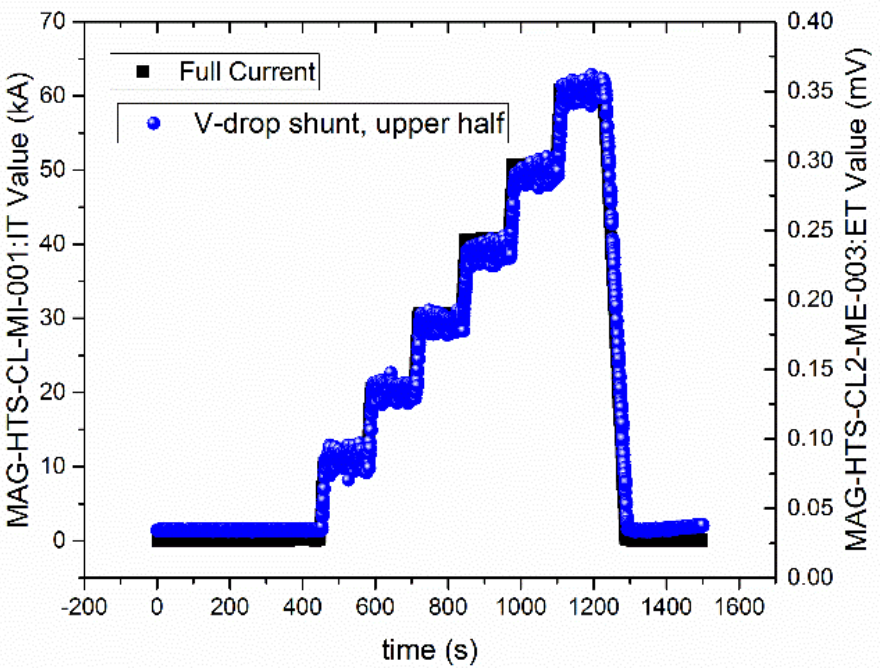

Figure 89 V(t) and I(t) curves for the upper half of the shunt as a function of time for CL2.

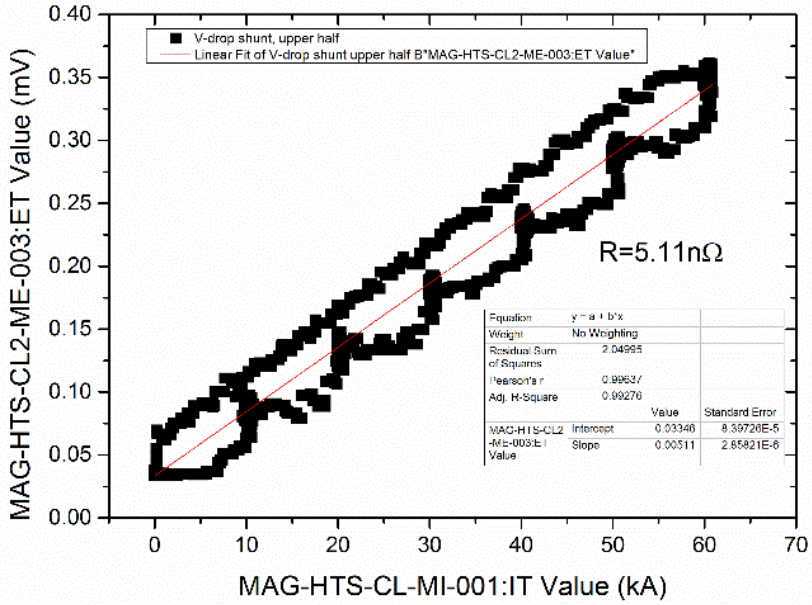

Figure 90 V-I characteristic curve to obtain the resistance on the upper half of the shunt for CL2 before shifting the time of the two data sets (i.e. V(t) and I(t)).

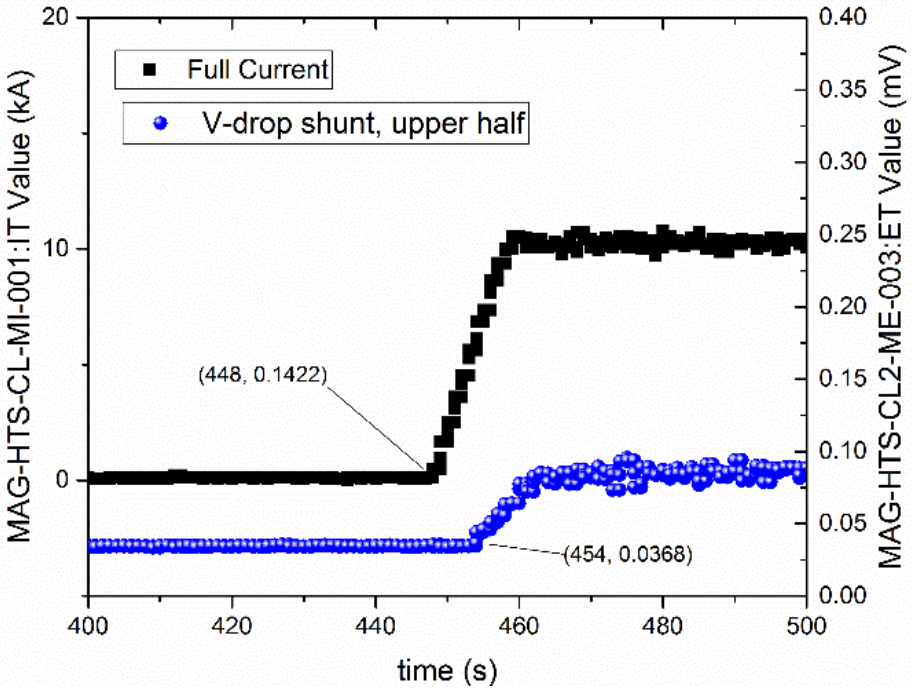

Figure 91 Magnification of the V(t) and I(t) curves for the upper half of the shunt of CL2 to estimate the time shift between CODAC and QDS acquisition systems (6 s).

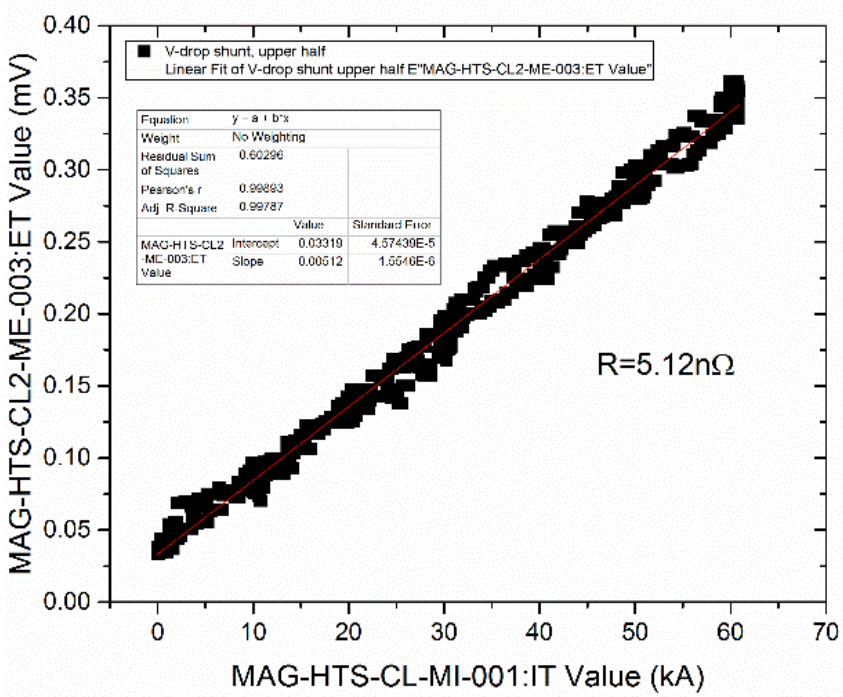

Figure 92 V-I characteristic curve to obtain the resistance on the upper half of the shunt for CL2 after shifting the time of the two data sets (i.e. V(t) and I(t)).

The difference between the resistance values found before and after the shift in time is only 0.01 nΩ.

C. Shunt bottom half for CL1 and CL2 (ME006): $R_{HTS-LTS}$

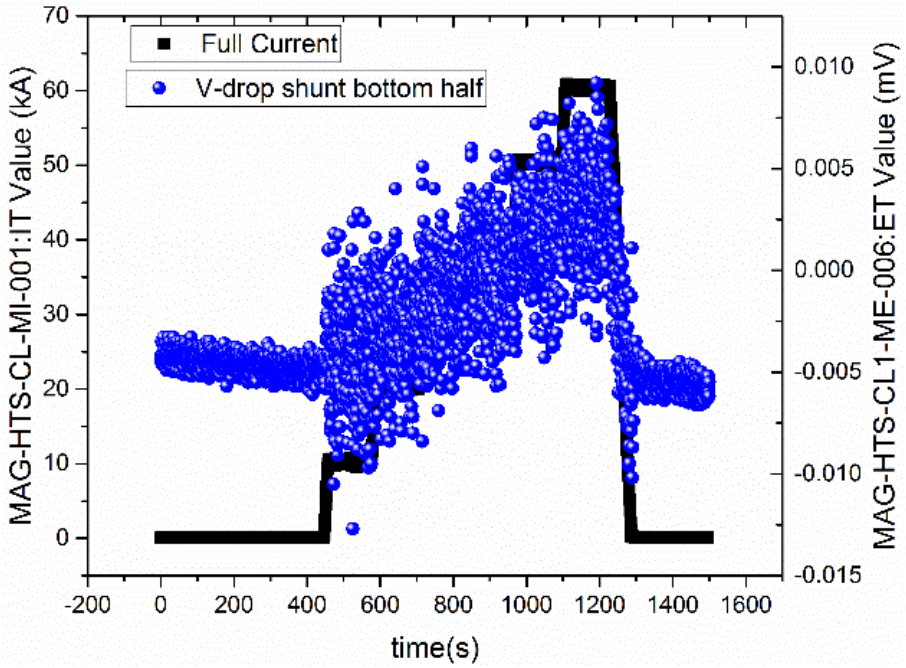

Figure 93 V(t) and I(t) curves for the bottom half of the shunt as a function of time for CL1. Unfortunately, in this case, the shift in time cannot be determined due to the fluctuation in the V(t) curve.

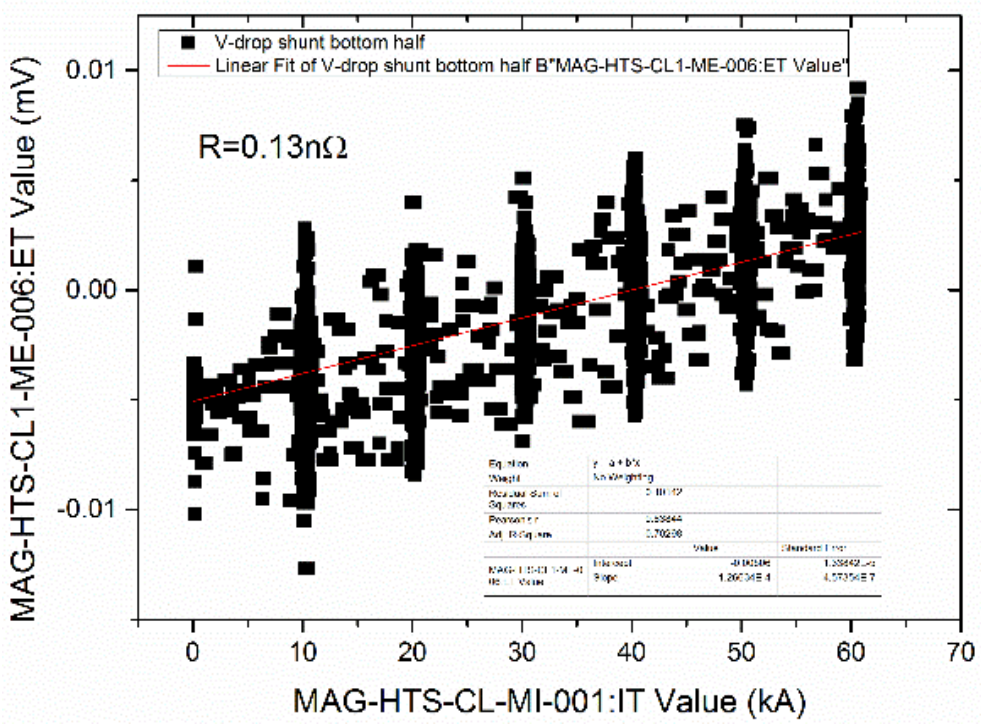

Figure 94 V-I characteristic to obtain the resistance on the bottom half of the shunt for CL1.

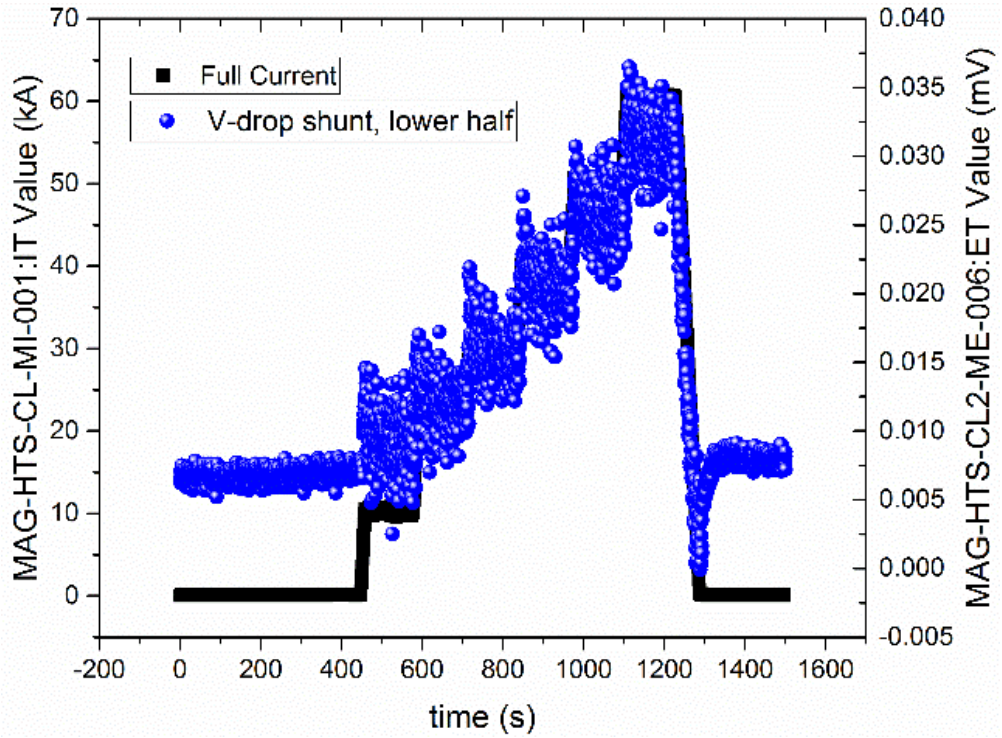

Figure 95 V(t) and I(t) curves for the bottom half of the shunt as a function of time for CL2. Unfortunately, in this case, the shift in time cannot be determined due to the fluctuation in the V(t) curve.

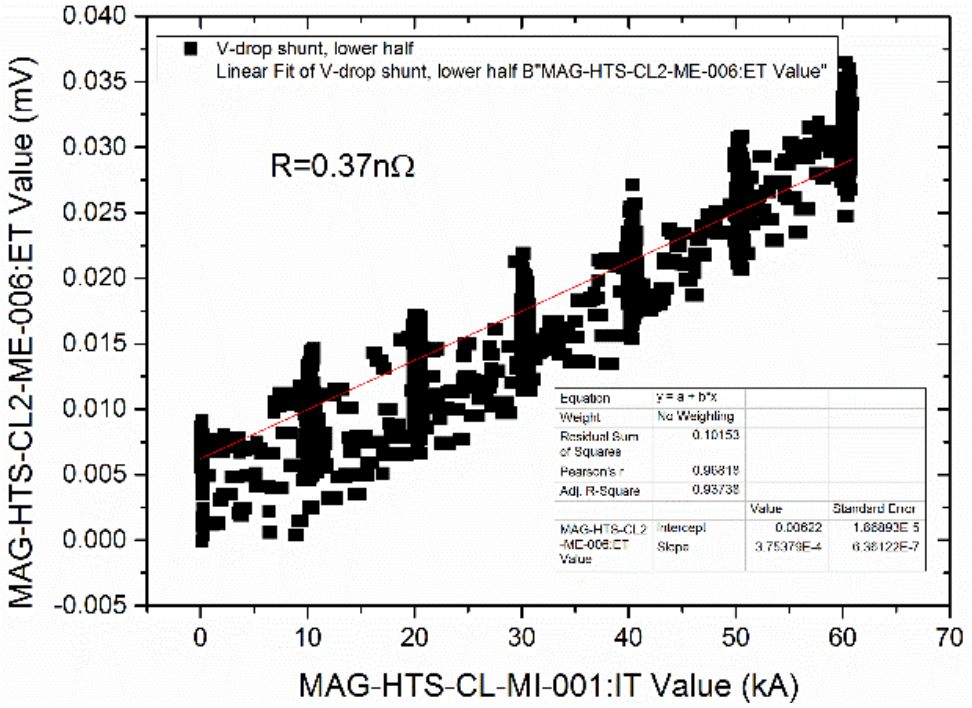

Figure 96 V-I characteristic to obtain the resistance on the bottom half of the shunt for CL2.

To obtain more precise values for these resistances it is necessary to repeat the V measurements on both the current leads.

D. LTS linker and twin box joint for CL1 and CL2 (ME008): $R_{TWIN\ BOX\ (LTS-LTS)}$

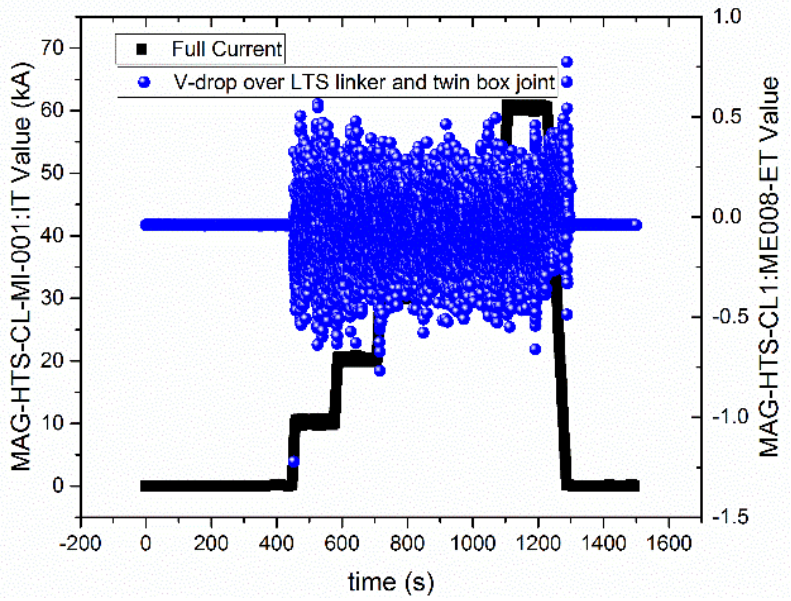

Figure 97 V(t) and I(t) curves for the LTS linker and twin box joint as a function of time for CL1. Unfortunately, in this case, the shift in time cannot be determined due to the fluctuation in the V(t) curve.

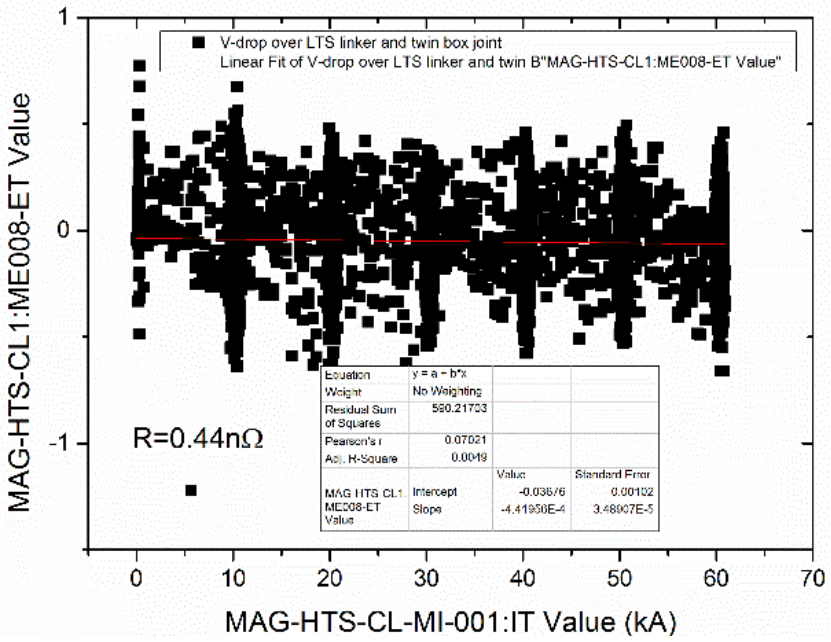

Figure 98 V-I characteristic to obtain the resistance over LTS linker and twin box joint for CL1.

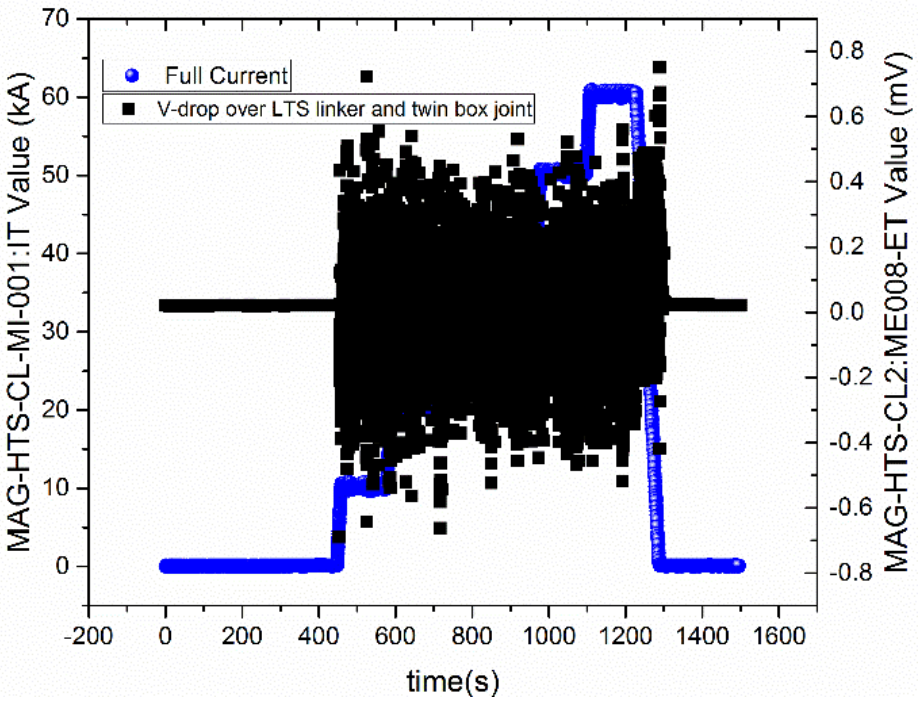

Figure 99 V(t) and I(t) curves for the LTS linker and twin box joint as a function of time for CL2. Unfortunately, in this case, the shift in time cannot be determined due to the fluctuation in the V(t) curve.

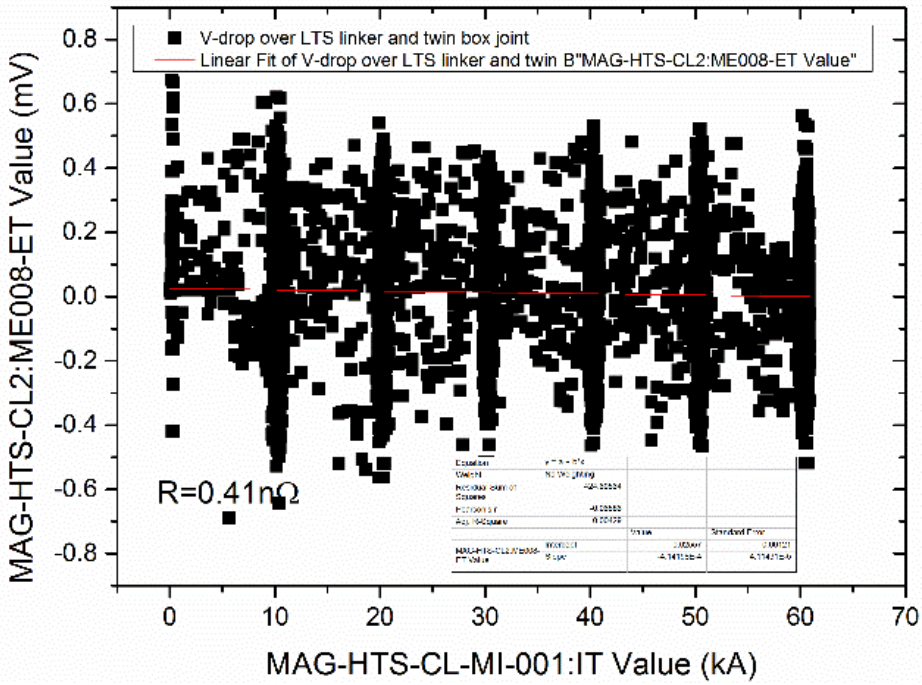

Figure 100 V-I characteristic to obtain the resistance over LTS linker and twin box joint for CL2.

To obtain more precise values for these resistances it is necessary to repeat the V measurements on both the current leads.

E. Flexible and terminal for CL1 (ME001): $R_{FLEXIBLE-Cu\ TERMINAL}$

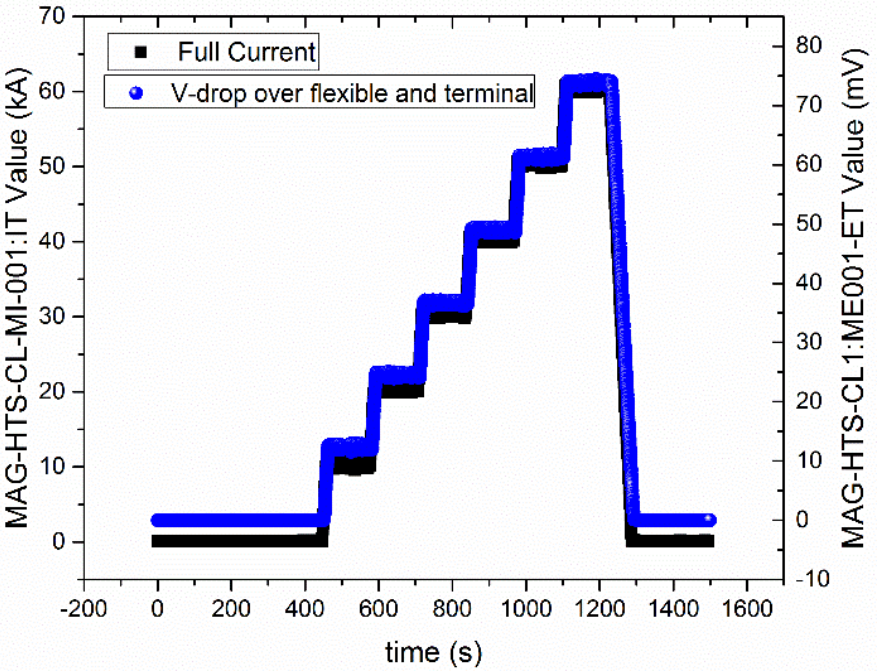

Figure 101 V(t) and I(t) curves for the flexible and terminal as a function of time for CL1.

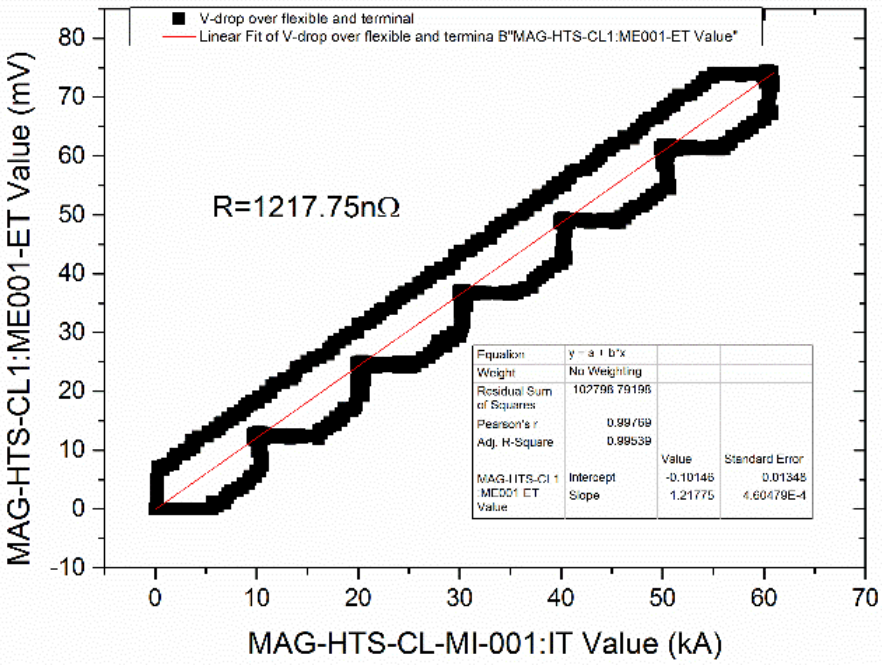

Figure 102 V-I characteristic to obtain the resistance over flexible and terminal for CL1 before shifting the time of the two data sets (i.e. V(t) and I(t)).

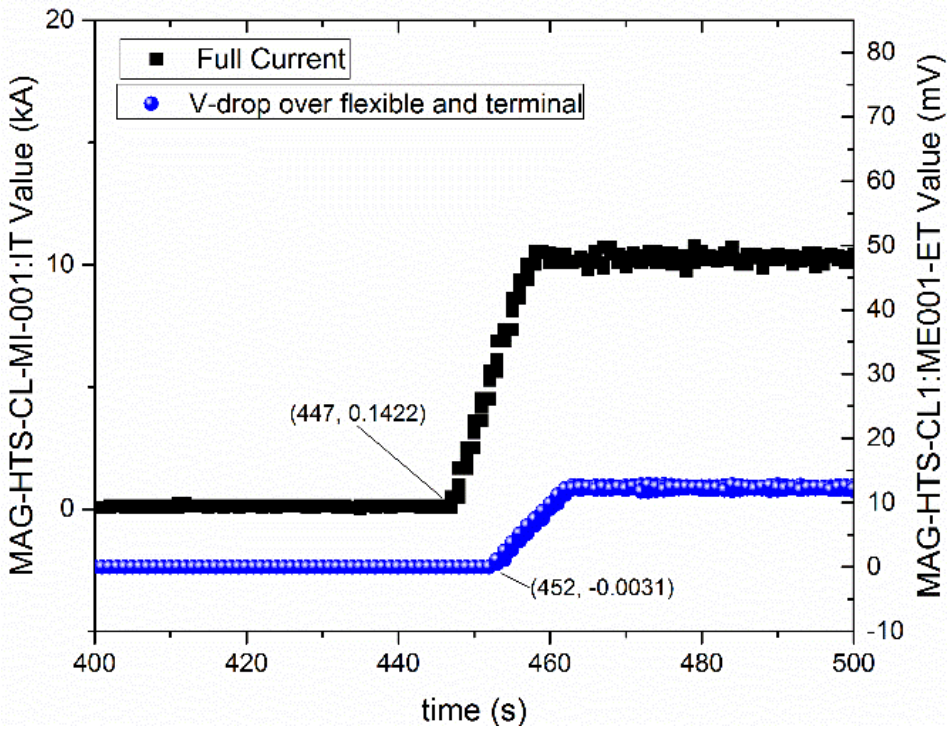

Figure 103 Magnification of the V(t) and I(t) curves for the flexible and resistance of CL1 to estimate the time shift between CODAC and QDS acquisition systems (5 s).

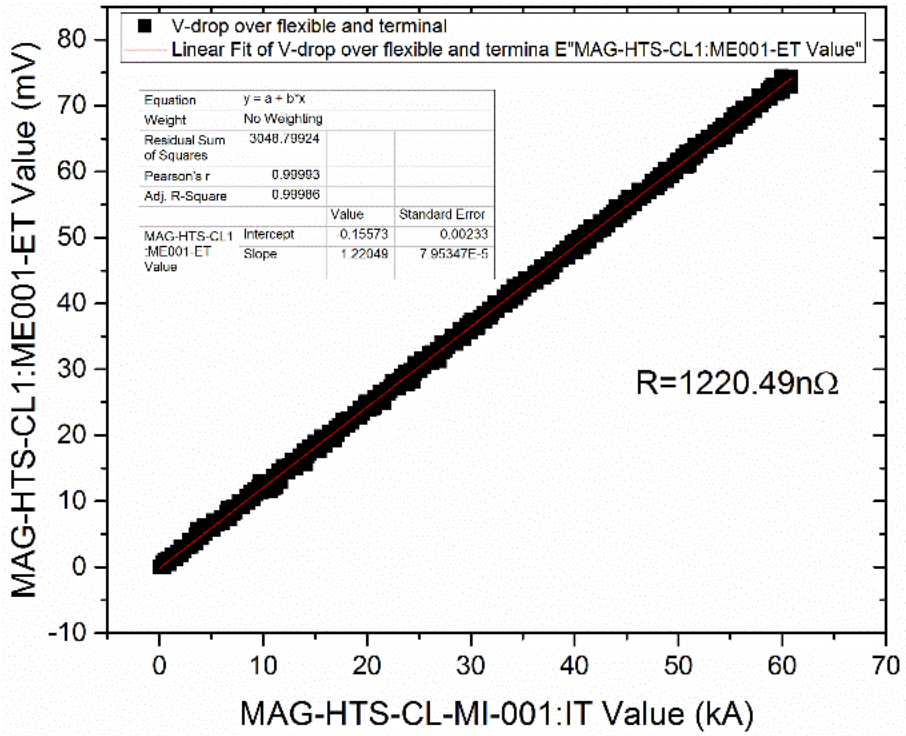

Figure 104 V-I characteristic curve to obtain the resistance on the resistance and flexible for CL1 after shifting the time of the two data sets (i.e. V(t) and I(t)).

The difference between the resistance values found before and after the shift in time is only 2.74 nΩ.

F. Flexible and terminal for CL2 (ME001): $R_{FLEXIBLE-Cu\ TERMINAL}$

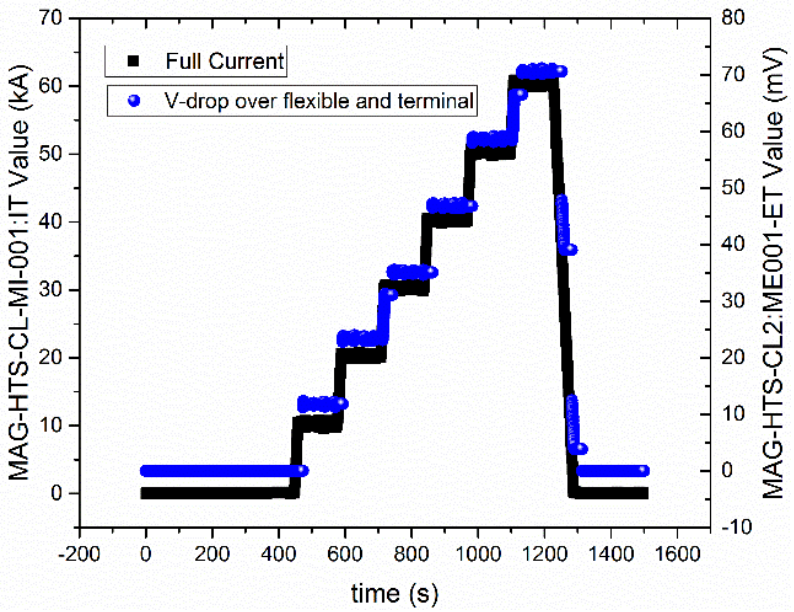

Figure 105 V(t) and I(t) curves for the flexible and terminal as a function of time for CL2.

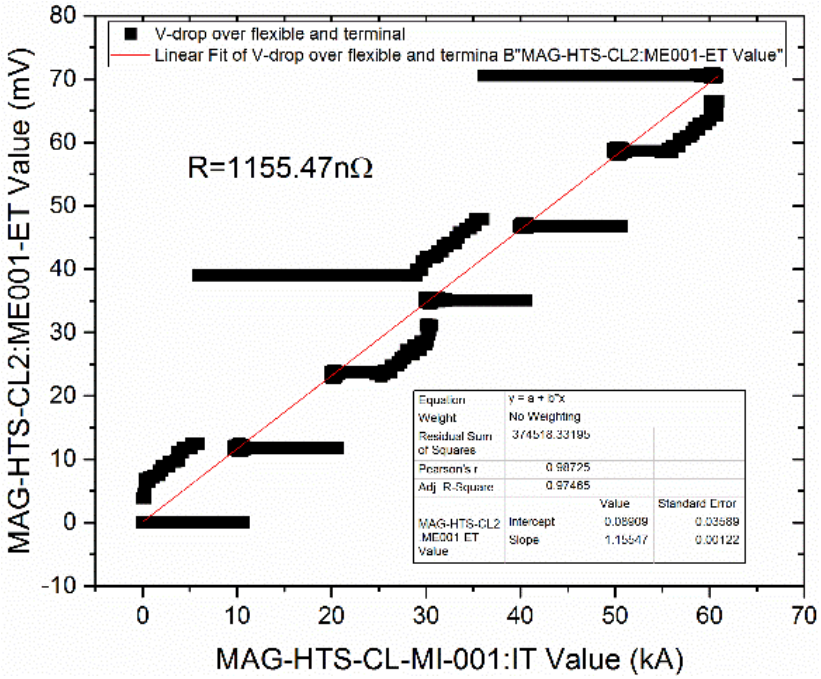

Figure 106 V-I characteristic to obtain the resistance over flexible and terminal for CL2 before shifting the time of the two data sets (i.e. V(t) and I(t)).

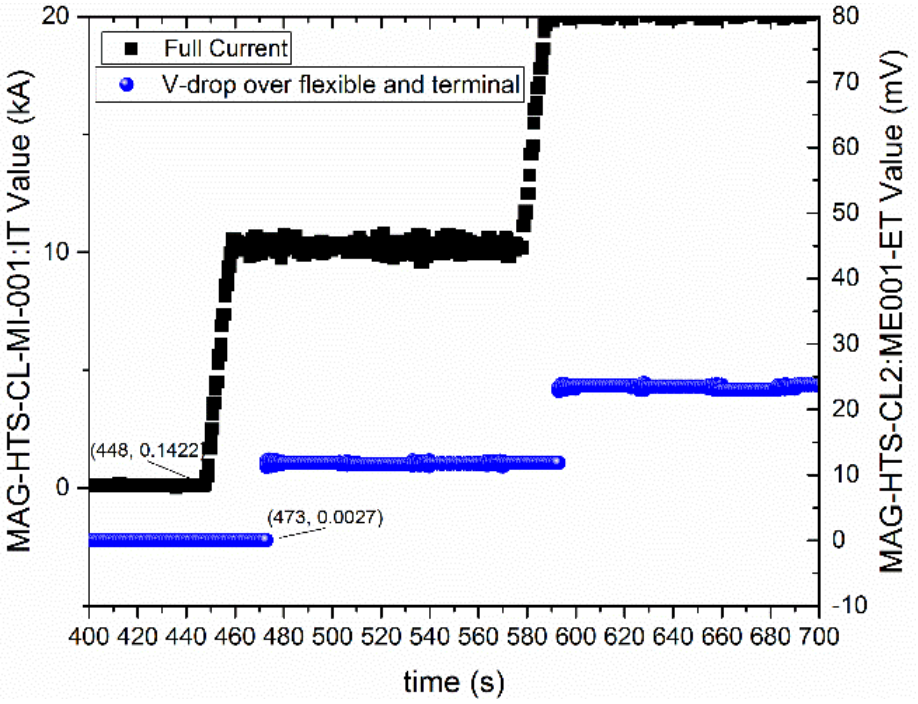

Figure 107 Magnification of the V(t) and I(t) curves for the flexible and resistance of CL2 to estimate the time shift between CODAC and QDS acquisition systems (25 s).

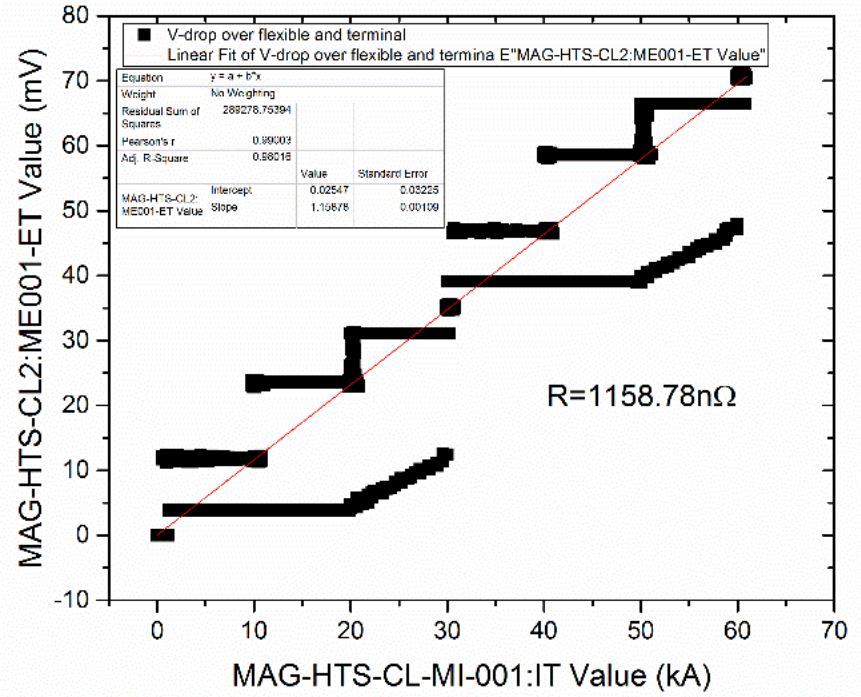

Figure 108 V-I characteristic curve to obtain the resistance on the resistance and flexible for CL2 after shifting the time of the two data sets (i.e. V(t) and I(t)).

The difference between the resistance values found before and after the shift in time is only 3.31 nΩ.

The V-I characteristic curves (Figure 106 and Figure 108) present several discontinuities due to the missing V(t) data (as shown in Figure 107).

Table 9 *Comparison between the joint resistance experimental results (as obtained from the analysis at ASIPP* **[3]** *and at CERN) and the ITER requirement.*

Parameter [nΩ]	ITER requirement	CL1		CL2	
		ASIPP	CERN	ASIPP	CERN
$R_{65K\ Cu\text{-}HTS}$ **ME003**	10	5.14	5.02 before 5.03 after	5.25	5.11before 5.12 after
$R_{HTS\text{-}LTS}$ **ME006**	1	0.14	0.13	0.44	0.3754
$R_{TWIN\ BOX\ (LTS\text{-}LTS)}$ **ME008**	2	0.37	0.44	0.26	0.414
$R_{FLEXIBLE\text{-}Cu\ TERMINAL}$ **ME001**	100	170	1217.75 before 1220.49 after	170	1155.47

From such analysis it is possible to conclude that the "hysteretic" like shape of the V-I curves is due to the time shift (about 6 s) between the V data (acquired with the QDS system) and I data (acquired with the CODAC system).

In Table 9 the comparison between the experimental values and the ITER requirements are reported and there is a very good agreement for the resistances $R_{65K\ Cu\text{-}HTS}$ (ME003), $R_{HTS\text{-}LTS}$ (ME006) and $R_{TWIN\ BOX\ (LTS\text{-}LTS)}$ (ME008) while some issues were found for the terminal to flexible contact resistance (ME001).

Indeed the ME001 PV includes the terminal (R_T), the contact from the terminal to the flexible ($R_{T\text{-}F}$), the flexible (R_F) and the contact from the flexible to Al bus-bus ($R_{F\text{-}Al\ bus\ bar}$) and all these four resistances have to be considered in series, i.e.:

$$R_{TOT} = R_T + R_{T\text{-}F} + R_F + R_{F\text{-}Al\ bus\ bar}$$

From the model it is possible to estimate the flexible resistance (R_F) as follows: the total cross-section of the Cu flexible(s) is 61440 mm^2 and the length is about 1 m thus R_F= 273 nΩ. Unfortunately no other information can be found for R_T, $R_{T\text{-}F}$ and $R_{F\text{-}Al\ bus\ bar}$ thus, as discussed

in the weekly meeting of the 18th of November 2015, further tests are planned for next January 2016. The solution to measure the flexible to RT terminal contact resistance that was proposed consists to add 8 additional V-taps as shown in Figure 109.

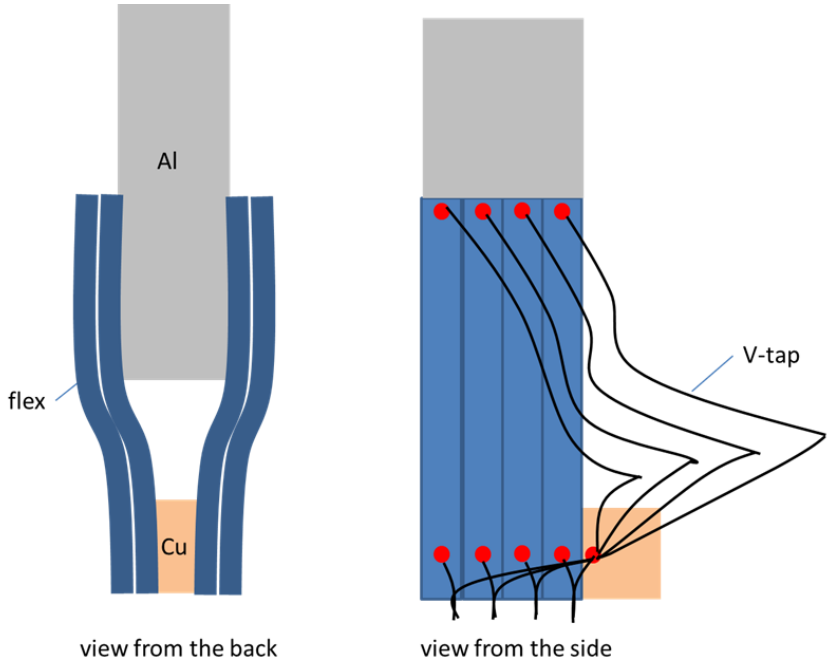

Figure 109 Proposition to measure the flexible to RT terminal contact resistance (Courtesy of P. Bauer)

SUMMARY

In this note the test measurements performed in Hefei on TF prototype CLs are analysed and discussed in details.

The main results can be summarized as follows:

1. LOFA tests (Case 4.1): the experimental minimum LOFA time for CL1 and CL2 are well behind the ITER requirements;
2. Steady state test (Case 4.1): both the experimental values for the mass flow rate and the pressure drop fully satisfy the simulated values as well as the ITER requirements;

3. Under/Over current tests (Cases from 6.1 to 6.5): as expected, the mass flow rate and the pressure and voltage drop over 50 K GHe circuit in HEX increase with the current;
4. Stand by (Case 3.2): the pressure drops in HEX in stand by mode are about two times lower than for the steady state; also the mass flow rate is lower than the nominal value, i.e. 1.22 instead than 4.65 g/s. Some instabilities during the CL1 measurements have been found;
5. Over cooling (Cases 5.10 and 5.11): the voltage drop over HEX for case 5.11 (45 K HEX inlet tempertaure) are higher at lower mass flow rate than in the steady state regime (50 K HEX inlet temperature); no voltage drop data available for case 5.10;
6. Temperature profile: the experimental values acquired with 4 temperature sensors (MT006, MT004, MT009B, MT003) are in good agreement with the temperature profile obtained by means of 3D FE thermo-hydraulic and electrical model.
7. Joint resistances: very good agreement for the resistances $R_{65K\ Cu\text{-}HTS}$ (ME003), $R_{HTS\text{-}LTS}$ (ME006) and $R_{TWIN\ BOX\ (LTS\text{-}LTS)}$ (ME008) while some issues have been found for the terminal to flexible contact resistance (ME001).

ACKNOWLEDGMENT:

The authors wish to thank P. Bauer for having provided the TF prototype data and for the many useful discussions during several meetings.

Distribution List:

TE-MSC-SCD (CERN); Arnaud Devred (arnaud.devred@iter.org); Pierre Bauer (Pierre.Bauer@iter.org).

References

[1] ASIPP, "ASIPP_Test Procedure for ITER Current Leads Prototypes- A-FED-DOC-ZY-15," 2015.

[2] P. Bauer, S. Lee, R. Maekawa, F. Michel, T. Spina and Y. Yang, "TF HTS Prototype Lead Test-Run II Summary (IO)- Nov. 4th 2015," 2015.

[3] K. Ding, *Test results of the prorotypes of TF HTS current leads,* at ITER site for Conductor Meeting, 16.09.2015.

[4] M. Sitko, A. Ballarino and B. Bordini, “Thermo-hydraulic and electrical model of the 68kA HTS ITER current lead,” EDMS Nr. 1396106, CERN, Geneva, June 2014.

[5] P. Bauer, S. Lee, R. Maekawa, F. Michel, T. Spina and Y. Yang, “TF HTS Prototype Lead Test-Run II Summary (IO),” Nov. 4th 2015.